

NORTHWESTERN UNIVERSITY

Dynamics of Fascin in Filopodia

A DISSERTATION

**SUBMITTED TO THE GRADUATE SCHOOL
IN PARTIAL FULFILLMENT OF THE REQUIREMENTS**

for the degree

DOCTOR OF PHILOSOPHY

**Field of Cell and Molecular Biology
Integrated Graduate Program in the Life Sciences**

By

Yvonne Sarah Aratyn

CHICAGO, ILLINOIS

December 2007

**© Copyright by Yvonne S. Aratyn 2007
All Rights Reserved**

ABSTRACT

Dynamics of Fascin in Filopodia

Yvonne S. Aratyn

Filopodia play a central role in proper cell navigation; they extend from the cell surface and scan the local environment to guide the cell to its proper destination. These dynamic events require precise mechanisms for the turnover of key molecules which determine the morphology of filopodia. As of yet, such mechanisms are undefined and compose a major gap in our understanding of filopodia function. Therefore, we investigated the properties and interaction of actin and the actin cross-linking protein, fascin, which are essential for filopodia formation. Using expression of phospho-mimetic mutants, we determined that actin bundling in filopodia is dependent upon fascin dephosphorylation at serine 39 while phospho-fascin is predominantly unbound and freely diffusing in filopodia. Fluorescence recovery after photobleaching (FRAP) analysis revealed that fascin exchanges rapidly in filopodia and that this exchange was recapitulated *in vitro*, indicating that its dynamic behavior is intrinsic to the fascin cross-linker. A computational model indicated that simple diffusion from a fascin pool in the cell body was not sufficient to keep up with observed rates of filopodial elongation. Rather, fascin exchange along the length of the filopodium enables the ready supply of fascin to growing filopodial tips. Altogether, these results suggest that filopodia have selected for dynamic cross-linking to form adequately stiff bundles and allow for remodeling.

Scientific Acknowledgments

I owe my extreme gratitude to John Peloquin for protein purification, Leong Chew and Oana Danciu for technical support (at the microscope and at the bench), Ed Taylor and Shin Kojima for guidance in data analysis and theoretical derivations of kinetic parameters in this study, and Thomas E. Schaus for computational and analytical analysis.

This study was carried out with the financial support of the Cell and Molecular Biology Department at Northwestern University and the National Research Service Award from the National Institute of Health.

Dissertation Dedication

This dissertation is dedicated to all of the individuals who provided immense support throughout my life and my graduate studies:

To my parents:

Henrik and Lidia Aratyn – For giving me an international upbringing, which involved an education of various languages, culture, and traditions. For instilling the importance of hard work and higher education. For encouraging me not to give up even when ‘the going gets tough’. For the continued financial support during my poor years as a graduate student (one day, I’ll return the favor). And, above all, for being both my best friends and wonderful parents.

To my graduate advisors:

Seth Lichter – For introducing me to the cytoskeletal field and being supportive of my transition to the IGP for the completion of my doctorate.

Gary Borisy – For providing me (an engineer with little pipetting experience) the opportunity to study cell biology. For challenging me and encouraging me to advance my research to the ‘next’ level, despite my incessant whining. For including me as part of his family, especially in Woods Hole, MA, where he and Sally generously offered a wing of their house for my 3-week stay.

Ed Taylor – For his scientific and moral support throughout my graduate studies, especially within the final year.

To my friends:

Lisa, Denise, Julie, Kristen, Abby, Beata, and Kelly – For being my best cheerleaders. For listening to me go on and on about my research. For lifting my spirits when they were down and, just as important, for genuinely celebrating my accomplishments.

To my lab members:

Oana, Shin, Tom, and Derek – For providing numerous scientific discussions and many laughs, you were both my teachers and my friends. I’ll never forget those CMB Holiday parties that ended up at my apartment for continued debauchery.

To my drinking buddies:

Tom, Derek, Abby, Shan, James, Lauren and Kelly – For our exclusive wine club, where so many wine glasses became victims of our fun times together.

To my committee members:

Drs. Gary Borisy, Ed Taylor, James Bartles, Sarah Rice, Leong Chew, and Cara Gottardi who formed an amazing scientific sounding board. I learned so much from these cell biology, biochemistry, and microscopy experts!

To my better half:

Tom Schaus –For opening my eyes! For making me laugh! For adventures in travel! For making my happiness your priority! For being the other half of our two-part team! You have stolen my heart!

LIST OF ABBREVIATIONS

Actin binding site	ABS
Adenosine triphosphate	ATP
Adenosine diphosphate	ADP
Dubellco's Modified Eagle Medium	DMEM
Deoxyribonucleic acid	DNA
Ethylenediaminetetraacetic acid	EDTA
Fetal bovine serum	FBS
Fluorescence loss in photobleaching	FLIP
Fluorescence recovery after photobleaching	FRAP
Green fluorescent protein	GFP
Kilodalton	kD
Phosphate buffered saline	PBS
Polyacrylamide gel electrophoresis	PAGE
Polyethylene glycol	PEG
Protein kinase C	PKC
Room temperature	RT
Small interfering ribonucleic acid	SiRNA
Sodium dodecyl sulfate	SDS
Tetramethylrhodamine	TMR
Wild type	WT

Original Publications

This thesis is based on the following articles,

- I. Vignjevic D, S.I. Kojima, Y. Aratyn, O. Danciu, and G. Borisy. (2006). Role of fascin in filopodial protrusion. *J Cell Biol.* 174, 863-875.
- II. Aratyn, Y., T.E. Schaus, E.W. Taylor, and G.G. Borisy. (2007). Intrinsic dynamic behavior of fascin in filopodia. *Mol. Biol. Cell.* 18:3928-3940.

Material that is in preparation for publication is also presented.

TABLE OF CONTENTS

CHAPTER 1

GENERAL INTRODUCTION AND BACKGROUND	14
STATE OF THE FILOPODIUM: THEN AND NOW	14
ACTIN ORGANIZATION AND TURNOVER IN FILOPODIA	15
FILOPODIA FORMATION	17
<i>FILOPODIA EMERGENCE VIA A FOCAL RING</i>	<i>17</i>
<i>CONVERGENT ELONGATION MODEL</i>	<i>17</i>
<i>NUCLEATION OF PARALLEL BUNDLES BY FORMINS.....</i>	<i>18</i>
KEY MOLECULAR PLAYERS INVOLVED IN FILOPODIA FORMATION	21
REVIEW OF ACTIN BUNDLES: LESSONS ON FORMATION AND ELONGATION	23
<i>WHAT IS THE ORIGIN OF ACTIN BUNDLES?</i>	<i>23</i>
<i>WHAT CONTROLS BUNDLE GEOMETRY?</i>	<i>24</i>
<i>WHY DO SOME ACTIN BUNDLE HAVE ON CROSS-LINKER AND OTHERS</i>	
<i>HAVE MORE?</i>	<i>26</i>
FASCINATING FACTS ABOUT FASCIN	27
DISCOVERY OF FASCIN	27
FASCIN STRUCTURE	30
REGULATION OF ACTIN BUNDLING	33
FASCIN:ACTIN STOICHIOMETRY IN ACTIN BUNDLES	33
THE ROLE OF FASCIN IN FILOPODIA FORMATION	34
MECHANICAL PROPERTIES OF FASCIN CONTAINING BUNDLES	34
ROLE OF FASCIN IN CELL ADHESION AND MOTILITY	35
CORRELATION TO HEALTHY DEVELOPMENT AND DISEASE.....	36
WOUND HEALING	36

NEUROLOGICAL DISORDERS	36
CANCER METASTASIS.....	37
CHAPTER 2	
RESEARCH RESULTS	40
GENERAL OVERVIEW.....	40
LOCALIZATION OF FASCIN IN FILOPODIA	42
DYNAMICS OF FASCIN IN FILOPODIA	44
DYNAMICS OF T-FIMBRIN IN FILOPODIA	46
FASCIN UNDERGOES RAPID LOCAL EXCHANGE IN FILOPODIA AND SIMULTANEOUS SLOW EXCHANGE WITH CYTOPLASM POOL	48
FRAP DATA REVEAL KINETIC-OFF RATE FOR FASCIN IN FILOPODIA.....	52
ROLE OF FASCIN PHOSPHORYLATION IN FILOPODIA FORMATION	54
<i>THE CHARACTERISTIC CYCLES OF FASCIN ASSOCIATION AND DISSOCIATION ARE AN INTRINSIC PROPERTY OF THE FASCIN-ACTIN INTERACTION</i>	<i>56</i>
<i>FASCIN-MEDIATED ACTIN BUNDLING IN FILOPODIA REQUIRES THAT FASCIN BE IN THE NON-PHOSPHORYLATED STATE</i>	<i>59</i>
FASCIN UNDERGOES FREE DIFFUSION IN FILOPODIA WITH A MODERATE DIFFUSION COEFFICIENT, $D = 6\mu\text{m}^2/\text{s}$	64
INCORPORATION OF FASCIN CROSS-LINKS IN FILOPODIA.....	67
<i>FILOPODIA CONTAIN RATIOS OF ONE FASCIN PER 25-60 ACTIN</i>	<i>67</i>
<i>MOST FASCIN MOLECULES IN FILOPODIA ARE BOUND AT ANY INSTANT</i>	<i>72</i>
DYNAMIC FASCIN CROSS-LINKING ALLOWS FOR INCREASED FILAMENT BUNDLING AT GROWING FILOPODIAL TIPS	75
CHAPTER 3	
DISCUSSION.....	81
TARGETING OF FASCIN TO FILOPODIAL TIPS	81

ADVANTAGES OF DYNAMIC CROSS-LINKING IN FILOPODIA	82
FASCIN PHOSPHORYLATION ACTS AS A MOLECULAR SWITCH FOR FILOPODIA FORMATION	83
FILOPODIA REPRESENT SEMI-ORDERED BUNDLES OF ACTIN	85
FASCIN DYNAMICS HAVE IMPLICATIONS ON THE MECHANICS AND REMODELING OF FILOPODIA	87
FASCIN TURNOVER IS A KEY PROCESS IN FILOPODIAL ASSEMBLY	90
CHAPTER 4	
SUMMARY OF CURRENT WORK AND FUTURE PERSPECTIVES.....	91
LESSONS FROM FILOPODIA: HOW DO ACTIN BUNDLES GROW?	91
ROLE OF FILOPODIA IN CANCER METASTASIS	98
CHAPTER 5	
APPENDIX.....	101
A. THEORETICAL MODEL FOR THE DERIVATION OF k_{off} FROM FRAP DATA	101
B. DESCRIPTION OF NUMERICAL DIFFUSION-REACTION MODELS	104
C. EFFECTIVE DIFFUSION OF FASCIN IN FILOPODIA	106
D. DETERMINATION OF THE OPERATING FASCIN:ACTIN RATIO IN FILOPODIA	107
CHAPTER 6	
MATERIALS AND METHODS	109
PROTEIN PURIFICATION.....	109
<i>ACTIN</i>	109
<i>FASCIN</i>	109
IN VITRO BUNDLING ASSAY	110
CELL CULTURE	112

PLASMIDS	112
QUANTITATIVE IMMUNOBLOTTING	117
IMMUNOFLUORESCENT STAINING OF FIXED CELLS	119
MICROSCOPY	119
<i>EPI-FLUORESCENT MICROSCOPY</i>	119
<i>FRAP AND FLIP</i>	119

CHAPTER 7

REFERENCES	121
CURRICULUM VITAE	130

LIST OF FIGURES

FIGURE 1. STRUCTURE OF FILOPODIA AND LAMELLIPODIA	16
FIGURE 2. MODEL FOR THE REGULATION OF ACTIN DYNAMICS IN FILOPODIA	17
FIGURE 3. MECHANISMS FOR FILOPODIA FORMATION	20
FIGURE 4. COMPONENTS INVOLVED IN FILOPODIA FORMATION.....	22
FIGURE 5. SEQUENCE ALIGNMENT OF FASCIN ISOFORMS	29
FIGURE 6. FASCIN STRUCTURE AND PUTATIVE ACTIN BINDING SITES	32
FIGURE 7. LOCALIZATION OF FASCIN IN B16 MELANOMA CELLS	43
FIGURE 8. LOCALIZATION AND DYNAMICS OF FASCIN AND ACTIN IN FILOPODIA	45
FIGURE 9. LOCALIZATION AND DYNAMICS OF T-FIMBRIN.....	47
FIGURE 10. QUANTITATIVE ANALYSIS OF FASCIN EXCHANGE IN FILOPODIA	50
FIGURE 11. RECOVERY OF CYTOPLASMIC FASCIN IN FILOPODIA IS RELATIVELY SLOW	52
FIGURE 12. KINETIC ANALYSIS OF FLUORESCENCE RECOVERY OF FASCIN IN FILOPODIA REVEALS k_{off}	53

FIGURE 13.	MODEL OF PHOSPHORYLATION-REGULATED FASCIN KINETICS	55
FIGURE 14.	FASCIN IS DYNAMIC IN RECONSISTUTED FILOPODIA-LIKE BUNDLES	58
FIGURE 15.	LOCALIZATION OF FASCIN MUTANTS IN FILOPODIA	61
FIGURE 16.	DYNAMICS OF FASCIN MUTANTS IN FILOPODIA	63
FIGURE 17.	PHOSPHO-FASCIN UNDERGOES PURE DIFFUSION IN FILOPODIA	66
FIGURE 18.	WESTERN BLOTS REVEAL AMOUNT OF FASCIN IN CELL LYSATES	68
FIGURE 19.	PERCENT FASCIN LOCALIZED TO FILOPODIA	70
FIGURE 20.	PERCENT FASCIN BOUND IN FILOPODIA	73
FIGURE 21.	EFFECTIVE FASCIN TRANSPORT TO TIPS OF GROWING FILOPODIA REQUIRE DYNAMIC CROSS-LINKING	78
FIGURE 22.	OPTIMAL CONDITIONS FOR FILOPODIAL ELONGATION	80
FIGURE 23.	ILLUSTRATIVE MODEL OF FASCIN DYNAMICS AND ORGANIZATION IN FILOPODIA.....	85
FIGURE 24.	RAPID FASCIN EXCHANGE MAY ENDOW FILOPODIA WITH A RATE-DEPENDENT RESPONSE MODE TO MECHANICAL STRESS	89
FIGURE 25.	SCHEMATIC MODEL OF ACTIN DIFFUSION ALONG FILOPODIA	95
FIGURE 26.	ACTIN DIFFUSION CANNOT ADEQUATLY SUPPLY MONOMERS TO GROWING TIPS OF LONG FILOPODIA	96
FIGURE 27.	ACTIN DIFFUSION CAN SUPPORT SHORT, GROWING FILOPODIA	97
FIGURE 28.	<i>IN VITRO</i> ASSAY	111
FIGURE 29.	A SCHEMATIC ILLUSTRATION OF pEGFP-FASCIN VECTOR	113
FIGURE 30.	SEQUENCE OF HUMAN FASCIN1	115
FIGURE 31.	PROTEIN STANDARD CURVE	118

LIST OF TABLES

TABLE 1.	FASCIN EXPRESSION IN HEALTHY TISSUE AND DISEASE	39
TABLE 2.	PARAMETERS USED IN REACTION-DIFFUSION MODEL OF FASCIN IN FILOPODIA	76
TABLE 3.	PARAMETERS USED IN NUMERICAL MODEL OF ACTIN DIFFUSION IN FILOPODIA	94
TABLE 4.	SCHEMATIC ILLUSTRATION OF pEGFP-FASCIN	114

Chapter 1: General Introduction and Background

State of the filopodium: then and now

Many cells move about by crawling over surfaces, rather than by using cilia or flagella. An experiment led by Albrecht-Buehler in 1976 showed that the direction of cell crawling is preferential rather than random, motivating the question; how do motile cells scan and decode positional information? At least part of the answer lies in fibrous-like cellular projections, named filopodia, which have been shown to have a substrate exploring function (Albrecht-Buehler, 1976). Once filopodia protrude from the cell surface, they rapidly scan the local environment until they attach to the substratum. Subsequently, cells extend their leading edge, or lamellipodium, in the direction of the filopodia and also adhere to the substratum while the rear of the cell is dragged forward by traction (Albrecht-Buehler, 1976; Gundersen and Barret, 1980; Zheng et al., 1996). Effectively, filopodia function as exploratory organelles which the cell uses to navigate to its proper destination.

Recent years have seen great advances in imaging technology, such as sophisticated single molecule measurements and live cell fluorescence microscopy, along with the development of computational models that have allowed for the testing of long standing hypotheses and the generation of new ones. Accordingly, our understanding of filopodia and their role in cell migration has significantly increased. In particular, the molecular basis for filopodia formation is fairly well understood and many of the molecular players involved have been identified. Nonetheless, information concerning how filopodia are coordinated spatially and temporally remains limited. Therefore, this thesis work emphasizes questions regarding the dynamics of filopodia, including, what are the cytoskeletal proteins involved in filopodia formation? Where and when do they act? Are they stable over the lifetime of filopodia or do they turnover? If they are dynamic then what implications does their reorganization have on the remodeling and physical properties of filopodia? To address the aforementioned questions, we used the latest microscopy techniques, such as fluorescence photobleaching (FRAP and FLIP), to study phenomena in the cellular context and extended them for use on *in vitro* systems to dissect regulatory

features of filopodia formation that were irresolvable *in vivo*. Furthermore, we contributed a numerical model to investigate the biological significance of our research findings in the framework of filopodia growth. Altogether, this work introduces novel experimental techniques, confers an understanding of how the cell assembles and extends its filopodia, and encourages continued study of assembly mechanisms of cellular actin bundles.

Actin organization and turnover in filopodia

Filopodia are composed of bundles containing approximately 15-20 parallel actin filaments (Lewis and Bridgman, 1992) that are tightly organized (Fig. 1), with 8-35nm spacing (Meyer and Aebi, 1990; Kureishy et al., 2002). Filopodia are long, slender protrusions that can grow more than 70 μ m in length and reach 250-400nm in diameter (McClay, 1999). Within the bundle, filaments are arranged with their barbed ends oriented toward the tip of the filopodium and pointed ends toward the cytoplasm (Lewis and Bridgman, 1992). The polarity of actin filaments is fundamental to the mechanism of actin assembly in cells (Pollard and Borisy, 2003). Actin polymerization occurs by assembly of ATP-actin at the barbed end. Upon incorporation of ATP-actin into the filament, ATP is hydrolyzed to ADP and phosphate is released. Hydrolysis of ATP reduces the strength of binding between monomers, thereby, promoting depolymerization (or disassembly) at the pointed end. The balance between actin polymerization at the barbed end and depolymerization at the pointed end is referred to as treadmilling (Neuhaus et al., 1983). A free actin filament grows when the rate of barbed-end polymerization exceeds the rate of depolymerization. Filopodial extension results from the difference between the rate of tip polymerization and retrograde flow, the flow of actin toward the central domain of the cell by action of myosin contractility (Fig. 2) (Mallavarapu and Mitchison, 1999; Medeiros et al., 2006). Typical rates of filopodial growth range from 1-10 μ m/min (Mallavarapu and Mitchison, 1999; Aratyn et al., 2007), with bursts of up to 25 μ m/min (Sheetz et al., 1992; McClay, 1999).

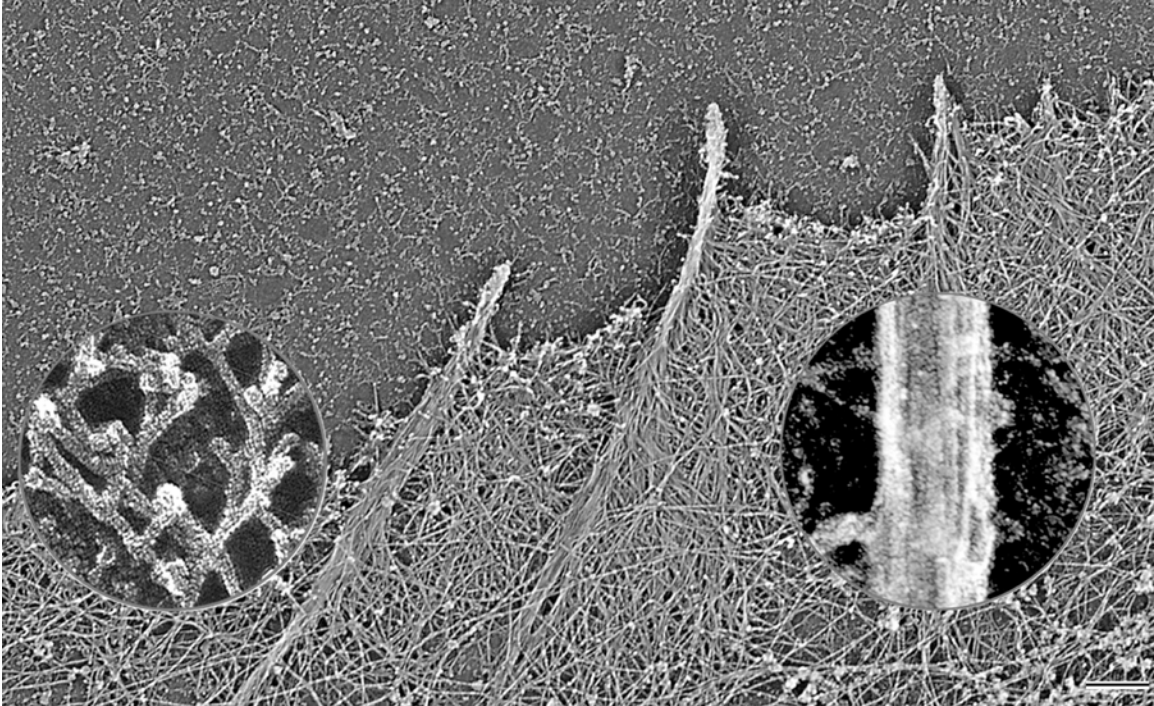


Figure 1. Structure of filopodia and lamellipodia

Lamellipodia are made of branched actin filaments. Filopodia contain an unbranched bundle of actin filaments, which are aligned axially and packed tightly together. Scale bar 200 nm. Electron micrograph was prepared in the lab by D. Vignjevic.

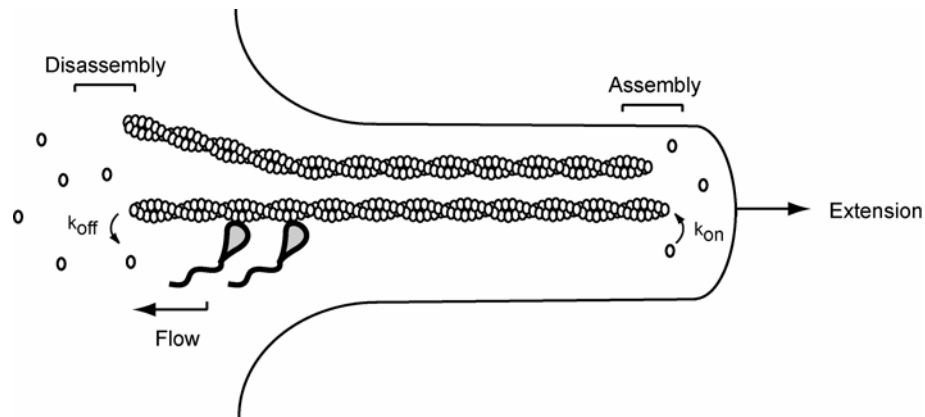


Figure 2. Model for the regulation of actin dynamics in filopodia

Filopodia extend by polymerization of actin filaments at the barbed end. Flow is driven by motors that pull on the filaments. The identity of the motors and what they pull on is not known, although myosin II (Wolenski et al., 1995; Ishikawa et al., 2003), V (Ishikawa et al., 2003), and XVa (Rzadzinska et al., 2004) have been reported to promote retrograde flow of filamentous actin. (Figure modified and adapted from Mitchison and Kirschner, 1988).

Filopodia formation

Filopodia initiation and elongation require the availability of free actin barbed ends, polymerization of actin into filamentous structures, and cross-linking of those filaments into bundles. Several spatial and temporal models have been proposed to describe mechanisms for filopodia formation. While none of the models are entirely exclusive, they highlight varying molecular events and key players.

Filopodia emergence via a focal ring

In this model, focal rings play a significant role in initiating and stabilizing filopodia (Steketee et al., 2001). They are proposed to develop at the base of the initiation site for filopodia formation. Actin filaments radiate from the ring, anchoring it indirectly to adhesion sites, thereby holding it stationary and taut within the cytoplasm. The focal ring acts as a nucleating center for new actin filaments, which are free to grow while using the ring as a basal adhesion. Filaments that extend outward from the ring and toward the cell membrane are bundled together and continue to grow into a mature filopodium.

Convergent Elongation Model for filopodia formation

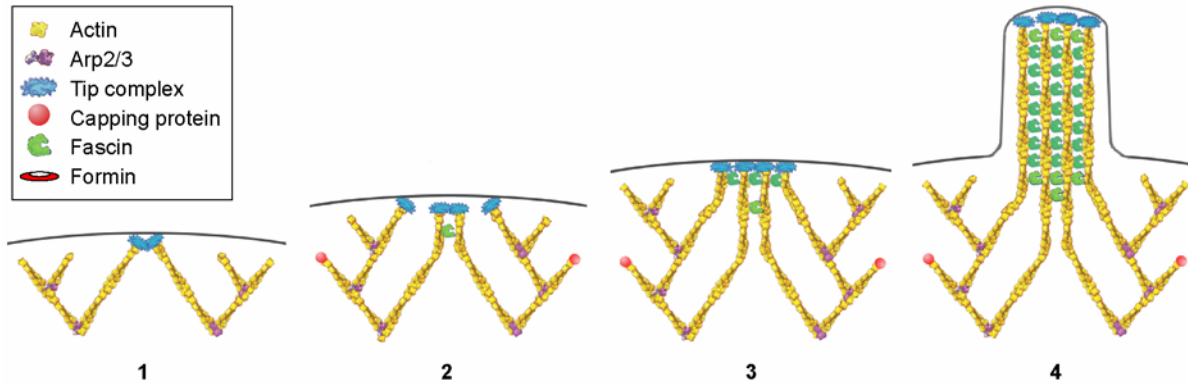
The Convergent Elongation Model (CEM) for filopodia initiation is based on a mechanism of self-organization. This model stipulates that filopodia arise from the gradual re-arrangement of the dendritic network, rather than from de novo actin filament nucleation (Fig. 3) (Svitkina et al., 2003). The idea of dendritic nucleation arose from *in vitro* and *in vivo* data that indicated that actin filaments could nucleate off the sides of pre-existing filaments (Mullins et al., 1998; Svitkina and Borisy, 1999). The reorganization of lamellipodial dendritic network to form filopodial bundles is thought to be mediated by the filopodial tip complex. Filaments formed by Arp2/3 (actin-related protein 2 and 3) complex-mediated dendritic nucleation gain protection against capping and can therefore elongate persistently at their barbed ends. The collision of the actin barbed ends cluster during filament elongation forming filopodial precursors, so-called Λ -precursors. The filopodial tip complex initiates filament cross-linking by

recruiting and/or activating fascin. Filament bundling via fascin initiates at the vertex of the self-organized precursors and facilitates the pushing efficiency of filopodia. Initiated filopodia elongate and treadmill at steady state, whereby barbed end growth is balanced by pointed end shrinkage. The filopodial tip complex remains associated with the growing tip, allowing for continuous elongation of filopodial filaments and mediating filopodia fusion on collision.

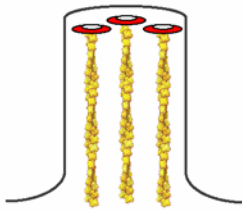
Nucleation of parallel bundles by formins

Yet another model for filopodia formation postulates that actin filaments are nucleated via a formin-mediated process, which involves the formation of actin bundles in an unbranched network (Kovar and Pollard, 2004; Zigmond et al., 2004; Pellegrin and Mellor, 2005). Formins are multi-functional proteins that are divided into two domains, the highly conserved formin-homology 2 (FH2) domain which interacts with the fast-growing barbed ends of actin filaments and the FH1 domain which binds profilin and profilin-actin (Pruyne et al., 2002; Sagot et al., 2002). These domains give formins the ability to inhibit end-to-end annealing of actin filaments (Kovar et al., 2003), compete with capping protein for barbed ends (Zigmond et al., 2003; Harris et al., 2004), and regulate actin turnover at filopodial tips (Schirenbeck et al., 2005). Together, this data suggests a mechanism in which formins promote filament elongation by allowing for insertional polymerization of actin at barbed ends of filopodial bundles.

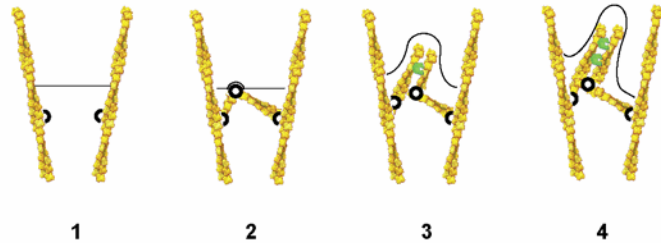
A. Convergent Elongation Model for Filopodia Formation



B. Filopodia Formation via Formins



C. Filopodia Emergence via Actin Focal Ring

**Figure 3. Mechanisms for filopodia formation**

(A) Convergent elongation model for filopodia formation. Dendritic filaments (1) move laterally in the plane of the leading edge as they elongate, resulting in collisions of their barbed ends. Barbed end binding molecules associate to form a tip complex (2) which recruit fascin, resulting in cross-linking of actin filaments. (3) Continued recruitment of fascin together with actin polymerization promote filopodial elongation (4). (B) Formins nucleate the assembly of straight, parallel actin filaments into filopodia. (C) Schematic model of filopodia forming via an actin focal ring. (1) During extension of lamellar region, components essential for filopodia formation are made available as the cytoplasm fills in. (2) Actin focal rings (black open circles) provide an anchorage site and nucleate actin filaments. (3) Precursors to filopodia form as actin elongates and is cross-linked. (4) Mature filopodia form via continued polymerization and cross-linking.

Key molecular players involved in filopodia formation

Several key molecules have been implicated in the regulation of cytoskeleton reorganization and filopodia formation and are shown in Figure 4. The GTP-binding protein, Cdc42, has been shown to induce filopodia formation (Adams and Schwartz, 2000) and interacts specifically with Wiskott-Aldrich syndrome protein (WASP) (Pantaloni et al., 2001) providing a direct link to actin assembly through the activation of the Arp2/3 complex. Filopodia formation relies on the protection of barbed ends from capping at the working interface by the Ena/Mena/Vasp family that serve to inhibit capping protein (Vignjevic et al., 2003). Formins have also been found to protect barbed ends from capping at filopodial tips as well as promote actin polymerization (Zigmond et al., 2003; Harris et al., 2004). The structural integrity of filopodia is supported by cross-linking proteins (fascin, filamin, alpha-actinin, espin) (Bartles, 2000; Briher et al., 2004), proteins that polarize assembly (profilin) (Carlier and Pantaloni, 1997) and promote disassembly from the pointed ends (ADF/cofilin) (Bamburg, 1999), molecular motors that transport elongation machinery to the tips of filopodia (myosins X and XVa) (Belyantseva et al., 2003; Tokuo and Ikebe, 2004), signaling proteins (IRSp53) (Govind et al., 2001; Yamagishi, 2004), and proteins that connect the sides of filaments to the cell membrane (ezrin/radixin/moesin) (Yonemura, 1998).

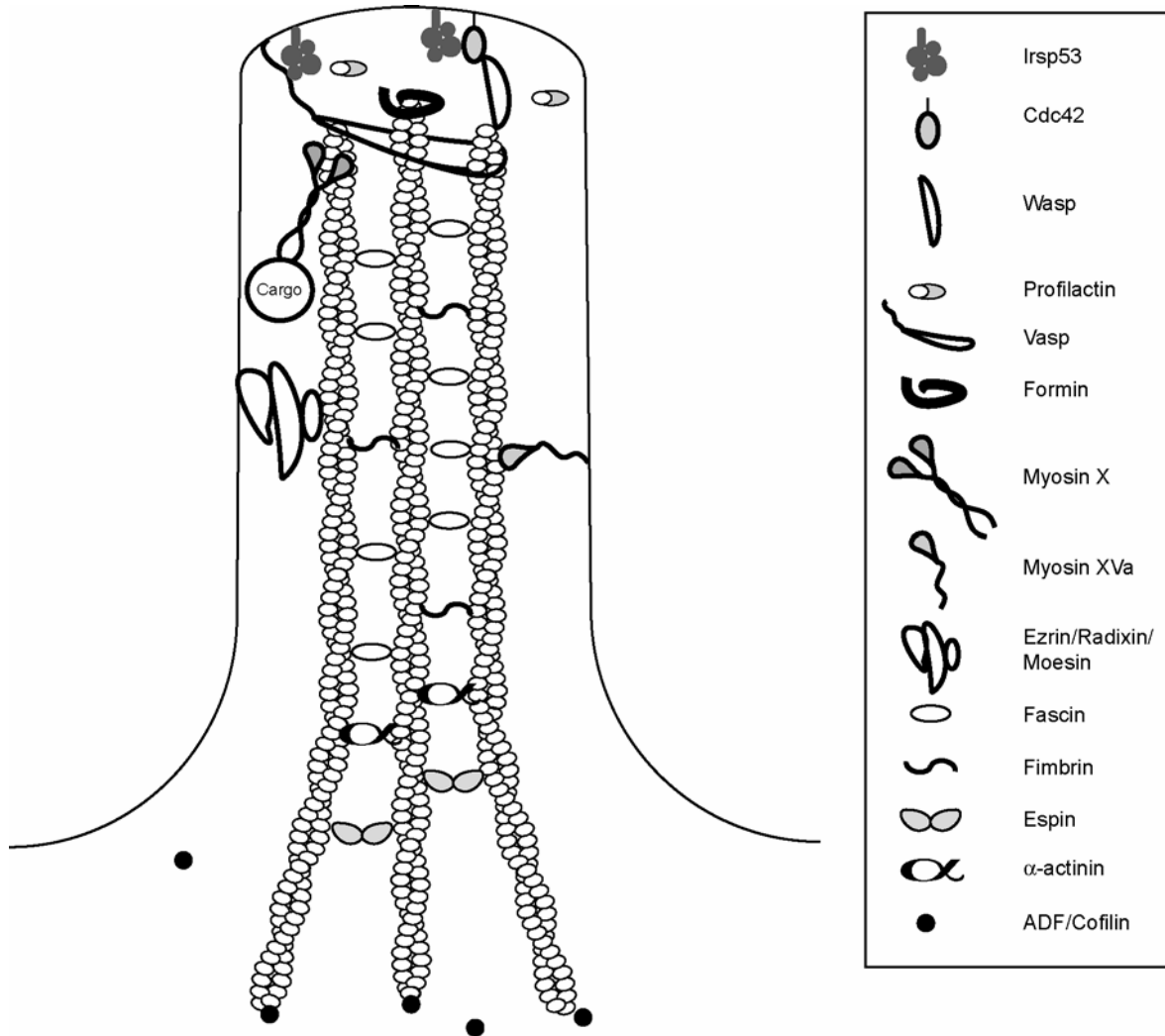


Figure 4. Components involved in filopodia formation

A brief review of actin bundles – Lessons on formation and elongation

While many of the key components and events involved in filopodia formation are fairly well outlined, many have yet to be sorted out. To bridge the gap between the known and unknown, it may be useful to examine features of other actin bundles. Filopodia share many composition principles with actin networks found in stereocillia, microvilli, *Drosophila* bristles, the nurse cell strut, fertilization cone, and acrosomal processes of sperm, to name a few. These structures are assembled in a specific location or particular developmental time and, therefore, can expose molecular mechanisms for bundle formation, in general. For this reason, it is worth comparing the similarities and differences between actin bundles as they can be advantageously used to study properties of filopodia. Here, we pose unanswered questions in the cytoskeletal field and compare and contrast features of actin bundles in an attempt to (partially) resolve them.

What is the origin of actin bundles?

Based on the assumption that all actin bundles possess a common mechanism of morphogenesis, Tilney and DeRosier proposed that cells harbor a bundle generating factory that manufactures short bundles, which compose the building blocks for longer bundles (Tilney and DeRosier, 2000). According to their hypothesis, the identity of these building blocks is microvilli, cellular extensions that are thought to increase the surface area of cells, thereby facilitating absorption and secretion. Microvilli are composed of roughly 20 actin filaments, bundled together with the same polarity, and grow 3-4 μ m long (Fath et al., 1990). They are nucleated from a dense material of unknown composition at the plasma membrane, which remains associated at the tip of the bundle as it grows. Other actin bundles are speculated to originate from microvilli, which are incorporated into more complex networks depending on the biological purpose of the cell. For instance, the fertilization cone, nurse cell strut, and *Drosophila* bristles contain microvillus-like actin bundles that are aggregated into larger discontinuous networks. In these cases, the actin bundles are composed of shorter units or modules that bind to each other, with each of

these modules derived from the core filament bundle in microvilli. Other actin networks, such as stereocilia and the acrosomal process of marine sperm, are also derivatives of microvilli but display continuous entities of actin bundles: Stereocilia (mechanosensitive protrusions in inner ear hair cells) form by the lateral addition of growing filaments to the microvillar bundle, exhibiting a characteristic staircase pattern. These bundles can grow up to 120 micron in length (Harrison et al., 2005; Rzadzinska et al., 2005; Rzadzinska et al., 2004). The acrosomal process initiates from small patch of dense material, just like microvilli, but then elongates into one continuous process that contain about 85 filaments at its base that taper off to 15 filaments near the tip (Tilney et al., 1981). Regardless of type, all the aforementioned bundles share common features; (1) filaments are unbranched and tightly bundled, (2) unidirectional polarization of filaments with their barbed ends located near the bundle tip, and (3) elongation by monomer addition at the barbed ends. Filopodia also exhibit these features and, in this context, may also be derived from microvilli.

What controls bundle geometry?

Actin bundles come in all shapes and sizes; some are short, some are long, some are narrow, and some are wide. For instance, the marine sperm acrosomal process (55 μm), fly bristle (65-350 μm), and long stereocilia (60-120 μm) are one to two orders of magnitude longer than microvilli (3-4 μm) (Tilney et al., 1981; Fath et al., 1990; Tilney et al., 2003; Rzadzinska et al., 2005). Furthermore, while the acrosomal process contains roughly 85 filaments and stereocilia have 30-300 in total, microvilli contain ~20 filaments and *Drosophila* bristles have between 10-50 filaments within each of their 12-18 bundles (Tilney and DeRosier, 1981; Tilney and DeRosier, 2000; Rzadzinska et al., 2004). These observations indicate that bundle length is independent on filament number, leaving us wondering what determines the diameter and length of actin bundles? Is there a single mechanism or is bundle geometry regulated by many factors? The answer to this question is largely unknown but parts of the answer have surfaced.

One might predict that the morphology of actin bundles is regulated, in part, by the ability of the cell to make components of the actin cytoskeleton available in the correct amounts and at the precise moment needed for bundle construction. By this method, microvilli and its counterparts might be generated sequentially, such that each component is assembled one by one to form the bundles. However, what signals the cell to stop making more and more of these components? It may be possible that regulatory molecules are made available to activate and inactivate the building blocks of actin bundles. In that way, only the active forms are utilized to generate microvilli and the others are left in the inactive state within the cytoplasm until the cell generates more bundles or lengthens existing bundles. Tilney and DeRosier proposed that the dense material at the tip (sometimes referred to as the 'tip complex') might play a regulatory role (Tilney and DeRosier, 2000). They propose that the tip complex acts as a bundle factory that limits the availability of cytoskeletal proteins during the nucleation event, such that it couples the concentration of components to the concentration of nucleation sites. In this case, the filament number in a nucleation site are specified and the average length of the bundles would be constant, independent of bundle width or rate of growth.

The dynamics of proteins that make up bundles has been shown to play a crucial role in length determination. For instance, the turnover of actin regulates bundle size and shape (Tilney et al., 2003). Bundle shape is controlled by assembly of monomers at the barbed end and disassembly at the pointed end, which orchestrates, in part, the movement of actin from bundle base to tip. In stereocilia, actin dynamics may play a role in regulating number of bundles, as they are fairly constant from one hair cell to the next. In early development, stereocilia bundles which are not incorporated into the staircase array, are depolymerized and the cytoskeletal components are recycled, possibly used to form new bundles or increase the size of existing bundles to form a mature stereociliary cluster (Tilney et al, 1992). The rate of actin delivery also plays a critical role in bundle length determination. While diffusion of actin monomers to the tip is one mechanism for delivery, another mechanism of transport is via myosin motors. For instance, myosin XVa has been implicated in regulating the length of stereocilia (Rzadzinska et al., 2004),

possibly regulating the delivery of growth components to bundle tips. Myosin X has also been found to localize to bundle tips in filopodia (Berg and Cheney, 2002). Other motor proteins, such as myosins II, V, and VI are speculated to regulate the flow of actin to the bundle base (Mitchison and Kirschner, 1988; Rzadzinska, 2004).

Actin cross-linking proteins also seem to play an important role in regulating the geometry of bundles. In an *in vitro* study, bundles with relative high concentration of fascin cross-linker to actin produced small bundles, while low fascin to actin ratios yielded larger bundles (Stokes and DeRosier, 1991). Based on these observations, a two-stage mechanism for bundle growth was proposed, which involves the rapid nucleation of short bundles with relatively high concentrations of cross-linker, followed by a slow growth phase, which involves continued bundle growth until the number of cross-linkers is exhausted. In stereocilia, the espin cross-linker regulate the formation and maintenance of actin bundle length; lack of espins results in the inhibition of bundle growth, while overexpression of espin induces long stereocilia (Belyantseva, 2003; Rzadzinska et al., 2005). The mechanism by which cross-linkers regulate bundle length remains unknown.

Why do some actin bundles have one cross-linker and others have more?

The above discussion naturally evokes the question of whether actin bundle shape is dependent on type of cross-linker. Afterall, each cross-linker requires a particular arrangement of actin filaments as each has a different set of actin binding sites. Therefore, the geometry of the actin helix in a filament specifies the maximum number and position for a specific cross-linker. The bonding geometry is more complex when actin bundles contain more than one type of cross-linker. For instance, microvilli contain three bundlers; villin, fimbrin and espin, stereocilia and *Drosophila* have two each; fimbrin and espin in the former and fascin and forked protein in the latter. What might be the purpose of having multiple bundling proteins? One possibility is that each protein serves a different role at various stages of bundle development. Or, accumulate at different times during the assembly process. In *Drosophila*, forked appears to initially form

bundles while fascin appears later (Tilney et al., 2000). What are the implications of sequential cross-linking? One cross-linker may be used to initially draw filaments close together such that they are spaced within reach of a second or third cross-linker, which function to tighten the bundle. ‘Tightening’ of the filaments may affect stiffness properties of bundles, which may be important for protrusion and shape maintenance/prevention of buckling (Tseng et al., 2002; Briehner et al., 2004).

While many actin bundles contain multiple cross-linking proteins, the minimum requirement for bundling is one cross-linker. For instance, actin bundles form *in vitro* by mixing filaments solely with alpha-actinin, T-fimbrin, or fascin. Filopodia formation is inhibited upon knockdown of fascin (Vignjevic et al., 2006), suggesting that other cross-linkers are not required for the formation of cellular protrusions. However, T-fimbrin and espins are not necessarily absent from these structures (Vignjevic et al., 2006). These results suggest that some cross-linking proteins may play a dominant role in bundle formation, while other bundlers are only called to duty later in the developmental stage and not at all if bundle formation is inhibited. It may even be possible that some cross-linkers function to trigger the activation of other cross-linkers in an indirect manner (via regulatory proteins), depending on whether they, themselves, are actively participating in bundling filaments. Such hypotheses have not yet been experimentally tested.

Fascinating facts about fascin

Since this thesis work is about filopodia, we studied its main cross-linking protein, fascin. Here, important properties about fascin are outlined that will be useful for understanding the basis of results discussed in Chapter 2.

Discovery of fascin

Fascin is a 55kD protein that was first discovered in the late 1970s from cytoplasmic extracts of sea urchin oocytes and coelomocytes and later found in HeLa cells in the mid 1980s (Bryan and Kane, 1978;

Otto et al., 1979; Yamashiro-Matsumura and Matsumura, 1985). The name, ‘fascin’, was derived from its ability to cross-link actin filaments into unipolar and tightly packed bundles (from the Latin, fasciculus, a bundle) (Otto et al., 1979). Fascin is well conserved across many species, including *Drosophila melanogaster*, echinoderms, and the platyhelminth *Schmidtea mediterranea* (Bryan et al., 1993; Kureishy et al., 2002; Sanchez et al., 2002; Adams, 2004). Vertebrate genomes encode three forms of fascin: the first cloned human fascin, fascin-1, which is highly expressed by mesenchymal tissues and in the nervous system; fascin-2, which was cloned from bovine and human retinal photoreceptor cells and shares 55% and 56% amino acid identity to first human fascin clone, respectively; and fascin-3, which was cloned from human testis and shares 27% identity to both fascin-1 and fascin-2 gene products (reviews: Kureishy et al., 2002; Adams, 2004). Sequence alignment of fascin proteins is given in Figure 3. The focus of this thesis work is on fascin-1, which, from this point onward, will be referred to as fascin.

Domain 1

Human fascin-1
 Mouse Fascin-1
Xenopus fascin
 Human fascin-2
 Bovine fascin-2
 Human fascin-3
 Mouse fascin-3
Drosophila fascin
 Sea urchin fascin

1 -----MTANGTAEAIVQFOGLNCKNYLTAEAFGRKVASASLKKKQMPLEPPPEAGSAAYCLASHLGRYLADKQGNITCEBEV--PFDCKRFLIVAHDDGRWLSQSEBARRRYFGGTEDELRSQCFACVTS--PABKWSVHLAAH
 1 -----MTANGTAEAIVQFOGLNCKNYLTAEAFGRKVASASLKKKQMPLEPPPEAGSAAYCEKHLGRYLADKQGNITCEBEV--PDQCRFLVAHDDGRWLSQSEBARRRYFGGTEDELRSQCFACVTS--PABKWSVHLAAH
 1 -----MSSGPTQLGNCNAYLTAEAFGRKVASASLKKKQMWLEPAGQDT--SAVLLSHLGRFLSADKQGNVSGESDT--AGTECRFLSAQAGDGRWLSQSEBILGRYFGGTEDELRSQCFSPSS--PABKWSVHLAAH
 1 -----MPTNGLHQVWKFOGLNCKNYLTAEAFGRKVASASLKKKQMPLEPPGAG--TAVLRSKSHLGRYLSABEDGRWAGAEAR--PFDCKRFLPQPDGRWLSQSEBGRIFEGGTEDELRSQCFATAIS--PABKWSVHLAAH
 1 -----MPTNGLHQVWKFOGLNCKNYLTAEAFGRKVASASLKKKQMWLEPPDPEG--TAVLFRSHLGRYLSABEDGRWAGAEAR--PFDCKRFLPQPDGRWLSQSEBGRIFEGGTEDELRSQCFATAIS--PABKWSVHLAAH
 1 -----MOETWTHRHPKAEDRVGLSWAGTVLFEAKNTVATAVLSGQRKQWLELVNSGHETQAVVRELVSWGTYLDCDQVFCYGRPR--TSHHGQFLRFRHRSIVLHGLGSRVLESNGKDICTSHVWTS--AYHMWTFRPAALH
 1 -----MAEYDWHRHPKAEDRVGLSWAGTVLFEAKNTVATAVLSGQRKQWLELVNSGHESQAVVRELVSWGTYLDCDQVFCYGRPR--TSHHGQFLRFRHRSIVLHGLGSRVLESNGKDICTSHVWTS--AYHMWTFRPAALH
 1 -----MAEYDWHRHPKAEDRVGLSWAGTVLFEAKNTVATAVLSGQRKQWLELVNSGHESQAVVRELVSWGTYLDCDQVFCYGRPR--TSHHGQFLRFRHRSIVLHGLGSRVLESNGKDICTSHVWTS--AYHMWTFRPAALH
 1 MNGAGCELHSGNGLISQQKQGWITGLINQGHYVTAETFGFKLVANASLKKKQMPLEPNTGES--IYLVSHNLYLSDPQGNVLCESDERDARTRGRFLVTSISEDSRGWALKNECVTLCGTFDKLVCTHAKVPG-ASBP-VTVHLAAR
 1 -----MPAMMKYHFGNLSGAVLTAEAFGRKVASASLKKKQMPLEPQESST--ISYLAVPSCKVLSADKQGNVSTEDRTEDELRSQCFATAIS--PABKWSVHLAAH

Domain 2

Human fascin-1
 Mouse Fascin-1
Xenopus fascin
 Human fascin-2
 Bovine fascin-2
 Human fascin-3
 Mouse fascin-3
Drosophila fascin
 Sea urchin fascin

140 POWNVSVIRRYVAHI SARP--ADELAVDRDVPWGVSLLTLAFQO---GRYSQTDHRRFRIDGRLVARPEPATGTLLEPFS--GKVAARDQGVYLPSGPSSTLKAGATATVGGDELRALEGS
 140 POWNVSVIRRYVAHI SARP--ADELAVDRDVPWGVSLLTLAFQO---GRYSQTDHRRFRIDGRLVARPEPATGTLLEPFS--GKVAARDQGVYLPSGPSSTLKAGATATVGGDELRALEGS
 132 PCFTLVSVIRRYVAHI SARP--GDELSVDRDVPWGVSLLTLAFQO---NRYSQTDHRRFLASDLSLEKPPPTHTVTLISA--GKVAAREGSVAVLSSGFTLKSANKSAGDELRALEGS
 139 PCVHLVSVIRRYVAHI CPR--EDEVAADGRDVPWGVDALTLIFQO---RNVCKSOSVDRSDRWPPEPRACVTLFEFA--GRAFIDQGHYLPVGHAGTILKAGNTRIPGAEDELRALEGS
 139 PCVHLVSVIRRYVAHI CTPQ--EDEVAADGRDVPWGVDALTLIFQO---RNVCKSOSVDRSDRWPPEPRACVTLFEFA--GKAFIDQGHYLPVGHAGTILKAGNTRIPGAEDELRALEGS
 144 VHMVLSVPTHCYVADPPT--MGRVYDAVAVFLELCGFLHFRD---GCHLETSTHFFSHVRLPFSQSSQTEHMKVPCGVFALDGGCGMLVPCVHLLGMCKPMRG--HEMFTLQHC
 144 VHMVLSVPTHCYVADPPT--MGRVYDAVAVFLELCGFLHFRD---GCHLETSTHFFSHVRLPFSQSSQTEHMKVPCGVFALDGGCGMLVPCVHLLGMCKPMRG--HEMFTLQHC
 144 VHMVLSVPTHCYVADPPT--MGRVYDAVAVFLELCGFLHFRD---GCHLETSTHFFSHVRLPFSQSSQTEHMKVPCGVFALDGGCGMLVPCVHLLGMCKPMRG--HEMFTLQHC
 153 POWVLSVIRRYVAHI SPS--ODELHVADNFPWGBDITLIFRAEGRVAVLITCNKLNANGLVQVNCEDCLFSAEITG--GHALRDGKATVSPKAVLKSRSVYTR--DELPSLSDS
 136 POWVAVNVRRYVAHI KTSBEGEDVFWDELVPWGBDITLIFVGLK--GNGVGEAFNG--GTFDQGLAGTANEDQVTFITFS--GHVLRDNNGHLVYDSGTRVLRSSVPLGTLK--ANTVFLDSDS

Domain 3

Human fascin-1
 Mouse Fascin-1
Xenopus fascin
 Human fascin-2
 Bovine fascin-2
 Human fascin-3
 Mouse fascin-3
Drosophila fascin
 Sea urchin fascin

260 CAQVVLCAVNERNSYTRQGDIDISANODEEDQETQLEIDRDTKCAFRPHTG---KWTLLATIGGGQSTAKSKNASCFIDIEWR--DRRTILASNGKFFV--KKNQGLAASVITAGLSEIDRKLIN
 260 CAQVVLCAVNERNSYTRQGDIDISANODEEDQETQLEIDRDTKCAFRPHTG---KWTLLATIGGGQSTAKSKNASCFIDIEWR--DRRTILASNGKFFV--KKNQGLAASVITAGLSEIDRKLIN
 251 CPQVVLCAVNERNSYTRQGDIDISANODEEDQETQLEIDRDTKCAFRPHTG---KWTLLATIGGGQSTAKSKNASCFIDIEWR--DRRTILASNGKFFV--KKNQGLAASVITAGLSEIDRKLIN
 258 HPQVVLCAVNERNSYTRQGDIDISANODEEDQETQLEIDRDTKCAFRPHTG---GWTLVTHGGIHTATAIQSANTVFMIEWR--GRRALASNGAVCKKNGQAAISSVFGKDEFFLKLIN
 258 HPQVVLCAVNERNSYTRQGDIDISANODEEDQETQLEIDRDTKCAFRPHTG---GWTLVTHGGIHTATAIQSANTVFMIEWR--GRRALASNGAVCKKNGQAAISSVFGKDEFFLKLIN
 262 PTWVLSKSKRRFLSVIYDAFCVABE LITQMSLEQEDSETPTLQFSANG---VMSQRHRVMDVHPVSDTFRHVN--CGRILASCEGAFGLAPSLVLANVLLPGRNEFFGLFAN
 262 PTWVLSKSKRRFLSVIYDAFCVABE LITQMSLEQEDSETPTLQFSANG---VMSQRHRVMDVHPVSDTFRHVN--CGRILASCEGAFGLAPSLVLANVLLPGRNEFFGLFAN
 274 LPQASFLGHRVYVYVGGVYVHANGDVEVNETQLEIDVNSAIDVHVRITQD---VYLAQRHRVHLDVHPVSDTFRHVN--CGRILASCEGAFGLAPSLVLANVLLPGRNEFFGLFAN
 258 CEGCAFEGCGYASIKQGEDVSKFLLVDEEDTEDTTQLETFEYETKVALVCDPKNKRDAVFWKTVAAQLQANGSKDQTDQFS--E--N--GNDVHVAIPGCKV--VRDNGHILFQDPS---KQVITFLIN

Domain 4

Human fascin-1
 Mouse Fascin-1
Xenopus fascin
 Human fascin-2
 Bovine fascin-2
 Human fascin-3
 Mouse fascin-3
Drosophila fascin
 Sea urchin fascin

383 RPTVLRGHEGFGR--VITGTDANRSDVDVDFBN--DGAANNVDSITGKVVWGSVMS--GTPVDFEFDFDYNVAVI--G--GVLVGDHAGL--ASABETDPA--SLVWY
 383 RPTVLRGHEGFGR--VITGTDANRSDVDVDFBN--DGAANNVDSITGKVVWGSVMS--GTPVDFEFDFDYNVAVI--G--GVLVGDHAGL--ASABETDPA--SLVWY
 374 RPTVLRGHEGFGR--MCTGDDNRSVDVDFBN--DGAANSKADATGKVVWGSVMS--CHPFSIFEFDFDYNVAVI--G--GVLVGDHAGL--ASABETDPA--SLVWY
 381 RPTVLRGLDFGVCHRR--G--SNQDITNRSVDVDFHLS--DGAANNVDSITGKVVWGSVMS--GTPVDFEFDFDYNVAVI--G--GVLVGDHAGL--ASABETDPA--SLVWY
 381 RPTVLRGLDFGVCHRR--G--SNQDITNRSVDVDFHLS--DGAANNVDSITGKVVWGSVMS--GTPVDFEFDFDYNVAVI--G--GVLVGDHAGL--ASABETDPA--SLVWY
 386 RFLVLRGKRYGVGSS--CHDLTQNDQDRHLDLPCRGTNHRQ--QGESWSTSTGCTFPGKFAINFCV--LQAGSSLLTLAPN--GFVYKRAVDSGHL--DADSDITRECVWE
 386 RFLVLRGKRYGVGSS--CHDLTQNDQDRHLDLPCRGTNHRQ--QGESWSTSTGCTFPGKFAINFCV--LQAGSSLLTLAPN--GFVYKRAVDSGHL--DADSDITRECVWE
 399 RPTVLRGLDFGVCHRR--G--SNQDITNRSVDVDFHLS--DGAANNVDSITGKVVWGSVMS--GTPVDFEFDFDYNVAVI--G--GVLVGDHAGL--ASABETDPA--SLVWY
 385 RFLVLRGLDFGVCHRR--G--SNQDITNRSVDVDFHLS--DGAANNVDSITGKVVWGSVMS--GTPVDFEFDFDYNVAVI--G--GVLVGDHAGL--ASABETDPA--SLVWY

Figure 5. Sequence alignment of fascin isoforms

Alignment of 9 cloned fascin proteins: human fascin1, mouse fascin1, *X. laevis* fascin1, human retinal fascin, bovine retinal fascin, sea urchin fascin, *D. melanogaster* singed protein, human testis fascin, and mouse testis fascin. The sequences are arranged by β -trefoil domain, as predicted based on the crystal structure of human fascin1 (1DFC). Color boxes denote conserved features: Black, conserved amino acids; Grey, conserved amino acid substitutions; red, protein kinase C-dependent phosphorylation sites; yellow, casein kinase II-dependent sites; blue, tyrosine kinase-dependent sites; pink, *D. melanogaster* singed protein which disrupt actin bundling activity.

Fascin structure

A crystal structure of recombinant human fascin at 2.9Å resolution reveals that fascin is a globular monomer that is folded into four β -trefoil motifs, each comprising six two-stranded β -hairpins (Fedorov et al., 1999; Protein Data Bank Accession number: 1DFC; Ponting and Russel, 2000). Since fascin is a monomer, it must contain at least two actin binding sites in order to cross-link filamentous actin. One site has been linked to residues 29-42, which is found within a highly conserved region (residues 11-50) between sequences of fascin from human, mouse and *Drosophila* (Kureishy et al., 2002). This region also contains a serine phosphorylation site, Ser39 (Yamakita et al., 1996; Ono et al., 1997). This phosphorylation site is followed by three lysine residues. If these basic amino acids do indeed interact with actin, phosphorylation at Ser39 could inhibit actin binding by creating a negative charge. The second putative ABS lies between residues 263 and 474, with Ser274 and Gly393 directly implicated in actin binding (Edwards, 1995; Cant et al., 1996). To date, there is no direct evidence that identifies the specific residues involved in fascin-actin binding.



Figure 6. Fascin structure and putative actin binding sites. (A.) Secondary structure of the four Beta-trefoil motifs. (B.) Two actin binding sites shown in red and green, with residues Ser39, Ser274, and Gly393 highlighted. Mutational analyses have shown that these residues disrupt actin binding and bundling.

Regulation of actin bundling

Actin-bundling is inhibited by Protein kinase C-alpha (PKC α) driven phosphorylation at serine 39 (Yamakita et al., 1996; Ono et al., 1997; Adams et al., 1999). The affinity of fascin for actin drops from $3.5\text{-}6.7 \times 10^6 \text{ M}^{-1}$ to $0.5\text{-}1.5 \times 10^6 \text{ M}^{-1}$ upon phosphorylation (Yamakita et al., 1996; Ono et al., 1997). Recently, mutational analysis has been used to study the regulation of fascin bundling in filopodia. The dephosphorylated form of fascin is mimicked by the mutation, S39A (Vignjevic et al., 2006). It localizes along the length of filopodia and induces an increase in both filopodia frequency (Vignjevic et al., 2006) and length (Yamashiro et al., 1998; Adams and Schwartz, 2000). In contrast, the phosphorylated form of fascin is mimicked by the mutation, S39E (Vignjevic et al., 2006). It yields weak localization along the length of filopodia and gives a 2.5-fold reduction in filopodia number (Vignjevic et al., 2006). Furthermore, the few S39E containing filopodia which do form are short-lived, suggesting that phospho-fascin, by itself, is insufficient at sustaining the architecture of filopodial bundles.

Fascin:actin stoichiometry in actin bundles

In vitro experiments revealed that spike-like bundles formed using fascin to actin ratios of 1:3 and 1:10, with saturation of bundling occurring at 1 fascin per 4.76 actin molecules (Bryan and Kane, 1978; Yamashiro-Matsumura and Matsumura, 1985). These studies were performed using a high concentration of fascin (2-9 μM). *In vitro* experiments using lower concentrations (0.45-1.8 μM) revealed that bundles frequently formed with fascin to actin ratios of 1:33 and 1:66 (Stokes and DeRosier, 1991). These bundles were poorly ordered, in contrast with the perfect hexagonal packing observed in the saturated bundles (Stokes and DeRosier, 1991). Instead, well-ordered bundles were observed with low fascin to actin ratios of 1:264 (Stokes and DeRosier, 1991). The challenge remains to determine the fascin to actin packing in filopodia.

The role of fascin in filopodia formation

Tight crosslinking of filamentous actin is necessary for the generation of stiff protruding filopodia (Svitkina et al., 2003; Vignjevic et al., 2003, Vignjevic et al., 2006). A mixture of Wiskott-Aldrich syndrome protein (WASP)-coated beads, actin, Arp2/3 complex and fascin was found to be the minimal requirement for assembly of parallel actin filaments *in vitro* (Vignjevic et al., 2003). These results were confirmed *in vivo* by a study that compared the ability of actin cross-linking proteins to form filopodia and implicated fascin as a major mediator for actin bundling in filopodia (Vignjevic et al., 2006). The same study determined that targeted depletion of fascin by SiRNA inhibits filopodia formation in B16F1 melanoma cells (Vignjevic et al., 2006). Reintroduction of fascin into those cells rescued filopodia formation, whereas other cross-linkers were unsuccessful or only partially able to form filopodia (Vignjevic et al., 2006).

Mechanical properties of fascin containing actin bundles

Several biophysical studies have investigated the ability of fascin to impart rigidity to *in vitro* actin bundles with the goal of understanding the mechanical properties of filopodia. Accordingly, the effect of cross-linking on the morphology of liposomes has been used to examine the rigidity of actin bundles. In large liposomes, polymerization of actin causes a morphological change from a spherical to a disc shape. Inclusion of fascin at ratios of 1 fascin per 16 actin resulted in the extension of straight, rigid projections from the surface of liposome discs. Neither alpha-actinin nor filamin triggered the formation of protrusions (Honda et al., 1999). Further studies using time-resolved rheometric measurements (measurements of flow and deformation) have been used to characterize viscoelastic properties of fascin containing actin-bundles (Tseng et al., 2001). They report that the formation of fascin-actin networks involves non-monotonic fluctuations in elasticity, and that such properties depend heavily on the concentration of fascin. In stark contrast, actin networks cross-linked with alpha-actinin display uniformly monotonic properties. Mixtures of fascin, alpha-actinin and actin formed networks that were more elastic

than the actin bundles formed by either cross-linking proteins, alone (Tseng et al., 2002). These data suggest that the sub cellular localization of different types of cross-linking proteins, or combinations of, may in part be determined by their ability to impart unique mechanical properties to actin bundles.

Role of fascin in cell adhesion and motility

The association of fascin with actin filaments is in part regulated by type of extracellular matrix (ECM) (Adams, 1997; Adams et al., 1999; Adams et al., 2000; Adams, 2002). Whereas some ECM components induce bundling of actin by fascin, others inhibit their interaction. For instance, cells plated on thrombospondin (TSP)-1, laminin, or tenascin-C display large arrays of fascin containing filopodia. In contrast, fully spread cells plated on vitronectin or collagen IV show diffuse distribution of fascin. Intriguingly, fascin-containing protrusions form transiently during initial cell spreading on fibronectin, but are subsequently lost when cells become fully spread (reviewed in Kureishy et al., 2002). The inhibition of actin bundling may be due to the regulation of fascin phosphorylation by ECM components (Adams et al, 1999).

In an effort to identify the mechanisms by which cell protrusions and contractile adhesions are coordinated to mediate either static or dynamic behavior, Parker et al. observed cultured cells plated on square ECM islands (Parker et al., 2002). The study reported that cells preferentially extended lamellipodia and fascin containing filopodia at the corner regions of the square islands, where cell-tractional forces were most heavily concentrated. Depletion of cell tension disrupted lamellipodial and filopodial extension. These results suggest a linkage between directional cell motility and mechanical interaction between cells and ECM and may explain different biological phenomena correlated with healthy development and disease.

Correlation to healthy development and disease

Wound Healing

During development and adulthood there are many morphological events that necessitate the sealing of multiple unobstructed epithelial edges to create a continuous epithelium. Recent wound healing assays have shown that when epidermal cells form intercellular contacts, filopodia penetrate and embed neighboring cells, which forces the cells to fuse together into a sheet (Vasioukhin and Fuchs, 2001; Jamora and Fuchs, 2002). The merging of wounded epithelial sheets involves the formation of many, long filopodia at the leading edge of the cells (Wood et al., 2002). These filopodia behave quite dynamic, sweeping laterally to sample the local environment and undergo cycles of extension and retraction at a rate of one micron per minute (Wood et al., 2002). At the final stages of wound closure, filopodia seem to regulate cell movement and recognition as they tug the cells close together, resembling stitching of the wound (Martin-Blanco and Knust, 2001; Wood et al., 2002).

Neurological disorders

Diseases of the Central Nervous System (CNS), which include senile dementia and Alzheimer's disease (AD), are characterized by pronounced cognitive impairment that usually manifests itself in the loss and decline of memory and intelligence. Memory is associated with structural modifications of the brain's neuronal network. Such changes have the potential to alter the number of neuronal synapses and their function in intercellular communication (Carey, 2002). Each synapse can undergo dynamic changes, potentially altering the efficiency of synaptic communication as well as the local architecture of the synaptic circuitry (Matus, 2000). The accuracy of the neuronal wiring along with the plasticity of synaptic networks represents the foundation of neuronal information processing and brain function (Wong and Wong, 2001).

One possible way in which brain tissue can respond to loss of neurons is by expanding dendrites and refining connections between neurons (Carey, 2002). A mechanism for facilitating synaptic communication is via rapid movement of dendritic filopodia (Wong and Wong, 2001; Sala, 2002; Yuste and Bonhoeffer, 2004). This movement involves extension, waving over long distances and retraction which are thought to regulate cell movement, cell-cell interaction and neuronal pathfinding (Yuste and Bonhoeffer, 2004). The regulation of actin bundling in filopodia by actin binding proteins plays an important role in characterizing growth cone behavior (Cohan et al., 2001). Fascin is highly expressed in growth cones (Cohan et al., 2001) and acts as the primary actin bundling protein necessary for generating filopodia (Svitkina et al., 2003; Vignjevic et al., 2006). The depletion of fascin results in inhibition of filopodia (Vignjevic et al., 2006), which is associated with growth cone collapse (Zhou and Cohan, 2001) and inaccurate pathfinding (Bentley and Toroian-Raymond, 1986).

Cancer metastasis

Cancer cells become metastatic by acquiring a motile, invasive phenotype. This process requires remodeling of the actin cytoskeleton and expression of exploratory, sensory organelles such as filopodia. Up-regulation of fascin promotes the formation of filopodia (Kureisy et al., 2002; Vignjevic et al., 2006) and could, therefore, be a significant component in the acquisition of invasive phenotypes in carcinoma (Hashimoto et al., 2005). Fascin is over expressed in many human cancers (summarized in Table 1) including breast, colon, and ovarian cancers (Hu et al., 2000; Grothey et al., 2000; Gonchurek et al., 2002; Jawhari et al., 2003; Pelosi et al., 2003a; Pelosi et al., 2003b; Hashimoto et al., 2006; Yoder et al., 2005). As an example, over 95% of invasive pancreatic tumors express high levels of fascin and up-regulation of fascin is very frequent in non-small cell lung carcinoma (Hashimoto et al., 2005). In addition to the high frequency of fascin expression in tumors, fascin expression mediates aggressive tumor metastasis (Yoder et al., 2005). For instance, high fascin staining has been observed at the margins of metastatic cancer cells, suggesting that cells at the boundary of tumors acquire a more motile and invasive phenotype than

cells in the center of the tumor (Wang et al., 2007). Furthermore, fascin expression is strongly correlated with poor patient prognosis and/or decreased disease-free survival in non-small lung cancer, esophageal, gastric, and breast carcinomas (Pelosi et al., 2003a; Hashimoto et al., 2005; Yoder et al., 2005). Therefore, current research emphasis is on studying fascin as a potential biomarker or therapeutic agent (Hashimoto et al., 2005). Understanding the mechanism for the formation of fascin-containing filopodia in cancer cells is vital to the progression of cancer research.

Fascin expression in human epithelia and carcinomas

Tissue	Normal epithelium	Carcinoma	Reference
Ampulla	N. D.	High focal or diffuse staining in 77% of carcinoma (n=56).	Van Heek et al. (2004)
Biliary duct	N. D.	Upregulated in 42% of CIS, 67% of invasive carcinomas (n=38)	Swierczynski et al. (2004)
Breast	N. D.	Positive in hormone receptor-negative tumors (n=58).	Grothey et al. (2000)
Colon	N. D.	High (n=10)	Jawhari et al. (2003)
Esophagus	Positive in basal layer	Increased (to>50% staining) in 95% of squamous cell carcinomas (n=200).	Hashimoto et al. (2005)
Lung	N. D.	High in NSCLC: 89% of tumors (n=220); Diffuse staining of tumor correlates with poor survival. Increased in the sarcomatoid component of pleomorphic lung carcinoma.	Pelosi et al. (2003)
Ovary	N. D.	High: focal or diffuse staining in borderline, primary and metastatic carcinomas (n=27). High in 18% of atypical proliferative mucinous tumors, 57% of primary carcinomas.	Hu et al. (2005)
Cervix	Weak	High fascin expression in 74% of neoplasms.	Kabukcuoglu et al. (2005)
Pancreas	Low/absent	Increased in 95% of 57 ductal adenocarcinoma (n=57). High: 97% of infiltrating adenocarcinomas (n=68)	Maitra et al. (2002)
Skin	Epidermal basal layer and outer root sheath and melanocytes are positive	High in locally-invasive areas of basal cell carcinoma, squamous cell carcinoma; Decreased in Merkel cell carcinoma and melanoma; Inverse correlation with metastatic potential of tumor type (n=78).	Goncharuk et al. (2002)
Stomach	N. D.	Increased in 25% of adenocarcinomas (n=214); Overall correlations with poor survival; Extent of tumor staining increased with depth of tumor invasion.	Hashimoto et al. (2004)

N.D.: Not Detectable, CIS: carcinoma in situ, NSCLC: non-small cell lung cancer

(table modified from Hashimoto et al., 2005)

Table 1: Fascin expression in normal epithelia and carcinoma

Chapter 2: Research results

General Overview

Filopodial turning, elongation, and retraction are key events involved in cell migration/neuronal pathfinding and require filopodia to be flexible enough to wave about yet rigid enough to protrude many microns past the cell surface. To identify the physical and molecular properties which underlie the reorganization of filopodia we must understand how actin filaments are cross-linked and how those cross-links are subsequently taken apart. Since fascin is the primary actin cross-linker in filopodia and is essential for filopodia formation (Vignjevic et al., 2006), we investigated features important to its function and dynamics. Specifically, we focused on questions regarding the initiation and elongation stages of filopodia formation as well as their maintenance and retraction: What is the origin of fascin in filopodia? How does fascin get delivered to tips of growing filopodia? How is it organized within actin bundles? How does that organization change over time and what implications does this reorganization of filaments have on filopodia dynamics and stiffness?

Filopodia are thought to form by a mechanism which involves the merging of filaments that elongate by polymerization of actin. Actin filaments that come in proximity to one another are cross-linked into unipolar parallel bundles to form mature filopodia (Svitkina et al., 2003; Vignjevic et al., 2006). There is, however, no established molecular mechanism that explains how fascin molecules are recruited to filopodia. One possibility is a higher affinity for actin filaments in filopodia than elsewhere in the cell. Activation by dephosphorylation is one way that has been reported to achieve this higher affinity (Ono et al., 1997; Yamakita et al., 1996; Adams et al., 1999; Vignjevic et al., 2006).

Cross-linking of actin filaments carries implications both for the elongation of filopodia and their response to mechanical stress. Cross-linking is presumed essential for filopodial protrusion as single actin filaments are insufficiently stiff to resist compressive forces (Mogilner and Rubinstein, 2005). Experimental support for this conclusion comes from observation of fascin-depleted filopodia which are typically bent and buckled under the cell membrane (Brieher et al., 2004; Vignjevic et al., 2006). It has

been established that elongation of filopodia is mediated by actin assembly at their tips (Mallavarapu and Mitchison, 1999). Presumably, a supply of fascin is also required to cross-link the newly polymerized actin. Otherwise, the nascent actin filaments would not be sufficiently rigid to support protrusion of the filopodium. To reach the growing (barbed) end of nascent actin filaments, fascin must be translocated from the cell body into the filopodium and out to the tip. However, when filopodia reach long lengths or elongate rapidly, diffusion, alone, may not be a sufficient mechanism for protein transport. What other mechanisms does the cell invoke to overcome the limitations of simple diffusion?

If filaments are physically attached to each other by cross-linking, how can they re-organize to relieve intra- and extra-cellular stresses without compromising structural integrity? Others have shown that dynamic interactions exist between α -actinin and actin filaments in stress fibers and that the dissociation rate of the cross-linker governs the mechanical properties of these bundles (Sato et al., 1987; Xu et al., 1998; Xu et al., 2000). We and others recently reported that fascin rapidly exchanges between filopodial actin filaments (Nakagawa et al., 2006; Vignjevic et al., 2006). The time-scale for fascin dissociation may provide clues as to how filopodia respond to mechanical stress which may have implications for the relationship of such response to cell morphology.

The purpose of this work is to advance our understanding of filopodia formation which currently lacks detailed information regarding the fascin-actin interaction and how that interaction influences the molecular organization, remodeling, and mechanical properties of filopodia during its dynamic lifecycle. Therefore, we undertook a quantitative, biophysical and kinetic analysis of fascin dynamics. We quantified kinetic rates for fascin turnover in filopodia and determined whether these rates are regulated or if they are intrinsic to the cross-linker. We probed the role of phosphorylation cycles in regulating the active pool of fascin available for actin cross-linking using phospho-mimetic fascin mutants. Finally, we examined the limitations of fascin transport by diffusion and developed a quantitative, computational model to analyze mechanisms for the delivery of cross-links to filopodial tips.

Localization of fascin in filopodia

A structure-based strategy and site-directed mutagenesis was used to identify potential actin binding sites (ABS) on fascin. The web-based software, Swisspdb viewer 3.7 (<http://ca.expasy.org/spdbv/>), provided a three-dimensional virtual model of fascin based on its crystal structure (protein data bank accession code: 1DFC). Using this model, we were able to identify amino-acid residues which were likely to be involved in actin binding. The phenylalanine residue at position 29 was implicated as a potential member of one possible ABS. This inference was based on the observation that F29 is solvent-exposed. Due to the hydrophobic nature of phenylalanine, it is probable that F29 is involved in intermolecular interactions, perhaps with actin. To test this idea, we constructed two mutants, F29A and F29E, which would potentially inhibit actin bundling and examined their localization in filopodia (Fig. 4). The mutant, F29A, was enriched toward the filpodial tip with weak staining along the length, similar to the pattern exhibited by S39E, the fascin phospho-mimetic mutant (Vignjevic et al., 2006). In contrast, the F29E mutant did not localize to filopodia at all. Instead, it was diffuse throughout the cell, which could have been a result of its inability to bind or bundle actin or protein misfolding. Extraction experiments, using phalloidin to stain actin, indicated no distinct change in the number and length of filopodia between cells transfected with wild type and fascin mutants, which implies that F29A and F29E are not dominant negative mutations. While filopodia can form by the action of endogenous fascin, our results indicate that mutations to F29 either precluded or dramatically weaken actin bundling. Tip localization of the F29A mutant may have resulted from interaction between the non-mutated domains and filopodial tip complex proteins.

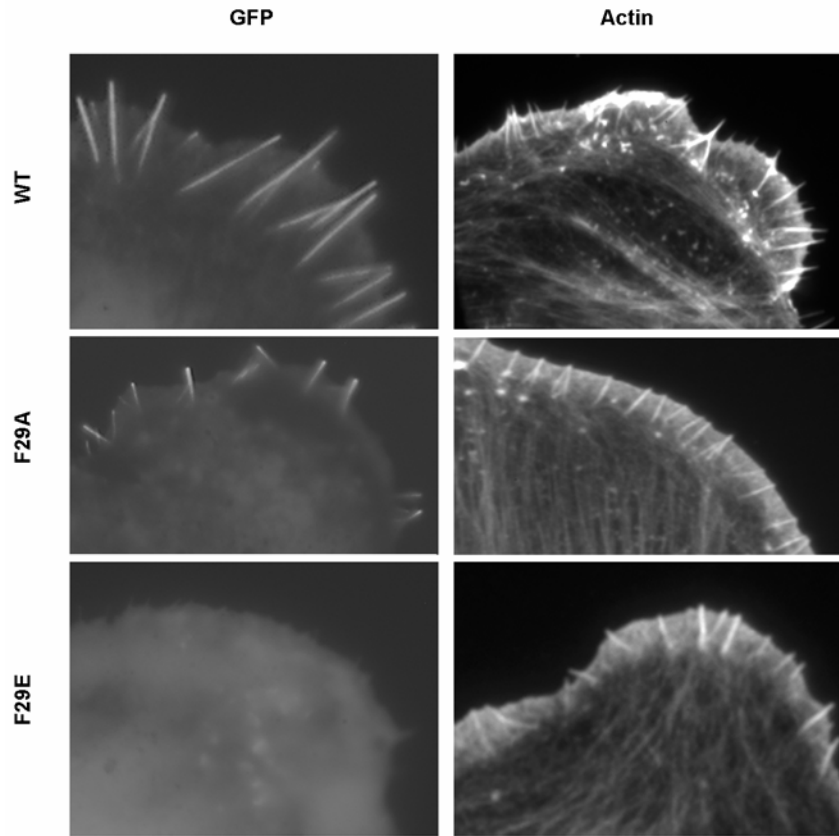


Figure 7: Localization of fascin in B16 melanoma cells. Distribution of (A.) wild type fascin, (B.) fascin-F29A and (C.) fascin-F29E in filopodia. The left column shows the localization of GFP-fascin wild type and mutants in B16 melanoma cells. Note that wild type fascin is distributed evenly along the length of filopodia while fascin-F29A is enriched at the tip, with weak expression along the shaft, and fascin-F29E is not recruited to filopodia at all. The right column shows the distribution of actin revealed by phalloidin staining in B16 cells expressing wild type and fascin mutants, respectively. No distinct differences in the number or length of filopodia were apparent between cells expressing wild type and fascin mutants.

Dynamics of fascin in filopodia

In live cells, fascin colocalizes with actin in filopodia (Vignjevic et al., 2006) with the exception of proximal regions of filopodial bundles where the amount of fascin with respect to actin is slightly lower (Cohan et al., 2001). Photo-activation and -bleaching studies have conclusively shown that actin is stably-bound along the length and over the life-time of filopodial filaments (Mallavarapu and Mitchison, 1999). Together, these data suggest a model for stable fascin association in filopodia. In the simplest version of this model, actin is bundled via fascin cross-links at the initiation site of filopodia formation and cross-links remain bound during filopodia elongation. Accordingly, Fluorescence Recovery After Photobleaching (FRAP) would reveal no significant recovery of either actin or fascin. Surprisingly, fluorescence recovery of GFP-WT fascin was rather rapid in filopodia, with half time of recovery $t_{1/2} = 8.6 \pm 1.2$ seconds ($n = 41$) in B16F1 cells and $t_{1/2} = 6.0 \pm 1.6$ seconds ($n = 24$) in Neuroblastoma 2a cells (Fig. 1A). In contrast and as expected, FRAP of GFP-actin in filopodia resulted in no detectable fluorescence recovery (Figs. 1B). Instead, bleached zones displayed retrograde flow, as previously shown (Mallavarapu and Mitchison, 1999). The time-scale for fascin exchange was consistent between phases of filopodial protrusion, retraction, and stationary periods. This result is consistent with findings in other cell types (Nakagawa et al., 2006), which indicates that the dynamic behavior is a conserved feature of the fascin protein.

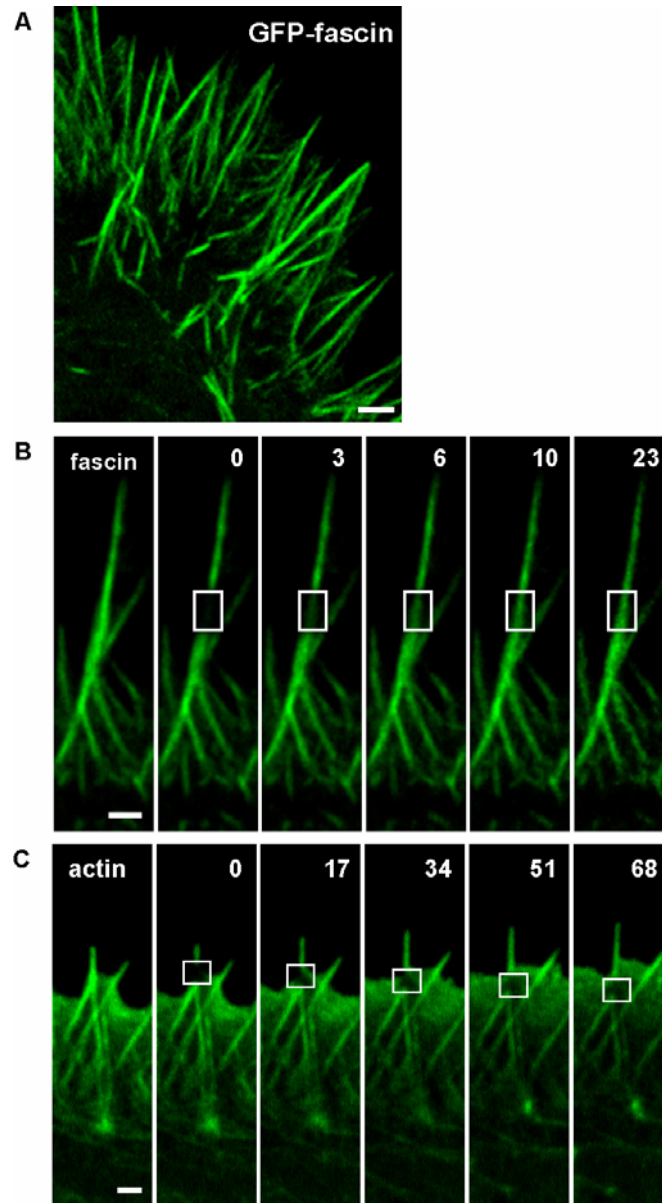


Figure 8. localization and dynamics of fascin and actin in filopodia. (A) GFP-fascin is enriched in filopodia of Neuro2a cells. (B) FRAP experiments reveal rapid recovery of fascin in filopodia, (C) but insignificant recovery of actin. Instead, actin undergoes retrograde flow. Time is given in seconds. Scale bar: 1 μ m.

Dynamics of T-fimbrin in filopodia

To determine whether dynamic cross-linking in filopodia is unique to fascin, we repeated photobleaching experiments on another actin bundling protein, T-fimbrin. We chose to examine this particular protein because, like fascin, T-fimbrin localizes throughout the length of filopodia in both B16F1 and Neuro2a cells (Fig.) and has the ability to rescue filopodia upon fascin knockdown (Vignjevic et al., 2006a; current study). Fluorescence recovery data revealed rapid exchange of GFP-T-fimbrin in filopodia (Fig.), with $t_{1/2} = 4.8 \pm 2.8$ seconds ($n = 15$). The similarity in recovery rates between fascin and T-fimbrin indicates that dynamic cross-linking proteins are common to filopodia and suggests that their localization and rapid turnover may be essential to filopodia remodeling and intimately connected to their physiologic function. In light of this finding, we further analyzed dynamic features of fascin in filopodia.

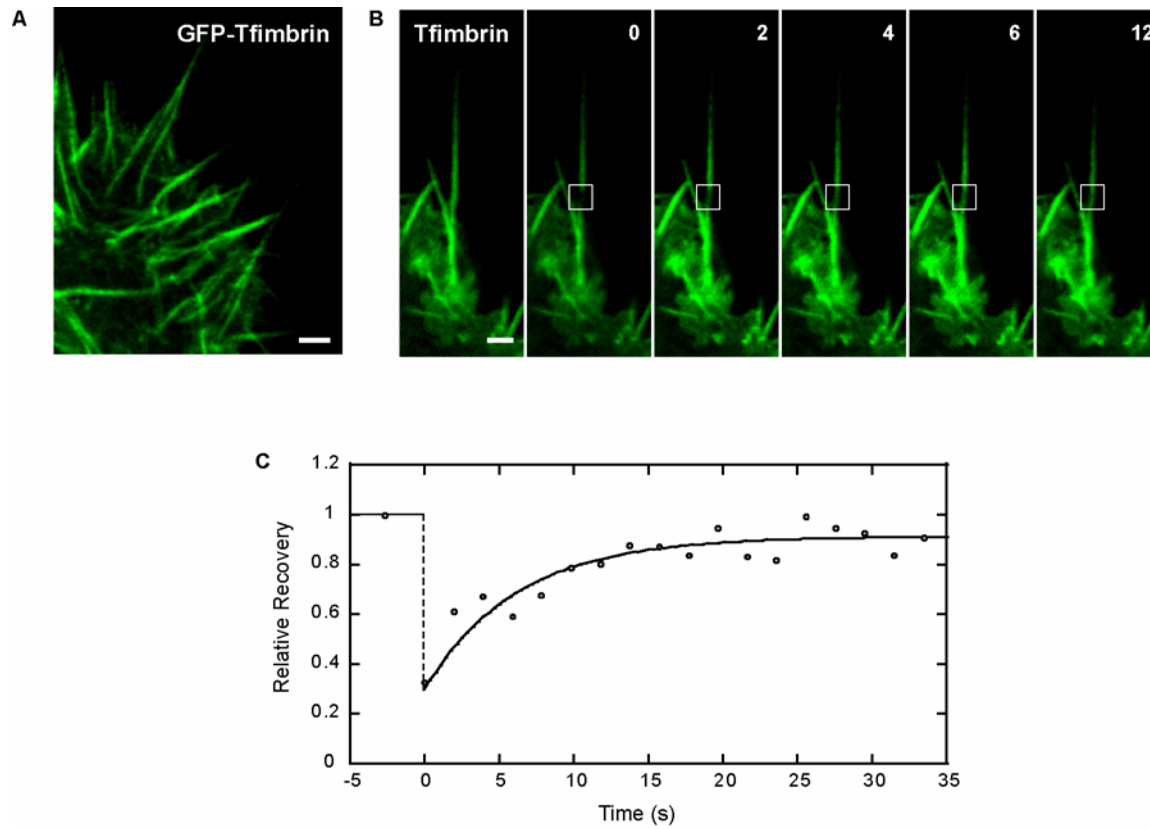


Figure 9. localization and dynamics of T-fimbrin. (A) GFP-Tfimbrin is enriched in filopodia of Neuro2a cells. (B) FRAP experiments reveal rapid recovery of T-fimbrin in filopodia. (C) Recovery profile reveals that the half time for T-fimbrin exchange in filopodia is approximately 5 seconds. Time is given in seconds. Scale bar: 1 μ m.

Fascin undergoes rapid local exchange in filopodia and simultaneous slow exchange with the cytoplasmic pool

Although our FRAP data demonstrates the existence of fascin exchange, by itself, it does not reveal the source of fascin turnover, specifically, whether the exchange is accomplished predominantly within the filopodium, with the cytoplasmic pool, or a combination of both. Assessing the source of fascin turnover requires the evaluation of recovery profiles as they provide information about the time-scale for protein exchange and the origin of that exchange. FRAP data were quantified by tracing the fluorescence intensity along bleached filopodia, normalizing for global loss of fluorescence during image acquisition along with pre-bleach intensity values, and plotted for varying times in the experiment (Fig. 2A). The trough in intensity at 0 seconds (thin grey line) corresponds to the region bleached in the experiment, while the nearly flat profile at 23 seconds (dashed black line) corresponds to the time when fluorescence had evenly redistributed within the filopodium. The average half time of this recovery was $t_{1/2} = 6.0 \pm 1.6$ seconds ($n = 24$). Although fluorescence within the filopodium became uniform by 23 seconds, it had not recovered to the pre-bleach level. Instead, it recovered to the average fluorescence at the post bleach time (0 seconds), indicating that little fascin exchange had occurred with the pool in the cell body (Fig. 1D, dotted line). Therefore, the initial recovery process predominantly represented a redistribution of fascin cross-links originally within the filopodium.

What is the significance of recovery that is uniform but to less than pre-bleach values? One possibility is that a fraction of the bleached molecules have been rendered immobile. Another possibility is the existence of a second, slower mode of recovery. Extending image acquisition to greater than 100 seconds showed essentially full restoration of pre-bleach fluorescence (Fig.2B). Since we could infer that the initial rapid recovery was predominantly due to intra-filopodial exchange, the secondary slow recovery process suggests two additional conclusions: first that essentially all the fascin has remained mobile and, second, that fascin in filopodial cross-links can exchange with the cytoplasmic pool of fascin.

FRAP experiments along the entire length of filopodia containing GFP-fascin revealed recovery times that matched those of the secondary recovery phase, confirming these conclusions (Supplemental Fig. 1).

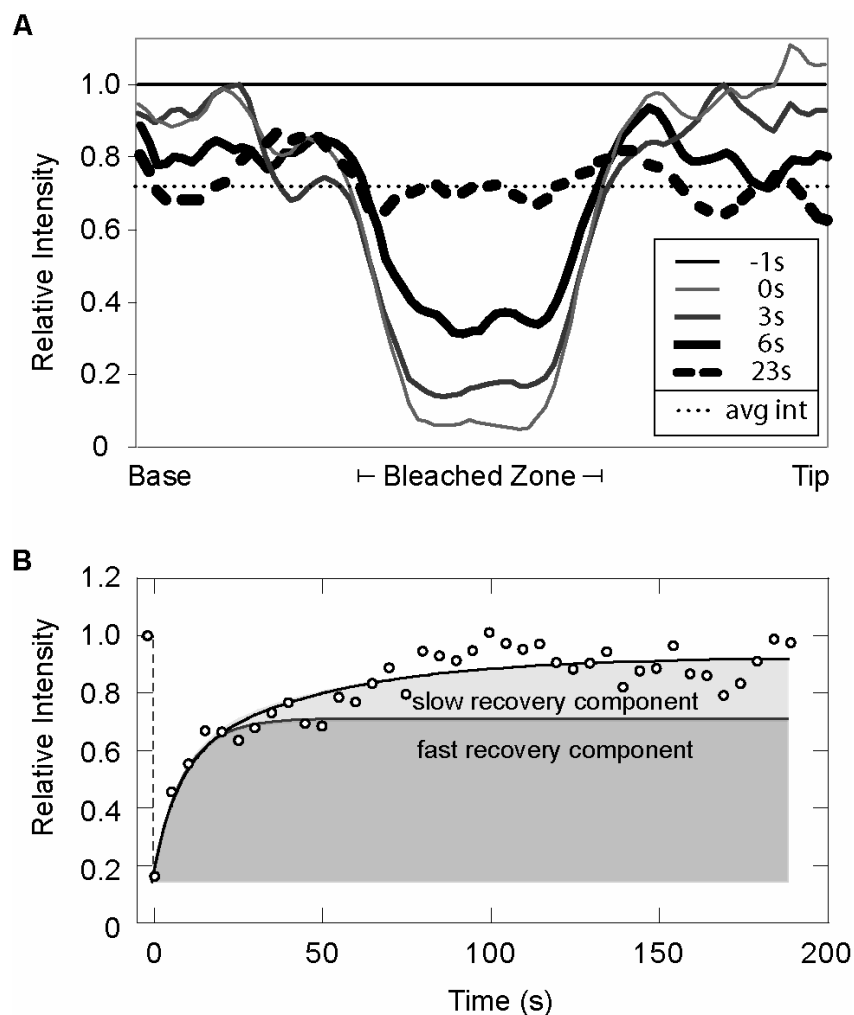


Figure 10. Fascin exchanges rapidly in filopodia.

(A) Recovery profile of bleached zone over time course of FRAP experiment. By 6 seconds, half of bleached cross-links have fully exchanged with neighboring molecules. The post-bleach average intensity along the filopodium matches the average intensity at the time when fluorescence has evenly distributed, or fascin has fully exchanged, suggesting that fascin turnover is primarily intra-filopodial on this time-scale. (B) At longer time-scales, the bleach zone recovers fully (to pre-bleach values), suggesting that filopodial-cytoplasmic exchange restores fluorescence to the pre-bleach intensity. The recovery profile is curve-fit with a double exponential function with a recovery constant for fast intra-filopodial exchange and a second recovery constant for slower filopodial-cytoplasmic exchange (see Materials and Methods). Fast and slow recovery components are shown in shaded regions, with the recovery profile for rapid intra-filopodial exchange separating the two.

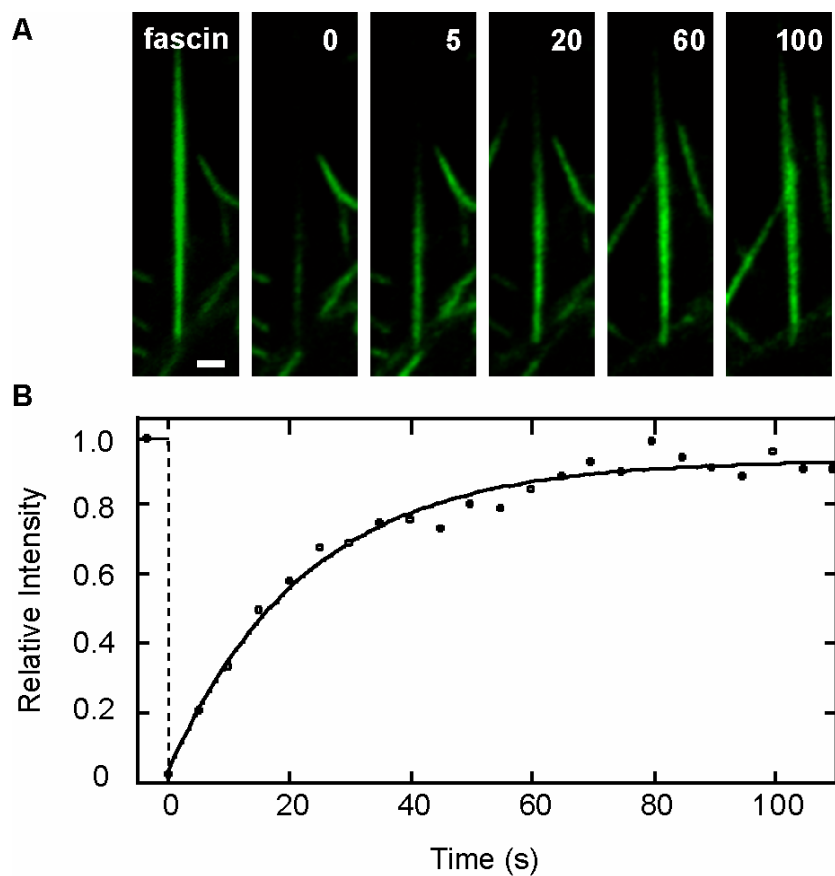


Figure 11. Recovery of GFP-fascin from the cell body into filopodia is relatively slow. (A) FRAP experiment on GFP-fascin in filopodia. Entire filopodia were bleached and monitored every 5 seconds for fluorescence recovery. Scale bar: 1 μm . Time given in seconds. (B) Average intensity of entire filopodium (normalized to pre-bleached state) plotted versus time and fit with a single exponential function. Recovery profile reveals fluorescence recovery to near pre-bleach intensity by 100 seconds, with $t_{1/2} \sim 20$ seconds, mimicking the slow recovery component between filopodial cross-links and the fascin pool from the cell body shown in Figure 10B.

FRAP data reveal kinetic off-rate of fascin in filopodia

What is the kinetic significance of the fast fascin recovery observed in the FRAP data? Is this recovery a measure of fascin association, dissociation, or a mixture of both events? Theoretical considerations indicate that in a simple binding reaction ($A + B \leftrightarrow AB$), recovery is exponential ($1 - \exp(-k_{off}t)$) and that the exponent k_{off} indicates the rate constant of dissociation from the complex (Appendix A; Sprague et al., 2004). On this basis, we calculate an off rate of $k_{off} = 0.12 \text{ s}^{-1}$.

We sought to confirm this value by independent Fluorescence Loss In Photobleaching (FLIP) experiments, which provided a more direct measure of the fascin dissociation rate constant in filopodia. Here, we repeatedly bleached a proximal domain of a filopodium containing GFP-fascin while monitoring the loss of fluorescence over time in a distal domain (Fig. 2A). Since the bleaching light was confined to the proximal domain, any loss of fluorescence in the distal domain was due to fascin molecules that dissociated from actin filaments in that domain and diffused into the proximal domain. If we assume that a fascin molecule typically diffused out of the distal zone before re-binding, the diminishing brightness of the distal domain was a direct indicator of the rate of fascin dissociation. The decay of fluorescence in the FLIP experiment was plotted versus time (Fig. 2B) and curve-fit using a single exponential function, $\exp(-k_{off}t)$, revealing an off rate, $k_{off} = 0.1 \text{ s}^{-1}$ ($n = 19$), corresponding to a half-time for fascin dissociation of ≈ 6 seconds. As expected, the half time for dissociation matches the half time of recovery from FRAP studies, shown by the complementary profiles of the curves plotted in Figure 2B, reinforcing the conclusion that fascin dissociates from actin filaments with $k_{off} = 0.12 \text{ s}^{-1}$.

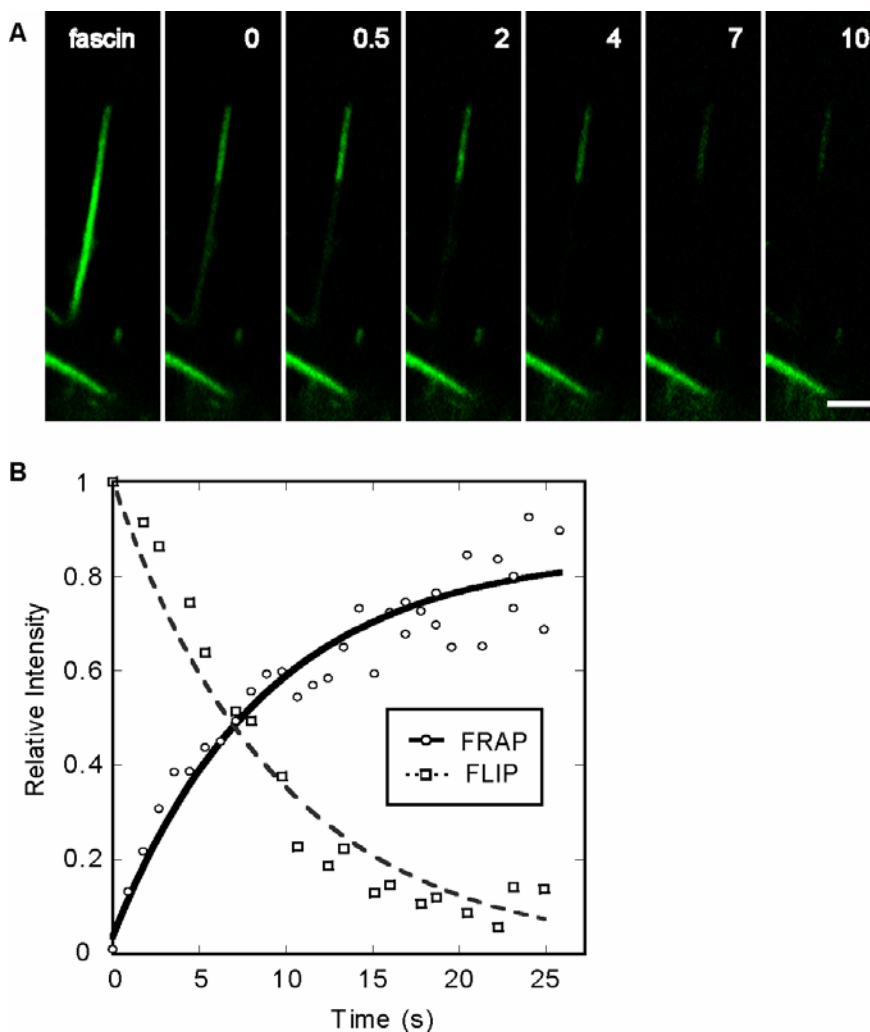


Figure 12. Kinetic analysis of fluorescence recovery of fascin in filopodia reveals k_{off} .

(A) FLIP of GFP-fascin in filopodia. Fluorescence decay near the tip represents exchange of GFP-fascin with bleached and endogenous cross-links. Scale bar: $1\mu\text{m}$. Time given in seconds. (B) Plot of relative intensity versus time in both FRAP and FLIP experiments on GFP-fascin in filopodia. Relative decay of fluorescence in FLIP experiment was curve fit with a single exponential function, $\exp(-k^{off} * t)$, and directly reveals a half-time of dissociation of 6 seconds. The corresponding FRAP curve shows a half-time of fluorescence recovery of 6 seconds as well. This half time also yields the dissociation rate of fascin from actin because, assuming that the total concentration of fascin remains unchanged in the filopodium over time, the recovered fluorescence is equal to the difference between the total amount of fascin and the amount that dissociated. Therefore, the FRAP data was curve fit with the function, $1 - \exp(-k^{off} * t)$, where $k_{off} = 0.12 \text{ s}^{-1}$.

Role of fascin phosphorylation in filopodia formation

Phosphorylation of fascin at serine 39 is important for its actin bundling activity *in vitro* (Ono et al., 1997; Yamakita et al., 1996) and proper localization *in vivo* (Adams et al., 1999; Vignjevic et al., 2006). These data suggest a model for the regulation of filopodial elongation. In the simplest version of this model, a pool of fascin is maintained in an inactive state by phosphorylation at serine 39. This inactive fascin is recruited to initiation sites of filopodia, where it is activated via dephosphorylation. Dephosphorylation induces a conformational change that allows for high affinity actin binding. Active fascin then crosslinks the new domains of actin filaments formed as filopodia elongate at their tips by incorporation of actin monomers. Breakdown of filopodia could occur by phosphorylation of fascin, followed by unbundling and depolymerization. In this model, phosphorylation could serve to regulate the dynamics and localization of fascin in filopodia.

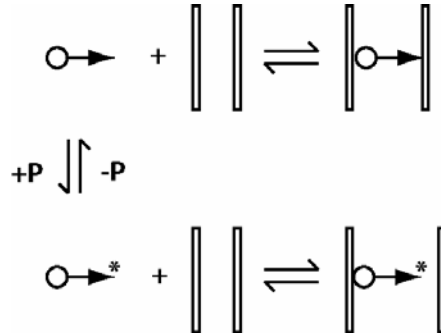


Figure 13. Model of phosphorylation-regulated fascin kinetics. Fascin cross-links actin filaments in its dephosphorylated (-P) state and weakly binds actin in its phosphorylated (+P) state.

The characteristic cycles of fascin association and dissociation are an intrinsic property of the fascin-actin interaction

To test the proposed model, we examined whether each cycle of fascin association and dissociation in filopodia is directly regulated, such as by enzymatic phosphorylation/dephosphorylation or by binding/dissociation of a G-protein, or if the ability to exchange is an intrinsic property of the fascin-actin interaction. To test for intrinsic fascin exchange in filopodia, we carried out FRAP experiments in reconstituted filopodia-like bundles composed strictly of purified fascin and actin proteins (Vignjevic et al., 2003), thereby excluding any proteins that potentially regulate fascin exchange. If the recovery behavior of fascin in purified bundles matched that in filopodia, then it would be evidence that fascin turnover is an intrinsic property of the cross-linker.

We tethered *in vitro* bundles to coverslips via a biotin-avidin interaction in a sealed perfusion chamber so that fluorescence recovery could be monitored over time (Fig. 3A). FRAP experiments revealed rapid fluorescence recovery of Alexa488-fascin (Fig. 3B, top panel). In contrast, fluorescence recovery of TMR-actin was negligible (Fig. 3B, bottom panel and Fig. 3C), confirming our *in vivo* result that fascin undergoes cycles of dissociation and association with actin. The recovery data was normalized for global bleaching and fit with a single exponential function as shown in Figure 3C. The half time of recovery for fascin *in vitro* is $t_{1/2} = 6 \pm 3$ seconds ($n = 28$), nearly identical to that found in filopodia (Fig. 3D). Because the time-scale for fascin exchange was recapitulated *in vitro*, we conclude that fascin exchange is an intrinsic property of the fascin-actin interaction and does not require assistance by an auxiliary molecule(s) for either binding or release from filopodial actin.

While the half-times for fast recovery were similar *in vitro* and in filopodia, *in vitro* fluorescence recovered fully to pre-bleach intensity levels within approximately 20 seconds, while full filopodial recovery required a slower component of exchange between the filopodium and cell body. The rapid full recovery *in vitro* was expected, as the bundles were surrounded by a large unbound pool of fascin that could undergo three-dimensional diffusion over shorter distances to unoccupied binding sites. In contrast,

full filopodial recovery required long-distance exchange with the cell body and diffusion through the more crowded filopodium.

Because such an intrinsic property precludes a multi-step association reaction (e.g., with a catalyst), we can use the value of a previously measured affinity constant ($K_A = 6.7 \mu\text{M}^{-1}$, Yamakita et al., 1996) and our measured k_{off} to calculate the kinetic on-rate, k_{on} , of the fascin-actin association reaction as follows: $k_{on} = K_A k_{off} = 0.8 \mu\text{M}^{-1}\text{s}^{-1}$.

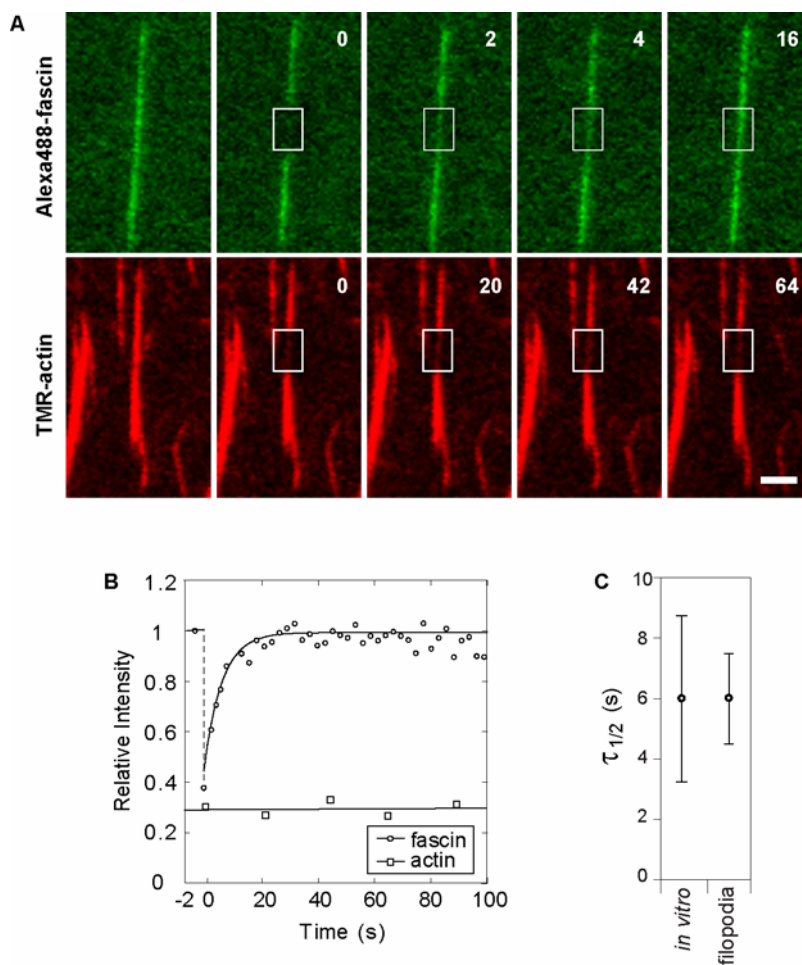


Figure 14. Fascin is dynamic in reconstituted filopodia-like bundles.

(A) Upper panel: photobleaching of Alexa488-fascin in reconstituted filopodia-like bundles reveals rapid recovery of fluorescence. Lower panel: photobleaching experiment on TMR-actin yields no fluorescence recovery. Bleached zone marked by boxes. Scale bar: 1 μm . Time given in seconds. (B) Recovery curves show intensity relative to pre-bleach value per time of the experiment for fascin and actin, with average half time of recovery for fascin of 6 seconds and recovery to pre-bleach level by 20 seconds. (C) Plots show the mean (circle) recovery half-times for FRAP experiments performed *in vitro* and *in vivo*, along with their respective 95% confidence intervals. The matching fast recovery kinetics for fascin in filopodia and reconstituted bundles reveal that dynamic exchange in filopodia is an intrinsic property of the fascin cross-linker.

Fascin-mediated actin bundling in filopodia requires that fascin be in the non-phosphorylated state

Several studies have shown that the formation and life-time of filopodia appear dependent upon the state of fascin phosphorylation; when activated by dephosphorylation, fascin yielded numerous, long-lived filopodia, whereas phospho-fascin yielded sparse, short lived filopodia (Yamakita et al., 1996; Adams, 1999; Anilkumar et al., 2003; Vignjevic et al., 2006). These observations suggest that phosphorylation limits the availability of fascin for actin bundling in filopodia. However, phosphorylated fascin is not excluded from filopodia (Vignjevic et al., 2006) and, therefore, its contribution to actin bundling needs to be tested. Here, we quantified and compared the preference for localization in filopodia and the turnover rates of fascin phospho-mimetic mutants to determine the extent of binding of phosphorylated fascin in filopodia.

To directly test whether the incorporation of fascin in filopodia was dependent on the phosphorylation state, we analyzed the fluorescence distribution of soluble GFP, GFP-tagged wild-type fascin, and GFP-tagged mutant fascin proteins that mimic the inactive phosphorylated (S39E) and active non-phosphorylated (S39A) states (Fig. 4A). Proteins were expressed in N2a cells (on a background of endogenous levels) because these cells generate many filopodia that are easy to study. We used confocal microscopy to obtain images of consistent optical depth so that measured intensities would indicate relative GFP concentrations, and we plotted the ratio of filopodial to lamellipodial fluorescence for each protein in Figure 4B. As a control for uniform optical depth, we first measured this ratio for GFP-expressing cells and found that $I_{fil}/I_{lam} = 0.9 \pm 0.1 \approx 1$ (n = 26), as expected for a uniformly soluble marker. Also as expected, wild-type GFP-fascin showed significantly greater preference for filopodia ($I_{fil}/I_{lam} = 7.4 \pm 1.0$, n = 27) than did diffuse GFP. While both mutants localized along filopodial shafts, the active S39A mutant showed strong preference for filopodia ($I_{fil}/I_{lam} = 10.0 \pm 2.9$, n = 27), while filopodia containing inactive S39E exhibited only marginal localization ($I_{fil}/I_{lam} = 1.3 \pm 0.1$, n = 27) and a

uniform diffuse fluorescence in the cytoplasm. The comparison of intensity distribution among fascin mutants implies that fascin incorporation in filopodia is strongly increased by fascin dephosphorylation.

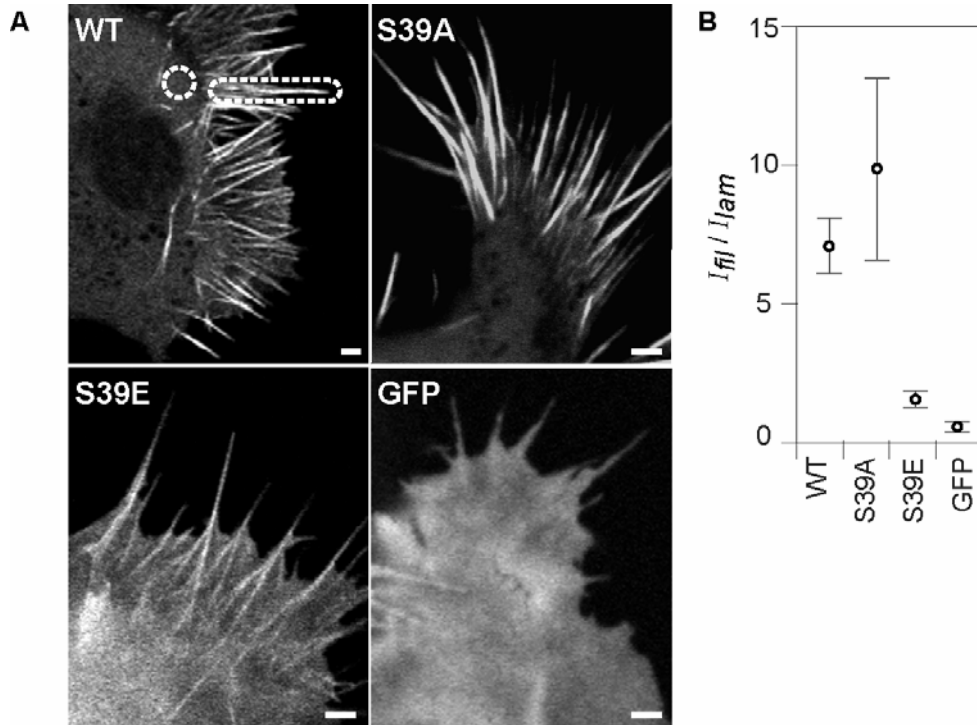


Figure 15. Localization of fascin mutants in filopodia.

(A) Fascin WT and phospho-mutant expression patterns in N2a cells. WT and S39A are enriched in filopodia while S39E shows weaker localization in filopodia. Soluble GFP localizes uniformly throughout cell. Scale bar: 1 μ m (B) The relative intensities of filopodia and cytoplasm for WT, S39A, and S39E fascin and those of soluble GFP, as measured in protruding filopodia and lamellipodia, indicated in dashed outlines of (A). Average relative intensity ratios, I_{fil}/I_{lam} , (circles) and 95% confidence intervals are similar and overlap for WT and S39A, while those for S39E and GFP are much lower and similar to each other, suggesting that S39E weakly localizes to filopodia.

The weak localization of phospho-fascin in filopodia suggests either limited access to, or low retention within, filopodia. We compared the mobility of fascin mutants using FRAP to test the dependence of fascin lifetime in filopodia on phosphorylation state. Filopodia containing GFP-tagged S39A mutant revealed recovery after photobleaching (Fig. 4C) with $t_{1/2} = 5.7 \pm 1.2$ seconds ($n = 34$) in B16F1 cells and $t_{1/2} = 6 \pm 2$ seconds ($n = 17$) in Neuro2a cells, which is nearly identical to that exhibited by the wild type fascin protein (Fig. 4E). These results suggest that the bound fascin cross-links in filopodia exist predominantly in the dephosphorylated state and that this feature is conserved among neuronal and non-neuronal cells. In contrast, the recovery profile for the GFP-tagged S39E mutant (Fig. 4D, left panels) closely resembled that of soluble GFP (Fig. 4D, right panels), with $t_{1/2} = 1.7 \pm 0.6$ seconds ($n = 13$) and $t_{1/2} = 0.5 \pm 0.2$ seconds ($n = 10$), respectively (Fig. 4E). Instead of revealing a distinct bleached zone, as in the wild-type and S39A FRAP experiments, the bleached zone and the region distal to it appeared to be generally non-fluorescent after photobleaching despite bleaching a zone of identical size ($1 \mu\text{m}^2$ area). We infer from the similar mobilities of GFP and the S39E mutant the neither appreciably bind actin. Instead, both GFP and S39E likely diffused into the bleached zone during the bleaching interval prior to redistributing into the distal domain of the filopodium, leaving the bleached zone and the region distal to it non-fluorescent.

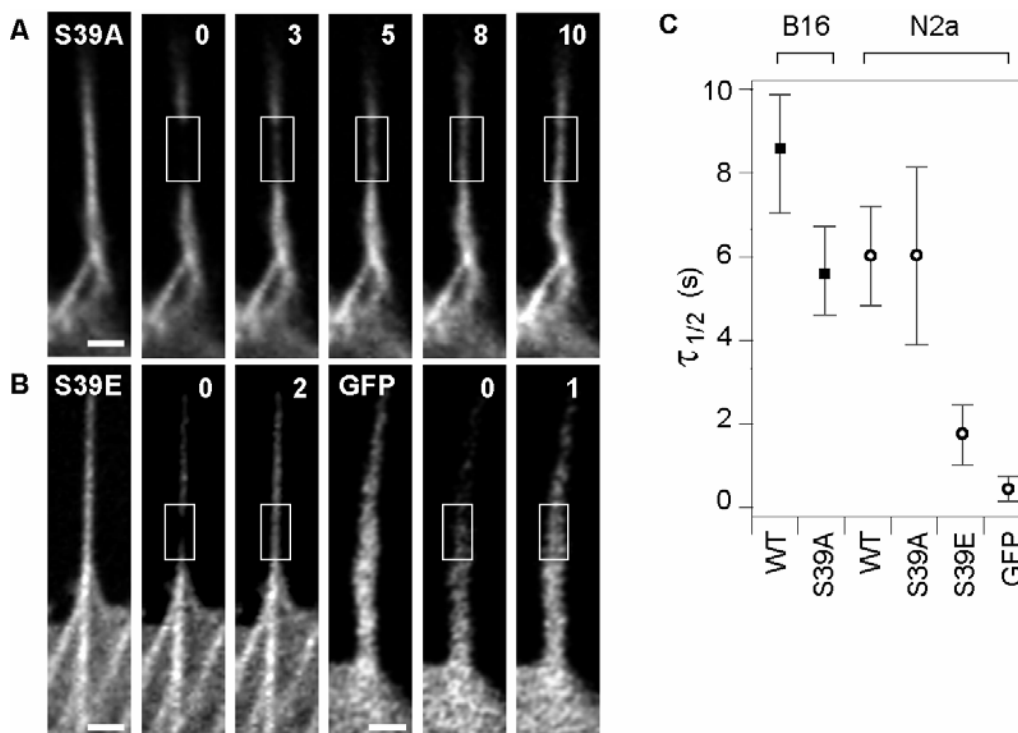


Figure 16. Dynamics of fascin mutants in filopodia.

FRAP experiments reveal recovery of (A) GFP-S39A fascin, (B) GFP-S39E fascin (left panels), and GFP (right panels) in filopodia. Scale bars: 1 μ m. Time given in seconds. While FRAP leaves a distinctly visible bleached zone in the S39A experiment, it leaves nearly the whole filopodium bleached in the S39E and GFP experiments even though the same size bleached zone was used to perform the bleaching experiments, suggesting that S39E undergoes a diffusion process similar to that of GFP in filopodia. (C) Plots show the distribution of half-times of recovery for fascin WT and mutants alongside GFP. While recovery of S39E and GFP occur in $t_{1/2} = 1.7 \pm 0.9$ seconds ($n = 13$) and $t_{1/2} = 0.5 \pm 0.3$ seconds ($n = 10$), respectively, the recovery is slower and similar for WT and S39A within and between N2a and B16 cells, with average $t_{1/2} = 6$ seconds, suggesting that filopodial filaments are primarily bundled by dephosphorylated fascin.

Fascin undergoes free diffusion in filopodia with a moderate diffusion coefficient, $D = 6 \mu\text{m}^2/\text{s}$

The tight packing of actin filaments and closely apposed plasma membrane of filopodia suggest an environment of limited diffusive mobility. We sought a measure of the diffusion coefficient of fascin in filopodia in order to understand the relative difficulty of movement compared to that in the cell body. Using experimentally-derived images of FRAP as inputs of filopodia cross-sections and initial and final protein concentrations, we simulated the recovery process of both GFP and GFP-S39E using a mathematical model of one-dimensional diffusion (Appendix A). Typical experimental recovery profiles and their simulation results are plotted versus time in Figure 5A. By matching the recovery half-times between experiment and simulation, we determined values of mean diffusion (D) coefficient for GFP and GFP-S39E of $7.5 \mu\text{m}^2/\text{s}$ and $5.1 \mu\text{m}^2/\text{s}$, respectively. Given the purely diffusive motion of soluble GFP, the Stokes-Einstein relationship predicts a diminished diffusion coefficient with increasing molecular weight: $D \propto M^{-1/3}$. We fit this relationship through the experimentally-determined diffusion coefficient of GFP, and plotted the experimental value for GFP-S39E on the same plot (Fig. 5B). The match between the experimentally-measured diffusion coefficient for GFP-S39E and the predicted value based on molecular weight confirms that the phospho-mimetic protein is not measurably slowed by actin binding or small network pore size in filopodia. Had the recovery process for GFP-S39E been significantly slowed by kinetics, the measured D value would have fallen below the curve.

The agreement between the experimentally-determined and predicted diffusion coefficients allows for the use of the Stokes-Einstein relationship to interpolate a free diffusion coefficient for native fascin in filopodia. Fascin's untagged molecular weight of 55kD corresponds to a diffusion coefficient of $D = 6 \mu\text{m}^2/\text{s}$ (Fig. 5B, discussion of effective diffusion in Appendix B). This value resembles the D value for GFP and, therefore, supports the conclusion that the FRAP recovery profiles used to calculate k_{off} were indeed kinetically-limited. It is also less than one-tenth the diffusion coefficient previously measured for

GFP in the cell body (Swaminathan, 1997), reflecting the increased rate of collisions with immobile proteins and/or the more tortuous paths within the tight filopodial network.

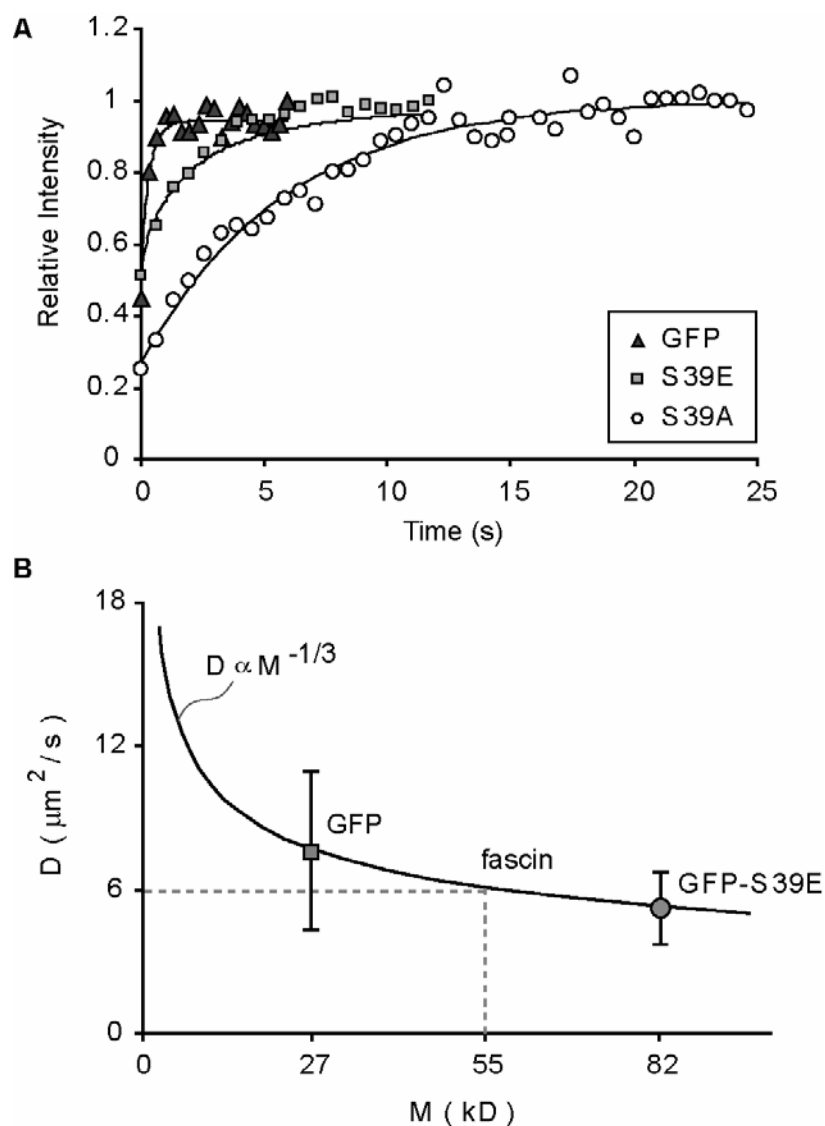


Figure 17. Phospho-fascin undergoes pure diffusion in filopodia.

(A) FRAP recovery curves for soluble GFP and fascin mutants, S39E and S39A (symbols). Simulations of recovery data (curves) yield diffusion coefficients for GFP and S39E. Recovery data with curve-fitting for S39A follows reaction-dominant process, plotted for comparison. (B) Median values of measured diffusion coefficients for GFP ($7.5 \mu\text{m}^2/\text{s}$, $n = 12$) and S39E ($5.1 \mu\text{m}^2/\text{s}$, $n = 14$) plotted versus molecular weight. Given a purely diffusive motion of GFP, the Stokes-Einstein relationship predicts a diminished diffusion coefficient with increasing molecular weight that matches S39E recovery data, suggesting the phospho-mimetic mutant is negligibly slowed by adhesion or small network pore size. This relationship allows for interpolation of diffusion coefficient for unlabeled fascin, yielding $D = 6 \mu\text{m}^2/\text{s}$.

Incorporation of fascin cross-links in filopodia

Individual actin filaments cannot impart sufficient stiffness to filopodia extended beyond the leading edge, but bundling by fascin allows for protrusion and maintenance of filopodia (Brierher et al., 2004; Mogilner and Rubinstein, 2005; Vignjevic et al., 2006). It is not known, however, what the fascin-to-actin ratio is in filopodia. Additionally, while our FRAP data reveal the existence of bound and free populations of fascin in filopodia, we do not know the fraction bound. We designed two approaches to calculate the relative fascin to actin concentration and solved for the ratio of bound to free fascin. Together, these relationships provide an estimate for the number of bound fascin molecules per actin in filopodia.

Filopodia contain one fascin cross-link per 25-60 actin monomers

To solve for the stoichiometry of fascin to actin in filopodia, we developed a two-part technique that involves quantitative immunoblotting and fluorescence ratiometry based on previously established methods (Zhai and Borisy, 1994; Wu and Pollard, 2005). Immunoblotting was employed to calculate the total number of fascin molecules in cells and fluorescence microscopy was performed to determine the proportion of cellular fascin molecules that localize to filopodia. The measurements were combined to calculate the number of fascin cross-links per actin residing in filopodia.

To determine the concentration of fascin in a cell, non-transfected cells were plated in a dish and counted by phase microscopy. Lysates of the counted cell population along with known amounts of pure fascin protein were loaded onto an SDS-PAGE gel and incubated with fascin antibody. The blot was visualized by chemilluminescence and shown in Figure 6A and Supplemental Figure 2. The intensity of the bands corresponding to amount of fascin in cell lysate and pure protein were quantified using NIH image software. We determined that B16 and N2a cells contain roughly 100-500nM (n = 20).

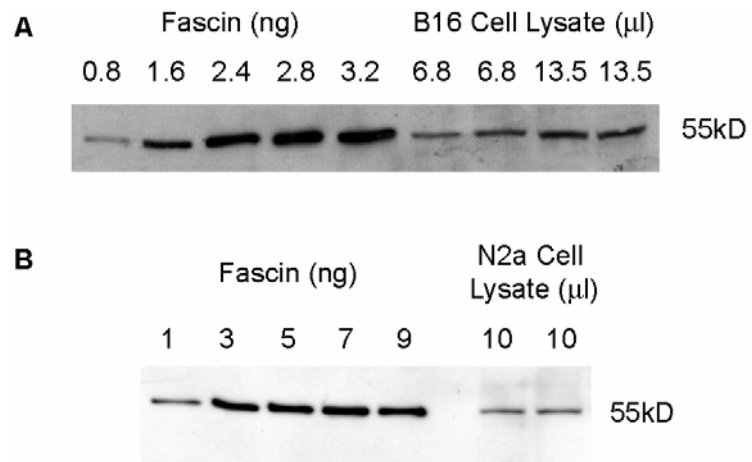


Figure 18. Western Blots reveal amount of fascin in cell lysates

Western Blots of (A) B16 and (B) N2a cell lysates (in duplicate) and varying amounts of pure fascin protein. Comparison of band intensity reveals that B16 cells typically contain 100-300 nM [fascin] while N2a cells typically contain 350-500 nM [fascin]. Appendix D reveals a calculation of fascin:actin ratio in filopodia based on estimates for fascin concentration.

Fluorescence ratiometry was used to determine the local concentration of fascin molecules in filopodia. Cells expressing GFP-fascin were imaged at varying expression levels in order to evaluate intensity variation in filopodial versus non-filopodial parts over a wide expression range. Figure 6B shows a typical epi-fluorescent image of a B16 cell expressing GFP-fascin with inset illustrated in Figure 6C. The solid line demarcates the perimeter of the cell, while the dotted line outlines the outer boundary of the cytoplasm. By assuming that intensity is proportional to protein concentration, the ratio of total fascin localized to filopodia was calculated by dividing the integrated intensity in filopodia by that of the entire cell; filopodia plus cytoplasm. The percent of fascin in filopodia was plotted versus average cell intensity for cells expressing GFP-fascin and fit with third order polynomial (Figure 6D, Supplemental Figure 2). The y-intercept of the fitted curve yields the percent of total cellular endogenous fascin crosslinks that localize to wild type filopodia to be about 10-30% (n = 118). Taken together, quantitative immunoblotting and fluorescence fractionation revealed that average filopodia contain one fascin crosslink per 25-60 actin monomers (calculation shown in Appendix D).

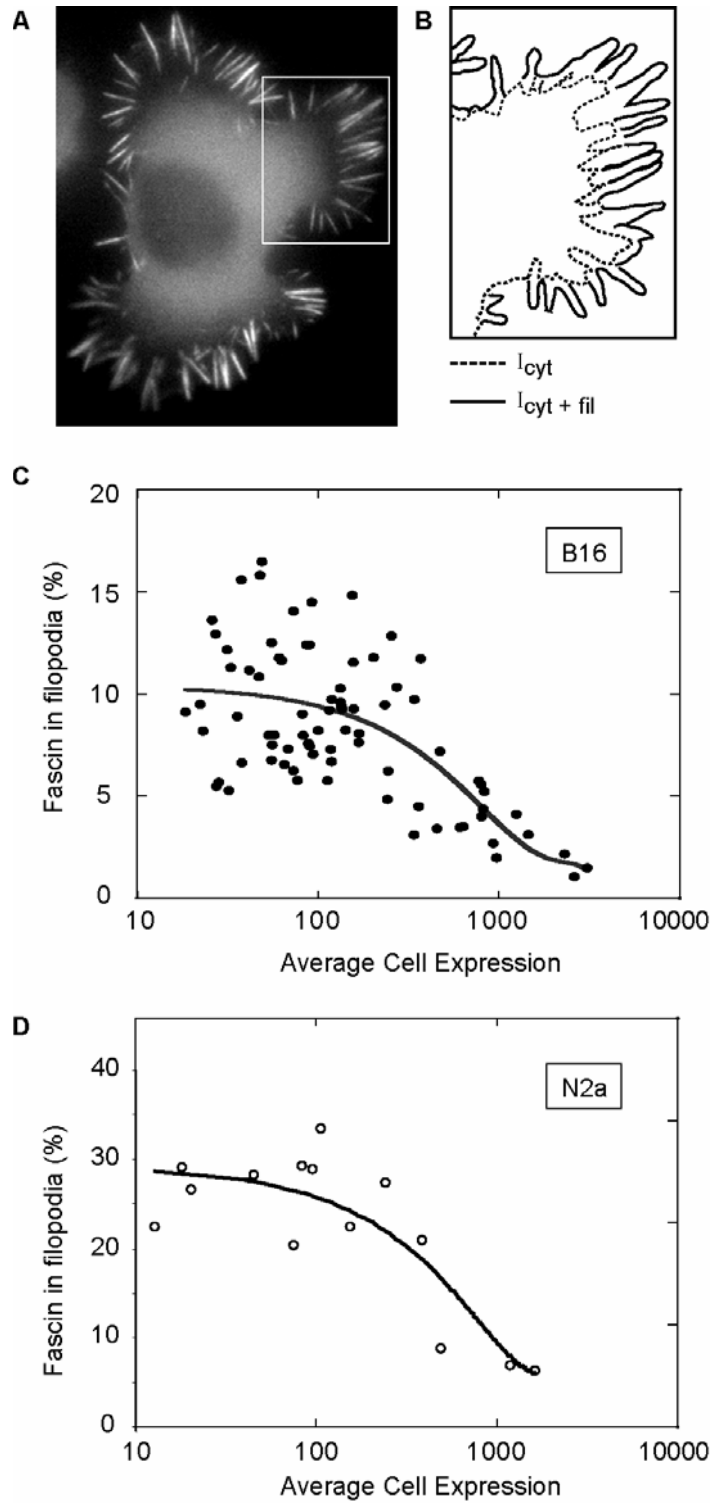


Figure 19. Percent fascin localized to filopodia

(A) Epi-fluorescent image of a B16 cell expressing GFP-fascin along with (B) schematic representation of inset. Peripheries of cell (solid) and cytoplasm (dashed) are outlined to indicate borders of integrated intensity measurements, where $I_{cyt + fil}$ is the total cell intensity and I_{fil} is the intensity of all filopodia in a cell. Percent fascin localized to filopodia was calculated using the expression, $(I_{cyt+fil} - I_{cyt}) / I_{cyt+fil} * 100$ and plotted versus average intensity in (C) B16 cells and (D) N2a cells for varying expression levels. The data was fit with a third order polynomial with y-intercept equal to the percentage of endogenous fascin that localizes to filopodia in wild type, non-expressing cells. Using this technique, we determined that approximately 11% of total fascin molecules in B16 cells localize to filopodia, or 11-33 nM [Fascin] reside in filopodia and about 29% of total fascin molecules in N2a cells localize to filopodia, or 100-145nM [fascin]. Comparison of fascin to actin concentrations in filopodia, we determined that B16 filopodia contain 1 fascin per 25-60 actin and that N2a filopodia contain 1 fascin per 27-41 actin.

Most fascin molecules in filopodia are bound at any instant

The stoichiometry of fascin to actin in filopodia determined above includes the total population of fascin molecules in filopodia; both bound and unbound fractions. Here, we used a fluorescence ratiometric technique to determine the proportion of fascin molecules that are bound. We examined the difference between intensity in filopodia and cytoplasm in confocal images of cells expressing GFP-fascin at varying expression levels. Confocal microscopy serves as an advantage to wide-field microscopy in that an image of the same optical depth is acquired. Therefore, intensity levels between different cellular structures, namely, filopodia and cytoplasm, can be directly compared. Figure 7A shows a representative confocal image of a B16 cell expressing GFP-fascin. Based on the assumption that the cytoplasmic pool in the cell body is unbound and that this concentration is uniform throughout the cell and filopodia, the per-pixel fluorescence intensity in the cell body (dashed circular region in Figure 7B) was taken as proportional to free fascin concentrations, while the fluorescence intensity in the filopodium (solid black outline in Figure 7B) was taken as proportional to the sum of bound and free fascin. The assumption that fascin is predominantly soluble in the cell body is supported by FRAP experiments in which rapid diffusion precluded any discernable bleached zone within lamellipodia or the cell body (data not shown). Dividing the fluorescence intensity in the cell body by the filopodial intensity therefore yields the proportion of unbound fascin population in the filopodium. Subtracting this value from one gives the proportion of bound fascin molecules in filopodia. We plotted the percentage of bound fascin molecules in filopodia against average intensity values in the cytoplasm of cells at varying expression levels (Fig. 7C and Supplemental Fig. 2C). To determine the percentage of bound fascin molecules in wild-type filopodia, we curve fit our data with a second order polynomial and extrapolated to zero cell intensity. The y-intercept of the curve revealed that, on average, 97% (B16 cells: $n_{\text{cells}} = 51$, $n_{\text{fil}} = 615$; N2a cells: $n_{\text{cells}} = 26$, $n_{\text{fil}} = 353$) of endogenous fascin molecules are bound in filopodia, with a range of 94-98%.

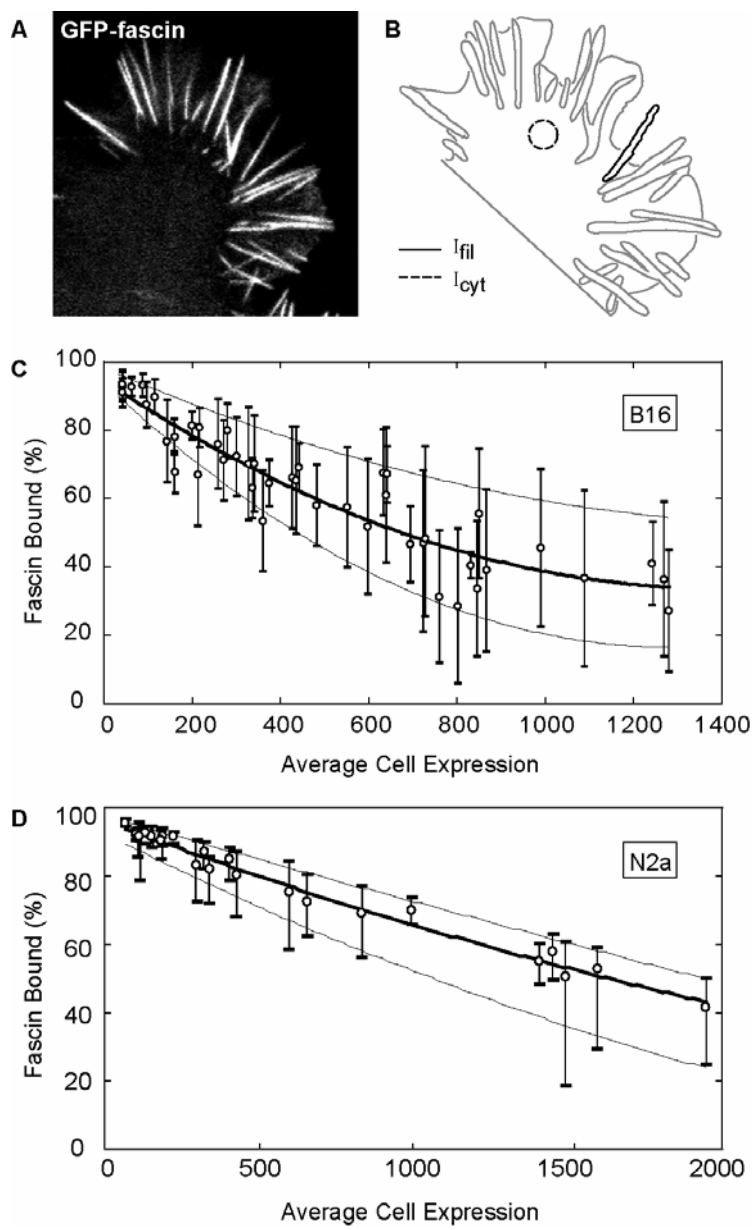


Figure 20. Percent fascin bound in filopodia.

(A) Confocal slice of a B16 cell expressing GFP-fascin along with (B) schematic representation of the same cell. Average intensities in filopodia (solid line) and cytoplasm (dashed circle) were measured. (C and D) Thus, the intensity in filopodia, I_{fil} , is proportional to total concentration of fascin, bound and unbound, while intensity in the lamellipodium, I_{cyt} , is proportional to amount of unbound fascin in filopodia. Percent fascin bound in filopodia of cells was calculated as $(1 - I_{cyt} / I_{fil}) * 100$ and plotted versus average cytoplasmic intensity over a range of expression levels. Both the range and mean values for percent fascin bound in filopodia were fit with a second order polynomial function, where the y-intercept yields the percent endogenous protein bound in filopodia of wild type, non-expressing cells. Using this method, we found that 94-98% of filopodial fascin is bound, with a mean value of 97%, independent on whether cells were non-neuronal or neuronal.

Dynamic fascin cross-linking allows for increased filament bundling at growing filopodial tips

Filopodial elongation requires actin assembly at their tips (Mallavarapu and Mitchison, 1999). Presumably, a supply of fascin is also required to cross-link the newly polymerized actin. Otherwise, the nascent actin filaments would not be sufficiently rigid to support protrusion of the filopodium. To reach the growing (barbed) end of nascent actin filaments, fascin must diffuse at a sufficient rate from the cell body over the entire length of the filopodium. Do binding reactions along the length preclude fascin delivery to the tips of long or rapidly-growing filopodia?

With the k_{on} and diffusion coefficient values reported in this study (Table 2), the average distance a fascin molecule diffuses before a binding reaction is $\approx 1.2 \mu\text{m}$. In filopodia significantly longer than this distance and with irreversible cross-links (i.e., $k_{off} = 0$), diffusing fascin would permanently fill binding spots nearest the base first, and an elongation rate that exceeds fascin supply would leave the tips very low in fascin (Fig. 8A). This rapid local transport but slow long-distance diffusion is the same phenomenon observed in the fast and slow recovery components of Fig 1. Diffusion with dynamic cross-linking ($k_{off} > 0$) might permit a sufficient supply rate to the tip region at longer lengths, however, by allowing dissociation of bound fascin and continued diffusion and re-distribution along the length of the filopodium.

Parameters	Value	Units
k_{off}	0.12	s^{-1}
k_{on}	0.8	$\mu M^{-1}/s$
D	6	$\mu m^2/s$
fascin:actin	1:25-60	
fascin (bound:free)	19-49:1	

Table 2: Parameters determined in this study

To quantify this predicted effect, we designed a numerical, 1D, reaction-diffusion model of filopodial elongation (Appendix A) and compared the ability of these two mechanisms to accommodate growth over a range of filopodial lengths. The value of k_{on} was kept constant at $0.8 \mu\text{M}^{-1}\text{s}^{-1}$ throughout all simulations, such that changing k_{off} was equivalent to changing K_A . Unoccupied binding sites at $[S] = 10 \mu\text{M}$ (Appendix A) were added to the tip of the model filopodium to simulate elongation rates of 1-4 $\mu\text{m}/\text{min}$, with typical rates of 2-3 $\mu\text{m}/\text{min}$ determined by subtracting the rate of actin retrograde flow from the rate of filopodial protrusion in FRAP data. A constant pool of free, active fascin $[F] = 0.1 \mu\text{M}$ was maintained at the base (cell body). Because growth extends unoccupied binding sites and k_{on} is finite, the extreme tip itself was always theoretically devoid of bound fascin. Accordingly, we compared concentrations of occupied binding sites, $[FS]$, at a position $0.5 \mu\text{m}$ from the filopodial tip. Plots could have alternatively been made of the bound fascin-to-actin ratio ($[FS]/([S]+[FS])$), but these curves would be of identical shape since the total binding site concentration ($[S]+[FS]$) is proportional to the actin concentration and remains constant along the length.

As expected, the advantage of fascin dissociation increased with filopodial length at typical rates of elongation. With irreversible cross-links, the profile of bound fascin concentration fell sharply toward the tip of 3 μm long filopodia (Fig. 8B, black curve). With dynamic cross-linking, the concentration of occupied sites near the base decreased due to a lower equilibrium (i.e., maximum) value, but increased by a factor of 1.5 near the tip (Fig. 8B, grey curve). When filopodia continued to grow to 10 μm , a markedly sigmoidal concentration profile indicated low fascin transport to the tip when $k_{off} = 0 \text{ s}^{-1}$, but a 100-fold increase in bound fascin concentration was observed with $k_{off} = 0.12 \text{ s}^{-1}$. Thus, a process which involves diffusion and rapid, irreversible association can supply fascin only to short filopodia, but dynamic cross-linking was required to sustain longer filopodia.

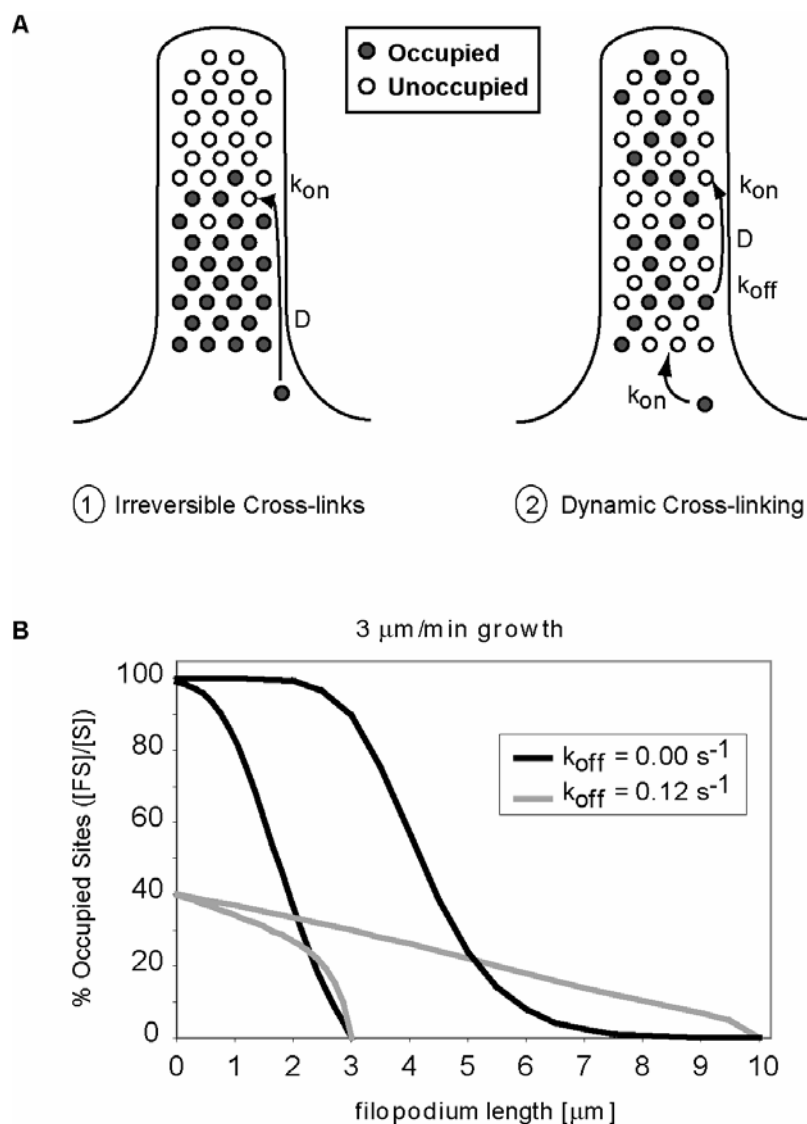


Figure 21. Effective fascin transport to tips of growing filopodia require dynamic cross-linking

(A) A numerical model was developed to compare the suitability of fascin delivery to tips of growing filopodia via diffusion with (1) irreversible cross-linking, and (2) dynamic cross-linking via dissociation. (B) Under mechanism 1, cross-linkers diffuse toward barbed-ends and attach permanently near the first available binding site ($k_{\text{off}} = 0$) precluding delivery to the growing tips of moderate or long filopodia (black curves). In mechanism 2, fascin dissociation allows for cross-links to contribute farther along the filopodial length and near the tips (gray curves).

Is there an optimal off-rate for delivery of fascin to filopodial tips? Figure 8C plots the concentrations of bound fascin $[FS]$ near the tips of growing, 3 μm filopodia as a function of k_{off} . Consistent with Figure 8B, tip concentrations initially increased with k_{off} . At higher k_{off} , however, concentrations decreased due to a diminishing equilibrium bound fascin concentration. The peaks in the curves represent an optimal value of k_{off} for maximum bound fascin concentration near the tips of growing filopodia. Our measured off-rate compares well with the range of dissociation rates, 0.05-0.25 s^{-1} , that are optimal for filopodia growing at rates of 1 to 4 $\mu\text{m}/\text{min}$.

Figure 8D plots the optimal k_{off} as a function of length for several growth velocities. At growth rates of 2 $\mu\text{m}/\text{min}$ and lengths of 3 μm , our measured value of $k_{off} = 0.12 \text{ s}^{-1}$ provides the highest bound fascin concentration near the tip. At 3 $\mu\text{m}/\text{min}$ filopodial growth rate, k_{off} is optimized for short, 0.8 μm filopodia. At slow growth rates of 1 $\mu\text{m}/\text{min}$, bound fascin concentrations near the tip would be higher with a decreased k_{off} at any length. Thus, the k_{off} measured in this study appears to be a good compromise among lengths to generate the highest tip concentrations of bound fascin at typical growth rates.

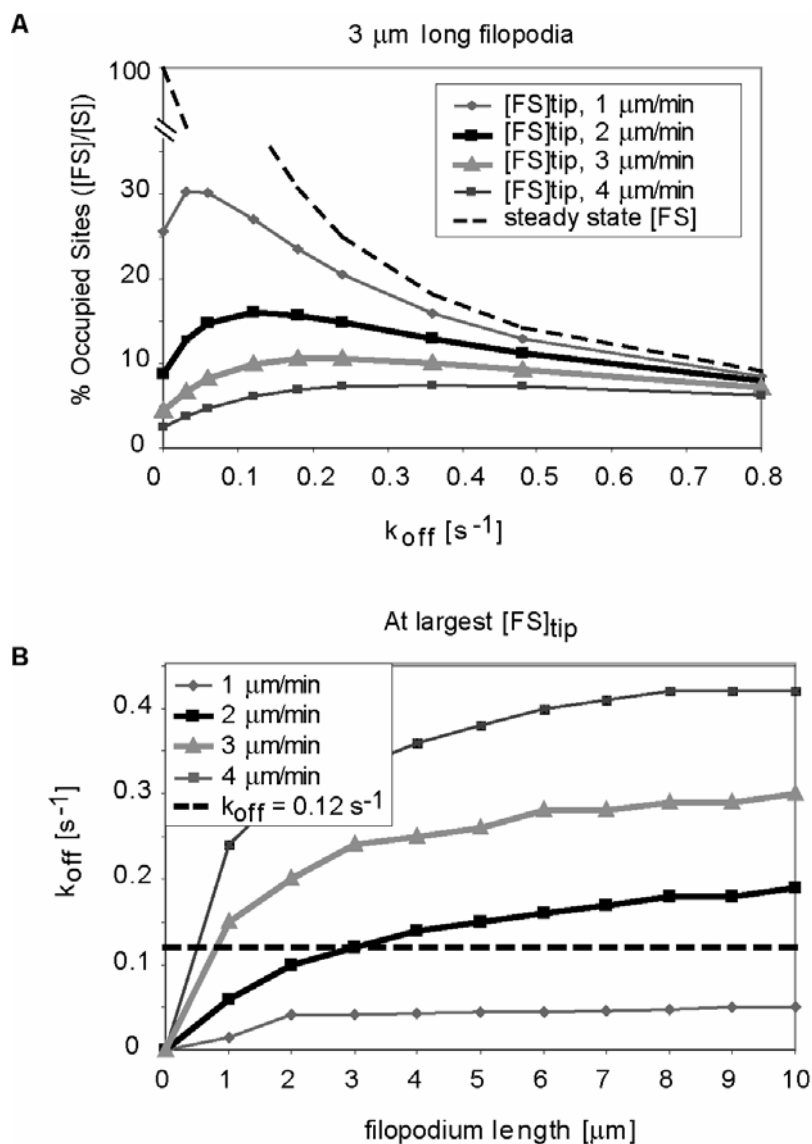


Figure 22. Optimal conditions for filopodial elongation

(A) The percentage of occupied binding sites near the tips of 3 μm filopodia was plotted against fasciin dissociation rate constants for growth rates of 1 to 4 $\mu\text{m}/\text{min}$. The curves reveal an increase in fasciin-actin complex concentration, $[FS]$, near tips for low rate constants, as well as a decrease at high rates due to a diminishing steady state bound concentration (dashed curve). The peaks in the curves reflect optimal off rates for given conditions. (D) A plot of the optimal off-rate for various lengths and growth speeds show that a value of $k_{\text{off}} = 0.12 \text{ s}^{-1}$ is optimal for 3 μm long filopodia growing at 2 $\mu\text{m}/\text{min}$.

Chapter 3: Discussion

Filopodia are highly dynamic cellular protrusions that require precise mechanisms for recruitment, maintenance, and turnover of their molecular components. In this study, we showed that filament bundling in filopodia requires fascin dephosphorylation, that instantaneous fascin cycling between filaments optimizes filopodial growth conditions, and that, on average, filopodia contain fascin:actin ratios of 1:25-60. Here, we explore the implications of these results on mechanisms for filopodia formation, assembly, and physical properties.

Targeting of fascin to filopodial tips

As a potent actin filament cross-linker, expressed fascin is capable of associating with actin filaments throughout a cell. Yet, it specifically localizes to filopodia, but not, for example, to stress fibers. This targeting specificity was also displayed by the constitutively active S39A fascin (Vignjevic et al., 2006) suggesting that dephosphorylation and phosphorylation of fascin are not necessary for regulating its specific targeting. One possible mechanism of fascin targeting to filopodia is that it specifically recognizes closely opposed parallel actin filaments. During normal filopodia formation, accumulation of closely spaced parallel filaments at the tips of Λ -precursors may serve as a site for fascin recruitment. Additional mechanisms may contribute to fascin exclusion from other bundles, for example, through competition with tropomyosin (DesMarais et al., 2002; Ishikawa et al., 1998).

Even if parallel aligned filaments are sufficient to recruit fascin, our localization data of the F29A and S39E mutants suggest an additional mechanism that coordinates filament elongation and bundling in growing filopodia in B16F1 cells. In the case of both mutants, the same putative ABS underwent site-directed mutagenesis while the other ABS was left untouched, presumably free to associate with actin, albeit weak. Despite this, both F29A and S39E were enriched at filopodial tips, suggesting a recruitment mechanism independent of actin bundling. Svitkina et al., 2003 showed that filopodial tips are associated

with a large protein complex. The composition of the tip complex is poorly characterized, but some components are known, including Ena/VASP proteins (Lanier et al., 1999; Rottner et al., 1999), myosin X (Berg and Cheney, 2002), Vav 1 (Kranewitter et al., 2001), Abi (Stradal et al., 2001), formins (Pellegrin and Mellor, 2005; Peng et al., 2003; Schirenbeck et al., 2005). Some of these or unknown component(s) of the filopodial tip complex might be responsible for recruiting fascin to filopodial tips. Interestingly, it was shown that neurotrophin receptor p75 specifically binds fascin in human melanoma cells (Shonukan et al., 2003) and thus is a candidate for recruiting fascin to the membrane. However, it is not known whether this protein is specifically enriched at filopodial tips. Another possibility for fascin targeting to filopodial tips is that fascin could preferably bind ATP-actin near the growing barbed ends. Concentration of fascin at the filopodia tips, which may also be coupled to activation by dephosphorylation, would enhance the availability of the cross-linker for actin bundling.

Advantages of dynamic cross-linking in filopodia

An important and unexpected finding in this work comes from the FRAP experiments, which demonstrate that fascin in filopodial bundles undergoes frequent cycles of association and dissociation rather than remaining stably bound to actin filaments. Importantly, fast dynamics was also observed *in vitro* and for the constitutively active S39A mutant, suggesting that fast fascin turnover is not coupled to cycles of phosphorylation and dephosphorylation. Such behavior of active dephosphorylated fascin may seem counterintuitive if one assumes that rapid dynamics is not consistent with the rigidity of actin bundles. However, a high dissociation rate does not necessarily imply a weak binding affinity. If the association constant is fast as well, the affinity can be sufficiently strong. Also, actin filaments in filopodia are very densely packed (1 fascin cross-link per 25-60 actin) and many fascin molecules participate in the formation of actin bundles.

What are the advantages of dynamic cross-links over stable ones? We showed that dynamic binding would enhance the availability of fascin molecules to cross-link newly polymerized actin

filaments at filopodial tips by decreasing the diffusion distance. This ensures timely filament bundling during filopodia elongation. If fascin was stably bound to actin filaments in filopodia and released only with filament disassembly at the rear, free fascin would need to diffuse through the whole filopodial length, on the order of micrometers, to reach sites of growth. Furthermore, the energy required to break an actin-fascin bond would be costly in comparison. Another possible advantage of dynamic cross-links is to allow for the transport of other molecules. For instance, myosin X is proposed to deliver its cargo towards the tip of filopodia (Berg and Cheney, 2002). The local de-bundling and re-bundling may transiently generate space for passage of such cargos. Finally, local stresses that are generated within filopodial bundles during motility, such as uneven tension, torque, bends, etc., can be more easily relieved by dynamic cross-links. Altogether, dynamic association/dissociation cycles of fascin may be advantageous for rapid growth and integrity of filopodia.

Fascin phosphorylation acts as a molecular switch for filopodia formation

Cells have the capacity to form filopodia in response to a variety of signals that arise from environmental cues, particular substrates, or other cells. Such a capacity implies the existence of a regulatory mechanism. In this work, we tested phosphorylation/dephosphorylation cycles in regulating key events in filopodia. Because fascin phosphorylation has been reported to inhibit actin bundling (Ono et al., 1997; Yamakita et al., 1996; Adams et al., 1999), we suspected that the role of these cycles may be to regulate fascin exchange in filopodia and to limit concentrations of fascin available for actin cross-linking. Unexpectedly, we found that the time-scale for fascin dissociation in reconstituted filopodial bundles mimicked those in filopodia, indicating that the dynamic exchange does not require an enzymatic reaction, but is an intrinsic property of the fascin cross-linker. On the other hand, photobleaching data on fascin phospho-mutants revealed that phosphorylation alters the mobility of fascin in filopodia. While the non-phosphorylated fascin mutant imitated wild-type kinetic reactions in filopodia, the phospho-fascin mutant underwent a predominantly diffusive process. The phospho-mimetic mutant, S39E, contains one

active binding site and one that is inactivated by a single-site mutation. While the non-mutated binding site is presumably free to associate with actin, it is likely that, without the cooperation of the other binding site, fascin does not undergo appreciable binding to filaments. Therefore, only the non-phosphorylated form appears to participate in filament cross-linking, while the purpose of fascin phosphorylation is likely to limit the size of that pool. On basis of our results, we propose that phosphorylation/dephosphorylation cycles serve as a molecular switch to turn fascin activity on or off, which in so doing determines whether or not filopodia form.

In summary, we propose a model for the formation and maintenance of filopodia (Fig. 9). In our model, activation of fascin by dephosphorylation allows for high affinity actin binding in filopodia. Actin cross-linking provides filopodia with the rigidity necessary for protrusion, while intrinsic fascin exchange between filaments allows for elongation and filopodial remodeling. Fascin inactivation by phosphorylation decreases the availability of fascin to bundle actin, which in turn inhibits filopodia formation.

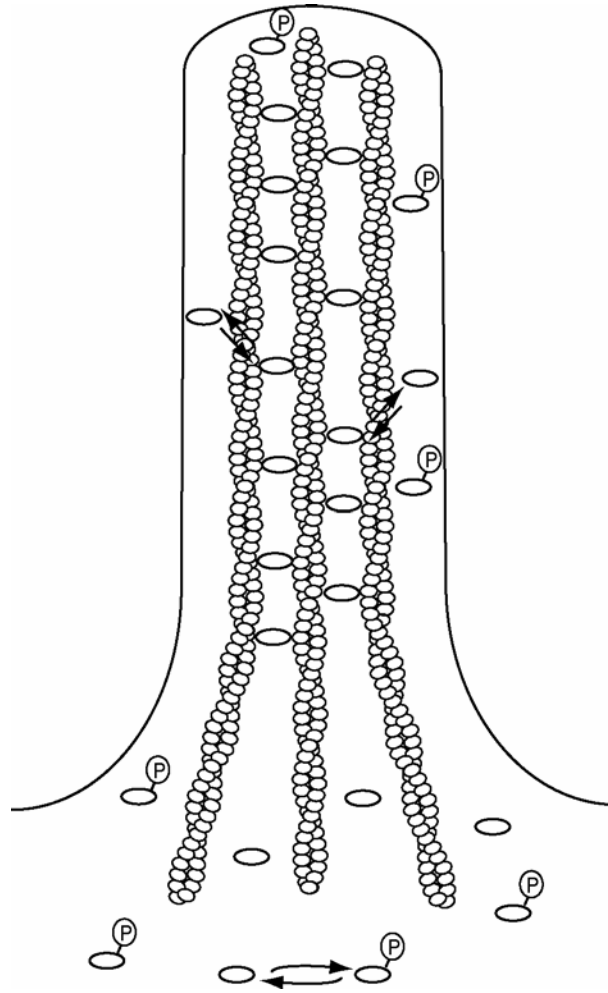


Figure 23. Illustrative model of fascin dynamics and organization in filopodia.

Fascin is activated by dephosphorylation, which allows for high-affinity interaction with actin filaments in filopodia. Active fascin undergoes intrinsic dynamic exchange, which facilitates and ensures efficient remodeling of the filopodium during shape changes.

Filopodia represent semi-ordered bundles of actin

Our study reveals that filopodia contain one bound fascin molecule per 25 to 60 actin monomers. Due to the dynamic nature of the cross-links, this ratio represents only partially occupied binding sites. The *saturation* stoichiometry can be calculated from equilibrium kinetics:

$$\begin{aligned} \frac{[\text{total number of binding sites}]}{[\text{actin}]} &= \frac{[S] + [FS]}{[\text{actin}]} = \frac{[FS]}{[\text{actin}]} \frac{1 + K_A[F]}{K_A[F]} \\ &= \frac{[FS]}{[\text{actin}]} \frac{1 + 6.7(0.1)}{6.7(0.1)} \\ &= (1 : 25 \text{ to } 1 : 60)(2.5) = 1 : 10 \text{ to } 1 : 24, \end{aligned}$$

where $[\text{actin}]$ is the filopodial actin concentration, $[F]$ is the soluble, active fascin concentration, and $[S]$ and $[FS]$ are the available and occupied binding sites on the filaments, respectively. Even more fascin could theoretically be bound in a perfect filament lattice. Considering each helix of an actin filament separately, if the pitch allowed for a 360 degree rotation precisely every 12 monomers, each monomer would contribute a 30 degree rotation. If these filaments were hexagonally-packed, for example, every second actin monomer in the helix would be aligned with an adjacent filament and perhaps accommodate a cross-link. Because each fascin is connected to two filaments, this repeating arrangement would result in a molecular ratio of 1 fascin per 4 actin monomers. (Note that each helix of each filament repeats this geometry, such that, neglecting bundle edge effects, the ratio remains 1:4 for the entire bundle). Indeed, lattices appearing hexagonal are apparent in some reconstituted or chemically-fixed bundles (Tilney and DeRosier, 1986; Tilney et al., 2000; Volkman et al., 2001), and bound ratios of up to 1:4.6 have been measured *in vitro* (Bryan and Kane, 1978; Yamashiro-Matsumura and Matsumura, 1985). It appears unlikely that the geometry of filopodia would allow for this precise packing, however. The pitch of each actin helix of a free filament is imperfect for hexagonal packing, rotating 360 degrees per approximately 13.7 monomers, or only 26.3 degrees per monomer. Because one bound fascin per 25 to 60 actin monomers equates to one cross-link every 6th to 15th monomer along a double helix, a torque aligning

the filament for hexagonal packing would result in an angle strain buildup of $(30 - 26.3)(6 \text{ to } 15) = 22$ to 56 degrees between successive cross-links on a filament. Electron micrographs of filopodia formed by convergent elongation in fact appear imperfectly packed (Svitkina et al., 2003), and Stokes and DeRosier have described bundles formed *in vitro* with one bound fascin per 33 to 66 actin monomers as plentiful but “poorly ordered,” both suggesting a somewhat reduced binding site concentration. The lower range of our bound fascin-to-actin ratio (1:25) would translate to a binding site to actin ratio of 1:4.6 if either K_A was as low as $2.3 \mu\text{M}^{-1}$ or the free fascin concentration, $[F]$, was as low as $0.03 \mu\text{M}$ (an order of magnitude lower than our measured 0.1-0.3 μM).

In summary, filopodia appear to represent semi-ordered bundles, reducing the possible fascin:actin ratio from a 1:4 theoretical value to 1:10 to 24. However, given their dynamic nature and limited soluble concentration, they only operate at ratios of 1:25 to 60 *in vivo*.

Fascin dynamics have implications on the mechanics and remodeling of filopodia

A key function of fascin as an actin cross-linker is its ability to stiffen filopodia. Individual actin filaments are insufficiently rigid to resist compressive forces (Janmey et al., 1991; Mogilner and Rubinstein, 2005), and filopodia in fascin-depleted cells are typically bent and buckle under the cell membrane (Vignjevic et al., 2006). While the function of stiffening would apparently be best served by high-affinity fascin binding, this counteracts the need for filopodia to undergo necessary remodeling (e.g. fusion of neighboring filopodia, accommodation to obstacles, or cycling between growth and breakdown). The dynamic nature of the fascin cross-links allows for both requirements.

The filopodium as a whole undergoes two main loading regimes, with a different mechanical response to each. Slow-scale displacement of the filopodium occurs on the timescales of cell motility itself, on the order of $1 \mu\text{m}/\text{min}$, and may occur over small or large distances. A growing filopodium may be displaced as it encounters other cells, for example, or be displaced by lamellipodial retraction or the motion of adjacent cells. Displacement may also occur on rapid timescales due to Brownian (thermal)

motion, under which a single, 10 μm -long actin filament bends considerably (persistence length, Isambert et al., 1995). We have shown that the half-time of fascin exchange in filopodia is 6 seconds, indicating a timescale of motion that divides two types of mechanical responses: displacement rates that build little strain in the cross-links over this time-scale result in little resistance to displacement from those cross-links, while rates that build up significant strain on this timescale encounter resistance due to the additional stiffness that fascin imparts to the bundle. This resistance rises with the filopodial fascin:actin ratio, which we estimated to be high, at 1:25-60. While it is difficult to predict the rate at which strain builds in the cross-links of a displaced filopodium without detailed knowledge of the system geometry, it is likely that the slow displacements do not build appreciable resistance from fascin over the course of a single binding period, while the displacement due to thermal motion almost certainly does. The dynamics of fascin exchange therefore mediate a differential, visco-elastic-like response to the two common loads, allowing slow remodeling but resisting rapid fluctuations with additional stiffness (Figure 10).

Similar stress-strain relationships have been observed in stress fibers incorporating alpha-actinin (Sato et al., 1987; Pollard et al., 1990). Like fascin mediated actin bundles, the mechanical properties of such actin networks depend on the rate of displacement, where the stiffness can increase by an order of magnitude at fast displacements. One significant difference is that the rate of dissociation of alpha-actinin is an order of magnitude faster than that of fascin (Xu et al., 2000). The variance in the time-scales of protein exchange between the two bundlers yield different limits for the rate of deformation. Such limits may be critical for the ability of actin bundles to withstand the different types of stresses they encounter in their respective subcellular locations. It would be interesting to compare such properties between filopodia and other protrusive actin networks such as pseudopodia, microvilli, and stereocillia.

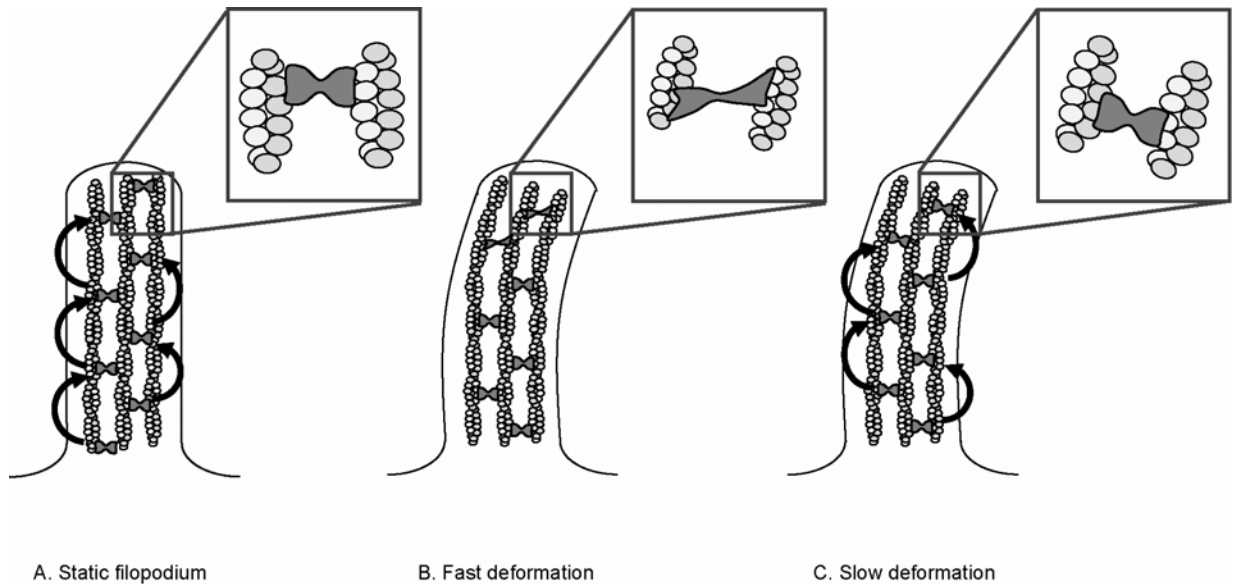


Figure 24. Rapid fascin exchange may endow filopodia with a rate-dependent response mode to mechanical stress.

Schematic models depicting the behavior of fascin in filopodial bundles under different rates of deformation. (A) Fascin undergoes continuous exchange within unstressed bundles. (B) Moderate rates of fascin exchange allow for filopodia to resist rapid deformations (C) but to reorganize when stress is applied slowly. In the latter case, fascin provides little resistance against the load since cross-links rearrange faster than filaments are displaced.

Fascin turnover is a key process in filopodial assembly

Filopodia are naturally subject to selective evolutionary pressures as dictated by their required sensory functions. Such pressures include the formation and maintenance of ordered parallel bundles; remodeling of filopodial structure at adequate rates under appropriate loads, with resistance to other loads; providing the necessary, perhaps non-uniform, stiffness along the filopodial length; and transport of cytoskeletal proteins to growing filopodial tips at rates compatible with elongation velocities. Such requirements must operate over filopodial lengths of 1 to 50 μm , diameters of only 0.1-0.5 μm (Mitchison and Cramer, 1996), and growth rates from a typical 2 $\mu\text{m}/\text{min}$ (Mallavarapu and Mitchison, 1999; current study) to as fast as 25 $\mu\text{m}/\text{min}$ (Sheetz et al., 1992). As our numerical analysis shows, filopodia growing at 2 $\mu\text{m}/\text{min}$ seem to operate near a k_{off} that delivers maximum fascin cross-links to the extending tip. Lower k_{off} values allow less dissociation of bound fascin and continued diffusion toward the tip, while higher values further limit the equilibrium bound concentration throughout the length. Among the pressures affecting filopodial rigidity and morphology, the optimal value of k_{off} to supply fascin to the tip at the typical growth rate appears to be of particular importance. Altogether, filopodia may have selected dynamic cross-links to form adequately stiff bundles at appropriate rates and allow for remodeling.

Chapter 4: Summary of Current Work and Future Perspective

This thesis research revealed a new conceptual framework for how filopodia form and grow: Initially, filopodia formation is triggered in part by fascin activation via dephosphorylation. Once filopodia form, fascin incorporates into semi-ordered actin bundles with a ratio of 1 cross-linker per 25-60 actin monomers. During the filopodial life time, fascin undergoes intrinsic dynamic exchange on the order of 10 seconds, which allows for filopodial growth to several microns, at a rate of 2 μ m/min. In total, this thesis work enhanced our understanding of filopodia and inspired several other questions; What is the nature of other protein-protein interactions in filopodia? What is the life-time of those interactions? And, what molecular players regulate the turnover of proteins in filopodia?

As future avenues of research on the cytoskeleton are considered, researchers within the field must take into account questions regarding both basic and clinical science. Without understanding the molecular mechanisms that govern cell behavior, we cannot begin to understand normal physiological development and disease. In view of that, this chapter highlights the following research objectives.

Lessons from filopodia: how do actin bundles grow?

Cell morphology is determined by the assembly of cytoskeletal proteins and the molecules which modify their organization. Over the past few years, valuable information about events which generate cell shape has become available, yet we still do not know the mechanisms that determine geometric parameters. In particular, we are limited in our understanding of the pathways that outline growth patterns of cellular actin bundles. The dissimilarity between various bundles, such as microvilli, *Drosophila* bristles, stereocilia, and filopodia only adds to the complexity. While *Drosophila* bristles are composed of modules of actin bundles (Tilney and DeRosier, 2005), microvilli, stereocilia and filopodial bundles are assembled in continuous entities of actin filaments (Tilney and DeRosier, 1986; Bartles, 2000; Svitkina et

al., 2003). These filaments are cross-linked by different actin bundling proteins, which sometimes act alone or in concert. At least one thing these bundles have in common is that their formation, elongation, and maintenance are dependent in part by the ability of the cell to deliver precise molecular components necessary for growth in a timely fashion. The supply of molecules to protrusive actin bundles can occur by at least two methods; diffusion of proteins inward from the cell body and by motor-driven transport. Here, we evaluate these factors and their influence on bundle growth.

In this thesis, we showed that filopodia require dynamic cross-linking of their actin filaments to grow and reach lengths longer than $3\mu\text{m}$. In contrast, a model which involved diffusion coupled with irreversible association of fascin cross-linkers could not keep up with physiological rates of filopodial elongation, only short or slow growing filopodia. This result prompts the question of how actin is sufficiently supplied to tips of growing filopodia since actin, unlike fascin, is stably bound along the length of filaments and mimics the aforementioned model. When filaments are long or fast growing, monomeric actin from the cell body has to diffuse several microns to reach the barbed end and has to do so fast enough to accommodate the rate of filopodial elongation. We predict that transport of actin by diffusion to growing filopodial tips can accommodate slow growing or short filopodia, but not long or fast growing bundles. To test our prediction, we devised a numerical, one-dimensional, reaction-diffusion model of filopodial elongation (schematic representation given in Figure 15A; T.E. Schaus, personal communication). Per the model, filopodia grow by free diffusion of actin from the base to tip along with biochemical reactions at the barbed end, by the following set of equations,

$$v = \frac{dm/dt}{N_{fil}} \delta \quad \text{kinematic: velocity relative to tip monomer incorporation}$$

$$\frac{dm}{dt} = -DA \frac{(C_{tip} - C_{base})}{l} \quad \text{diffusion: monomer supply to tip via Fick's law}$$

$$v = (k_{on} C_{tip} - k_{off}) \delta \quad \text{kinetic: velocity of protrusion relative to tip actin concentration,}$$

where m is the number of actin molecules (divided by Avogadro's number), v is the rate of elongation, A is the filopodial cross-sectional area, and δ is the actin monomer length, with all parameters for actin given in Table 3. Therefore, in this model there are three equations and three unknowns, which can be related to one another in graphical form. For instance, a plot of the rate of protrusion versus filopodial length shows that for the physiological average rate of protrusion, $2\mu\text{m}/\text{min}$, filopodia can grow to at most a micron long (Figure 15B). As the filopodium continues to grow, lower and lower actin concentration is available for tip polymerization (Figure 15C). Furthermore, the model shows that while free diffusion of actin to the tip can occur on the order of seconds in short filopodia, it takes over an entire hour for actin to diffuse and bind to the tip of 20 micron long filopodia (Figure 15D and E). In the cell, the rate of actin diffusion in filopodia could be slowed down by physical obstacles. Therefore, our model represents the extreme upper limit or fastest possible delivery of actin to filopodial tips under our assumptions, and yet this rate of growth is inconsistent with physiological behavior, which reveals that filopodia can grow to 20 microns on the order of just minutes. In summary, the model conclusively supports our prediction that diffusion of actin along the length of filopodia can only support short or slow growing filopodia.

Variable	Value	Units	References
A	1.1E-14	m^2	(assumed dia = 200nm)
D	6	$\mu\text{m}^2/\text{s}$	Aratyn et al., 2007
<i>Barbed end</i> k_{on}	12	$\mu\text{M}^{-1}/\text{s}$	Pollard, 1986
<i>Barbed end</i> k_{off}	1.4	s^{-1}	Pollard, 1986
δ	2.7	nm	Schaus et al., 2007
C_{base}	10	μM	assumption

Table 3: Parameters used in numerical study

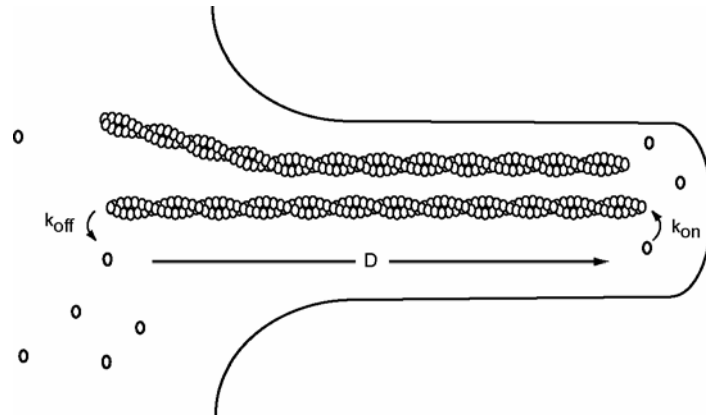


Figure 25. Schematic model of actin diffusion along filopodia

Schematic representation of free actin diffusion along filopodia with biochemical reaction at the barbed and plus ends of filopodial filaments.

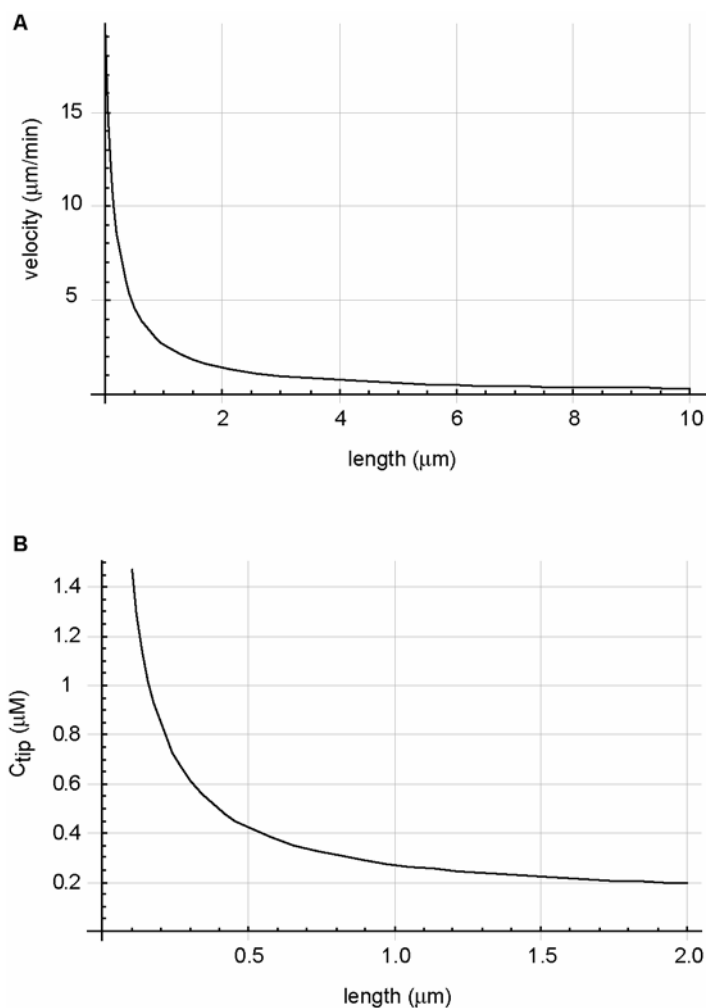


Figure 26. Actin diffusion cannot adequately supply monomers to growing tips of long filopodia

(A) Graphical comparison of filopodial elongation velocity by actin incorporation at the tip versus length of filopodia. The decaying curve reveals that as filopodia elongate, the rate of growth dramatically decreases. According to the model, at the measured average filopodial protrusion rate of $2\mu\text{m}/\text{min}$, filopodia can at best reach $1.6\mu\text{m}$ in length. However, physiological conditions allow filopodia to grow at the same rate for at least an order of magnitude longer (B) Plot of actin concentration at filopodial tip, C_{tip} , versus filopodia length. The model reveals that the tip actin concentration dramatically decays with filopodial growth.

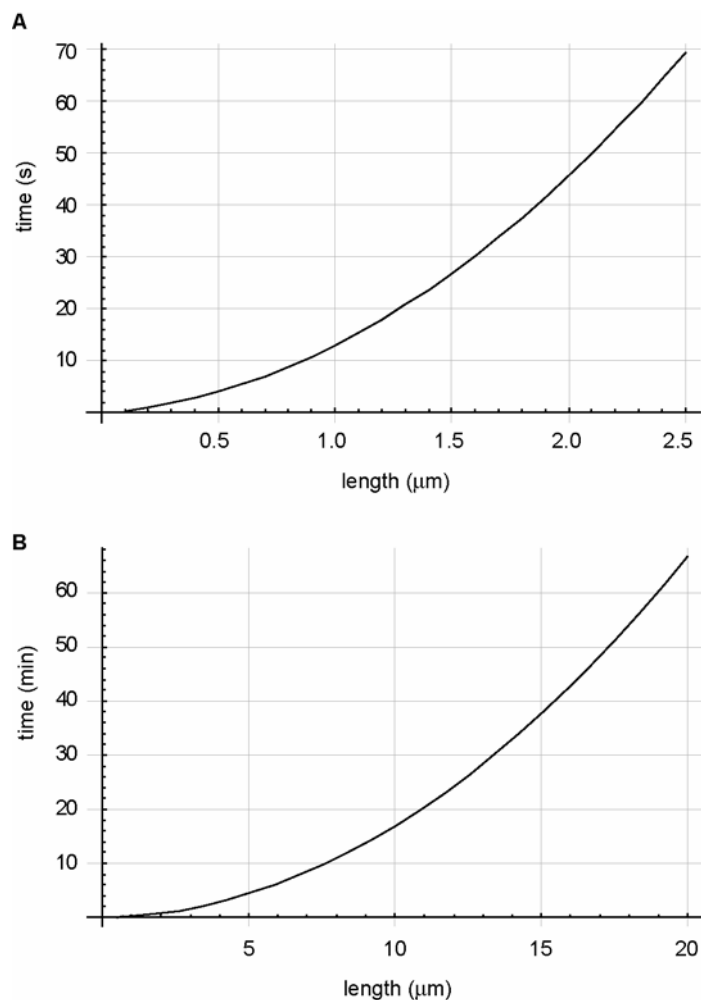


Figure 27. Actin diffusion can support short, growing filopodia

(A) Plot of time taken for filopodia to reach short lengths (0.5-2.5 μm). Filopodia can grow to short lengths within the order of 10 seconds. (B) However, actin delivery by diffusion does not allow for timely growth to long lengths (5-20 μm). For instance, the model reveals that it takes about one hour for filopodia to grow to 20 μm , which is much slower than physiological growth patterns, which allow filopodia to grow to similar lengths on the order of minutes. In summary, the model shows that actin diffusion, alone, cannot support typical growth rates of filopodial bundles.

Alternate mechanisms for actin delivery in filopodia need to be considered for long or rapidly growing filopodia. One possibility is that actin monomers dissociate from along the length of filaments, near the barbed end, such that they only have to diffuse short distances before reaching and assembling at the filopodial tip. Such dissociation may occur via a severing protein(s) or may be intrinsic to the actin molecule. However, this is an unlikely scenario since signs of actin dissociation would have been apparent in our FRAP studies, which revealed insignificant actin recovery after photobleaching. Another possibility is that filament fragments are made available along the filopodial length that can rapidly break apart and supply actin monomers to the tip when needed. For instance, *Drosophila* bristles contain short-lived snarls of uncross-linked actin bundles along the length (Tilney et al., 2003; Tilney and DeRosier, 2005). These snarls could come undone at the precise moment when monomers are in demand at the growing bundle tip. Since they are localized along the length, actin would only have to diffuse short distances and would, therefore, accommodate physiological growth conditions. Alternatively, filamentous fragments may be carried along the filopodial shaft by motor proteins, such as myosin XVa (Rzadzinska et al., 2004). Again, such fragments may dissolve into monomeric components near the tip to allow for filopodial growth. All possible explanations have yet to be experimentally tested.

Role of filopodia in cancer metastasis

Recent studies have shown that filopodia are strongly correlated with metastasis of cancer cells and poor patient prognosis (Hashimoto et al., 2005), however, the role and mechanism of filopodia in cancer are currently unknown. As metastasis remains the cause of roughly 90% of deaths from cancer (Gupta and Massague, 2005), the study of filopodia and cell motility are a serious research focus. The primary objective is to determine the role filopodia play in varying phases of metastasis (that is, the loss of cellular adhesion, increased motility and invasiveness, entry and survival in the circulation, exit into new tissue, and eventual colonization of a distant site). Recent studies revealed that filopodia may be involved in cell

migration and invasion during the initial steps of metastasis (that is, dissociation from primary tumor mass, invasion of basal membrane and migration towards the circulatory system) and during the final steps of metastasis (extravasation) (D. Vignjevic, personal communication). In between those stages and while in the circulatory system, the cells are likely to be passively carried by blood flow. It remains unknown how cells, once in transit, slow themselves down prior to exiting the blood vessel, what initiates the docking of those cells to their desired destination on the epithelium, and what role filopodia play during this process? It is possible that circulating cancer cells are attracted to chemoattractive gradients and extracellular matrix tracks that originate or terminate near the target organs or that signals emanating from metastatic cells enhance the permeability of blood vessels (Gupta and Massague, 2005). As presumed exploratory organelles, filopodia may decode such signals and navigate the cells to those sites. One possibility is that once the cells are within close proximity to the vascular wall, adhesion molecules near the tips of filopodia and along their shaft may make contacts and anchor the cells, or slow the cells from continued flow. This event could trigger the formation of more filopodia, which then, in a cooperative manner, guide the cell closer to the wall and eventually allow for extravasation. The same events may influence intravasation as well. Our idea that filopodia can generate surface attachments and pull cells toward vessels is based on experimental data on growth cone filopodia, which showed that when filopodial tips adhere to a surface, they can exert a pulling force (Heidemann et al., 1990; Smith, 1994; Suter et al., 1998; Suter and Forscher, 2000) that can transport attached objects toward the growth cone body or pull material from the growth cone anterogradely, resulting in engorgement of the filopodium and movement of the growth cone in the direction of the filopodium (Goldberg and Burmeister, 1986; Smith, 1994; Letourneau, 1996). Such ideas have partially been outlined in the ‘clutch’ model, which involves the formation of substrate adhesions between the filopodial actin bundle and the extracellular space, which restricts retrograde flow of actin by molecular motors, and generates tension that leads to the advancement of a crawling cell (Mitchison and Kirschner, 1988; Jay, 2000). However, the location and dynamics of ‘clutching’ (e.g. the force distribution versus time in filopodia) and motor

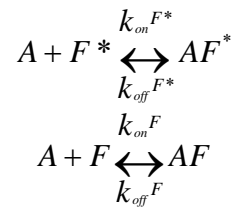
proteins which regulate actin flow have not been characterized. With further research and a better understanding of filopodia, perhaps the 'clutch' model can be applied to metastatic cells during intra and extra-vasation.

As technologies advance, we are likely to identify the molecular mechanisms associated with metastatic progression of cancer. Confirming the relevance of filopodia to metastatic motile behavior of cancer cells and dissecting the pathways that underlie it are important avenues for future research.

Chapter 5: Appendices

A. Theoretical derivation of dissociation rate constant from FRAP data

The objective of our FRAP study is to understand the dynamics of wild type fascin and its mutant forms in filopodia. The most commonly used approach to describe the mobility of proteins during FRAP experiments is to assume the spatiotemporal dynamics of these proteins to be diffusive in nature. We hypothesize that the following model takes place during the assembly and disassembly of filopodia: free actin, A , and free fascin, in its fluorescent form, F^* , and in its bleached form, F , are constantly binding together to create actin bound to fluorescent fascin complexes, AF^* , and actin-bound to bleached fascin complexes, AF ; while at the same time, constantly detaching from each other. Thus, we have two transitions that undergo a reversible process of binding and unbinding within a structure that can be assumed to be immobile and homogeneously distributed:

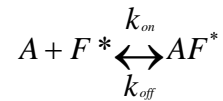


We shall make the following assumptions in order to solve for the rate constants

- The system, meaning the entire filopodium, is closed; thus, the concentration of available fluorescent fascin, bleached fascin and actin molecules remain constant throughout the recovery process. This assumption is confirmed in Figure 10.
- The system is in equilibrium during the binding and dissociation of fluorescent fascin and bleached fascin; thus, the concentrations of bound actin, $[AF^*] + [AF]$, remain constant throughout the recovery process.
- Diffusion occurs within a relatively short period of time compared to the recovery time inside the photobleached zone, thus, its own dynamics can be neglected. This assumption is confirmed in Figure 17.

- Bleached fascin does not rebind to actin; it simply diffuses out of the photobleached zone.
This is a reasonable assumption to make as the photobleached region is small compared to the length of the filopodium, and, therefore, the pool of bleached fascin is small in contrast to the available pool of free fluorescent fascin.
- The number of free fluorescent fascin molecules remains constant in the photobleached region throughout the assembly process. This is a reasonable assumption as when free fluorescent fascin binds to free actin it is replaced by diffusion.

After taking these assumptions into consideration, we are left with the following recovery model inside the photobleached region:



Differentiating the above equation with respect to time, we can calculate the variation of concentration of fluorescent fascin bound to actin, $[AF^*]$, and obtain a first degree inhomogeneous differential equation,

$$\frac{dA}{dt} = k_{on} [A] [F^*] - k_{off} [AF^*] (t)$$

Solving the above differential equation, we obtain,

$$\frac{dA}{dt} = -k_{off} \left([AF^*] (t) - \frac{k_{on}}{k_{off}} [A] [F^*] \right)$$

$$\frac{dA/dt}{\left([AF^*] (t) - \frac{k_{on}}{k_{off}} [A] [F^*] \right)} = -k_{off} dt$$

By integration, we obtain,

$$\ln\left([AF^*](t) - \frac{k_{on}}{k_{off}}[A][F^*]\right) = -k_{off}t + c$$

where c is a constant.

Taking the exponential of both sides of the above relation yields,

$$\left([AF^*](t) - \frac{k_{on}}{k_{off}}[A][F^*]\right) = \exp(-k_{off}t + c)$$

Thus, the general solution for our model is

$$[AF^*](t) = c' \exp(-k_{off}t) + \frac{k_{on}}{k_{off}}[A][F^*]$$

where c' is a constant.

We are able to solve for c' by applying the initial condition, $[AF^*](t=0) = [AF^*]_0$, to our general solution. Thus, $c' = [AF^*]_0 - \frac{k_{on}}{k_{off}}[A][F^*]$, where $[AF^*]_0$ is equal to the concentration of fluorescent fascin diffusing into the photobleached zone and binding to free actin during the photobleaching time.

We obtain the following equation that describes our model:

$$[AF^*](t) = \frac{k_{on}}{k_{off}}[A][F^*] - \left(\frac{k_{on}}{k_{off}}[A][F^*] + [AF^*]_0\right) \exp(-k_{off}t)$$

By inserting the following constants into the equation:

$$I_{PB} = [AF^*]_0$$

$$I_{\infty} = \frac{k_{on}}{k_{off}}[A][F^*],$$

where I_{PB} is intensity at photobleaching event and I_{∞} is intensity at the final time in the experiment. We obtain the following curve-fitting expression:

$$I(t) = I_{\infty} + (I_{PB} - I_{\infty}) \exp(-k_{off} t)$$

Due to the fact that the fluorescence intensity is non-uniform throughout the filopodium, primarily a result of varying levels of GFP upon transfection and technical reasons (alterations in the image mode acquisition), we will normalize the intensity values relative to the intensity at the prebleach time, I_0 , which yields the final curve fitting equation:

$$\frac{I(t)}{I_0} = \frac{I_{\infty}}{I_0} + \frac{(I_{PB} - I_{\infty})}{I_0} \exp(-k_{off} t)$$

We propose that the decay follows a first degree reaction and can, therefore, extract a half time for fascin dissociation in filopodia,

$$t_{1/2} = \frac{\ln 2}{k_{off}},$$

with mobile fraction (or the proportion of molecules able to undergo exchange), MF ,

$$MF = \frac{I_{\infty} - I_{PB}}{I_0 - I_{PB}}.$$

B. Description of numerical diffusion-reaction models

A numerical reaction-diffusion model of filopodia was created for the purposes of calculating diffusion coefficients from FRAP image sequences (Fig. 17) and predicting theoretical bound fascin concentrations along growing filopodia (Fig. 21-22). The model consisted of a 1D tube of varying cross-section, discretized into relatively small (constant, $\Delta x = 0.05 \mu\text{m}$ long), uniform-concentration segments along its length. Over small time steps ($\Delta t \approx 0.0025$ s), deterministic calculations of diffusion between adjacent segments (using Fick's law) and first- and second-order kinetic reactions within a segment were made. The filopodial base was assumed held at a constant soluble fascin concentration, while the tip was a reflecting boundary (i.e. a "wall"). The simulation was thus a discretization of the 1D diffusion-reaction equations, as follows:

$$\frac{\Delta[F]_i}{\Delta t} = -\frac{2D\Delta t}{\Delta x^2} \left[\left([F]_i - \frac{[F]_{i-1}Ac_{i-1} + [F]_iAc_i}{Ac_{i-1} + Ac_i} \right) - \left(\frac{[F]_iAc_i + [F]_{i+1}Ac_{i+1}}{Ac_i + Ac_{i+1}} - [F]_i \right) \right] \dots$$

$$\dots - k_{on}[F]_i[S]_i + k_{off}[FS]_i \quad [F] \text{ (fascin) diffusion and kinetics}$$

$$\frac{\Delta[S]_i}{\Delta t} = -k_{on}[F]_i[S]_i + k_{off}[FS]_i \quad [S] \text{ (empty fascin binding sites on actin) kinetics}$$

$$\frac{\Delta[FS]_i}{\Delta t} = k_{on}[F]_i[S]_i - k_{off}[FS]_i \quad [FS] \text{ (fascin-actin site complex) kinetics,}$$

where square brackets denote concentrations, the subscript i denotes the axial segment (position), Ac_i denotes the filopodial cross-sectional area of segment i , and k_{off} and k_{on} are the kinetic rate constants (given in Table 1). The following boundary conditions were applied:

$$[F]_{i=0} = [F]_{base} \quad \text{fascin concentration is fixed at base}$$

$$\frac{\Delta[F]_{i=tip}}{\Delta x} = 0 \quad \text{fascin gradient is zero (no diffusion) at tip}$$

$$\text{number of elements} = \frac{V}{\Delta x} t \quad \text{filopodial length grows at rate } V \text{ in time } t$$

In the experimental determination of diffusion coefficients (Fig. 5), sequential images of soluble markers undergoing FRAP provided data on the cross-sectional areas and marker concentrations along filopodia. The total number of labeled molecules assigned to each model segment was taken as the total intensity of the pixels in the corresponding image area. Because soluble markers in the pre-bleach image were at a uniform concentration, their total segmental intensity indicated the (significantly varying) cross-sectional area Ac_i of each axial segment i . Similarly, the first post-bleach image indicated the total number of labeled molecules per segment, but in the “initial condition” state. The model was therefore initialized with the filopodial length, respective segment cross sectional areas, and initial concentrations $[F]_i, (t = 0)$ equal to the total number of molecules in the first post-bleach image divided by the cross-sectional area at each segment. Filopodial length remained constant (i.e. $V = 0$) in both the images and these simulations.

Time-dependent diffusion calculations were then carried out (no kinetics were required here), and a recovery profile of the total filopodial fluorescence with time was plotted. This profile was compared to the experimental profile measured in the same manner, and the diffusion coefficient of the model was adjusted iteratively for a profile match. The diffusion coefficient used to attain a matching profile was then reported.

Calculation of the theoretical bound fascin concentration along the length of a growing filopodium (Fig. 21-22) used the same technique but calculated kinetics and simulated filopodial growth. From an initial length near zero, segments were added to the tip to match the desired filopodial elongation rate V , and appeared with a constant available fascin binding site concentration $[S]_i$ and constant Ac_i , but zero occupied sites $[FS]_i$. Each additional segment was accompanied by a shift in soluble concentration values toward the new segment, with the filopodial base segment drawing in fascin at the fixed base concentration. From an initial length near zero, each time step consisted of both diffusion calculations between segments and kinetic on- and off-reactions within them. The result was a bound fascin concentration value as a function of time and axial position.

Values measured from B16 cells were used in modeling. The soluble fascin concentration at equilibrium was equal to that of the cellular pool, $[F]$, and measured by quantitative western blotting to be 100 nM (Appendix B). To determine the total binding site concentration, we first calculated the available binding site concentration $[S]$ at equilibrium. Taking advantage of the data from Fig. 20, indicating the fraction of fascin in filopodia which are bound f_{bound} :

$$k_{on}[S][F] = k_{off}[FS]$$

$$[S] = \frac{k_{off}[FS]}{k_{on}[F]} = \frac{k_{off}[FS]/([FS]+[S])}{k_{on}[F]/([FS]+[S])} = \frac{k_{off}f_{bound}}{k_{on}(1-f_{bound})} = \frac{0.12}{0.8} \left(\frac{0.98}{0.02} \right) = 7 \mu\text{M}$$

The same calculation using a value of $f_{bound} = 0.95$ results in $[S] = 3 \mu\text{M}$. Using this range of 3 to 7 μM , we can calculate the total binding site concentration as:

$$\begin{aligned}
[S] + [FS] = \text{total binding site conc.} &= [S] \left(1 + \frac{k_{on}}{k_{off}} [F] \right) \\
&= (3 \text{ to } 7 \mu\text{M}) \left(1 + \frac{0.8}{0.12} 0.1 \right) = 5 \text{ to } 12 \mu\text{M}.
\end{aligned}$$

We therefore initialized each added filopodial segment with $[FS] = 0$ (no bound fascin) and $[S] = 10 \mu\text{M}$.

C. Effective diffusion of fascin in filopodia

While we have already found that the *free* diffusion coefficients of WT fascin (i.e., in its unbound state) is $6.0 \mu\text{m}^2\text{s}^{-1}$, its *effective* diffusion coefficient describes its overall motility. That is, instead of a full description of the kinetic and diffusive processes fascin alternates between, we may more simply describe the apparent motion as diffusion with a lower, effective diffusion coefficient. In general, the 1D diffusion coefficient of a molecule is the average distance traveled squared, divided by twice the time elapsed: $D = x_{\text{RMS}}^2/(2t)$. Because fascin molecules in filopodia are only free 2 – 6% of the time (Fig. 7), the time required to travel a distance x_{RMS} is the inverse, or 50 – 17 times the interval required for non-binding molecules with the same actual diffusion coefficient. The apparent, or effective, diffusion coefficients of active forms of GFP-tagged and WT fascin are thus only $0.12 - 0.35 \mu\text{m}^2\text{s}^{-1}$.

D. Determination of the operating fascin:actin ratio in filopodia

Quantitative immunoblotting was used to determine the concentration of cellular fascin protein to be 100-300 nM in B16 cells (350-500nM in N2a cells). That value was converted to number of fascin molecules per cell by dividing the amount of fascin protein by molecular weight of fascin (55 kD) and Avogadro's number, yielding $1.0-2.5 \times 10^5$ molecules per B16 cell ($3.0-4.6 \times 10^5$ per N2a cell). Using fluorescence microscopy, we determined the percent of total fascin molecules in a cell which localize to filopodia, 11% in B16 (29% in N2a). To calculate the number of fascin molecules in one filopodium, we

divided by the average number of filopodia per cell (number of filopodia in B16 cells = 30, n = 88; number of filopodia in N2a cells = 60, n = 30), or

$$0.11 \times \frac{1.0 - 2.5 \times 10^5 \text{ molecules}}{30 \text{ filopodia}} = 368 - 920 \text{ fascin / filopodium.}$$

Similar calculations yielded 1450-2200 fascin per N2a filopodium. We found that, on average, B16 filopodia were 3 μ m long (Vignjevic et al. 2006) and N2a filopodia were 8 μ m (current study). By assuming that filopodia contain 20 actin filaments (Lewis and Bridgeman, 1992; Mogilner and Rubinstein, 2005) and using the accepted incremental extension of an actin monomer of 2.7 nm, which gives 370 actin monomers per μ m of filament, we found that the filopodia contain:

$$\frac{370 \text{ actin monomers}}{\mu\text{m}} \times \frac{(20 \text{ filaments})(3 \mu\text{m})}{\text{filopodium}} \times \frac{\text{filopodium}}{368 - 920 \text{ fascin}} = 25 - 60 \frac{\text{actin monomers}}{\text{fascin}}.$$

Similar calculations yielded 27-41 actin per fascin in neuronal N2a filopodia.

Chapter 6: Materials and Methods

Protein Purification

Actin

Actin was purified from rabbit muscle as previously described (Spudich and Watt, 1971). TMR-actin was prepared by labeling F-actin with 5-(and 6) carboxytetramethylrhodamine succinimidyl ester (NHSR) (Molecular Probes) as described in (Isambert et al., 1995) and stored at -80°C. Biotinylated-actin was prepared with biocytin maleimide (Molecular Probes) by the method of Rock et al (Rock et al., 2000). Before use, labeled G-actin was recycled by polymerization for 2h on ice in the presence of 50mM KCl, 2mM MgCl₂, and 1mM ATP, sedimentation at 100,000 g for 1.5h at 4°C, resuspension in cold G buffer (2mM Tris-HCl, 0.2mM CaCl₂, 0.2mM ATP, and 0.5mM DTT) to a final concentration of 2 mg/ml, and dialysis overnight against G buffer using microdialysis buttons (Pierce Chemical Co.).

Fascin

Recombinant human fascin was prepared by a modification of the method of Ono et al. (Ono et al., 1997). *E. Coli* carrying the plasmid was grown at 37°C until the A₆₀₀ reached 0.6. Protein expression was induced by adding 0.1 mM IPTG at 20°C for 4 h. Cells were harvested by centrifugation and extracted with B-PER in phosphate buffer (Pierce Chemical Co.) plus 1mM PMSF and 1mM DTT. The lysate was centrifuged at 20,000 g for 20 min, and the supernatant was mixed for 1 h at RT with 2ml glutathione-Sepharose 4B (Amersham Biosciences) equilibrated with PBS plus 1 mM DTT. The glutathione-Sepharose was poured into a column and washed with 20ml PBS plus 1mM DTT. 80µl of thrombin (Amersham Biosciences) was added, and digestion was allowed to proceed overnight at 4°C. Flowthrough fractions were collected in 2 mM PMSF and concentrated by Centricon 10 (Amincon). Fascin was labeled with AlexaFluor 488 carboxylic acid, succinimidyl ester (Alexa 488-NHS, Molecular Probes). The pH of the fascin solution was raised to 8.3 by the addition of 1/20 volume of 0.1 M NaHCO₃, pH 9.3. A ten fold molar excess of Alexa 488-NHS was added from a stock solution of 25mg/ml in

DMSO and reacted for one hour at RT. Free dye was separated from labeled fascin on an Excellulose desalting column (Pierce).

***In vitro* bundling assay**

22mm x 22mm coverslips were cleaned with 70% ethanol and blown dry with air (same applies to microscope slides). Coverslips were coated with nitrocellulose (1% collodion in amyl acetate (Electron Microscopy Sciences)) and allowed to air dry for 1hr. Chambers were created by placing two strips of double-sided tape onto microscope slides, 0.5 inch apart, and placing coverslip (nitrocellulose coating face down) on top of taped slide. Neutravidin mix (1 μ l of 5mg/ml Neutravidin in 50mM PBS (pH 8.0) to 20 μ l actin polymerization buffer (10mM Imidazole (pH 7.0) 50mM KCl, 1mM MgCl₂, 1mM EGTA)) was infused into perfusion chamber and allowed to incubate at RT for 1min. Chamber was washed 2x with 1mg/ml BSA in actin polymerization buffer to block any non-specific binding. The bundle mixture* was infused into chamber. Chamber inlet and outlet was sealed with vasaline/lanolin/paraffin (1:1:1).

*Bundle mixture: To visualize TMR-actin in fascin-actin bundles, 1 μ M TMR-actin, 3 μ M unlabeled actin and 1 μ M Biotinylated-actin were added to an eppendorf tube and allowed to polymerize in actin polymerization buffer. 3 μ M unlabeled fascin was subsequently added to cross-link the filaments. To visualize Alexa488-fascin in fascin-actin bundles, 3 μ M unlabeled fascin and 1.5 μ M Alexa488-fascin were used to bundle filaments composed of 3 μ M unlabeled actin and 1 μ M Biotinylated-actin. Fluorescent actin and fascin had to be used in separate experiments as the fluorescent tags likely interfered with bundling. *In vitro* bundles were allowed to incubate at RT for 1hr. The following were used to inhibit photobleaching: 4.5mg/ml glucose, 0.86 mg/ml glucose oxidase (Sigma G-2133), and 0.14mg/ml catalase (Sigma C-3155) added to bundle mixture prior to imaging.

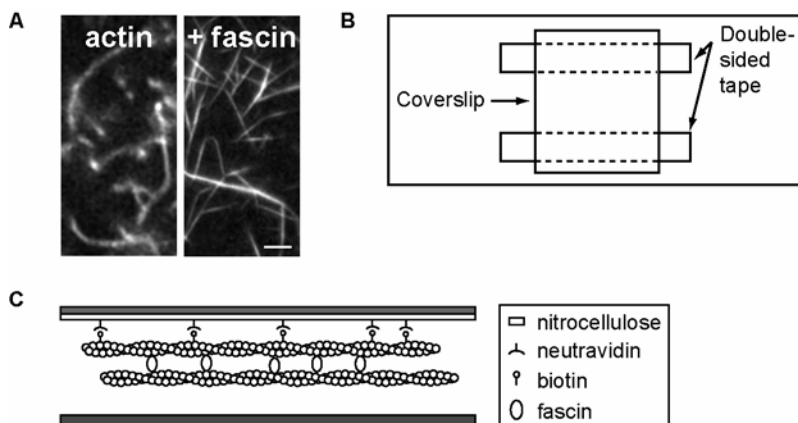


Figure 28. *In vitro* assay

(A) TMR-actin polymerized in the absence of cross-linking yields wavy, unbundled filaments. Addition of fascin resulted in the formation of thicker, stiffer actin bundles. Both viewed by wide field Epi-fluorescent microscopy. Scale Bar, 5 μ m. (B) Diagram illustrating the assay chamber. It consists of a microscope slide with 2 pieces of double-sided tape, spaced as shown. A nitrocellulose-coated coverslip was placed face-down on the tape. Solutions containing fascin-actin bundles were perfused in one side via a pipette. (C) Profile view of perfusion chamber design. Actin-fascin bundles were tethered to the nitrocellulose-coated coverslip in the chamber via a biotin-neutravidin interaction.

Cell Culture

B16F1 mouse melanoma and Neuro2a mouse neuroblastoma lines were provided by Drs. C. Ballestrem (Weizmann Institute of Science, Israel) and A. Ferreira (Northwestern University, Chicago, IL), respectively, and maintained in DMEM supplemented with 10% FBS at 37°C. Cells were plated onto coverslips, which were coated with 20µg/ml mouse laminin (Invitrogen) for 1hr and thereafter incubated with 1% bovine serum albumin in Phosphate Buffered Saline for 20min. Transfection of plasmids was carried out by FuGENE6 (Roche) transfection reagent in B16 cells and *TransIT-Neural* (Mirus) reagent for Neuro2a cells, both per manufacturers' instructions (transfection: 1µg DNA, 4µl FuGENE6 reagent or 1µl *TransIT-Neural* reagent, 100µl Optimem medium (Gibco)). For live cell imaging, cells were transferred into L-15 medium (Gibco) supplemented with 10% Fetal Bovine Serum (Atlanta BioScience).

Plasmids

pEGFP-actin construct was purchased from Clontech. pEGFP-Fimbrin was provided by Dr. J. Bartles (Northwestern University, Chicago, IL). pEGFP-fascin construct was provided by Dr. J. Adams (Cleveland Clinic Foundation, Cleveland, OH). QuikChangeII site-directed mutagenesis kit (Stratagene) was used to create point mutations.

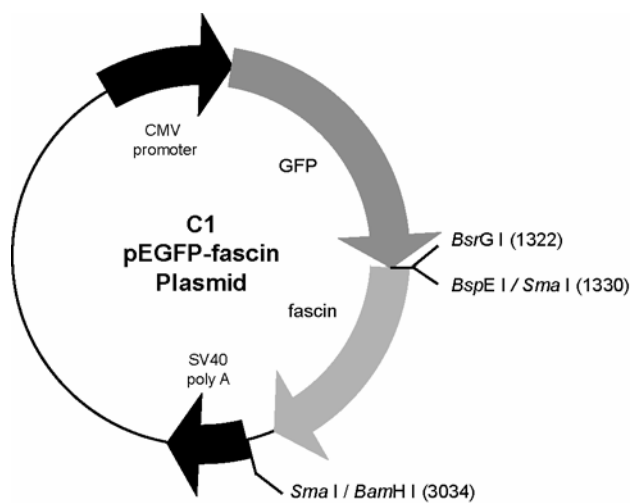


Figure 29. A schematic illustration of pEGFP-fascin vector. Total nucleotide length is 6.2kb, with fascin insert having 1.5kb. Not shown: plasmid is coded for kanamycin resistance.

Name	Primer Name	Primer Sequence (5' to 3')
S39A	S39A-F	GTGAACGCGTCCGCCAGCGCCCTGAAGAAGAAGCAGATCTGGACG
	S39A-R	CGTCCAGATCTGCTTCTTCTTCAGGGCGCTGGCGGACGCGTTCAC
S39E	S39E-F	GTGAACGCGTCCGCCAGCGAACTGAAGAAGAAGCAGATCTGGACG
	S39E-R	CGTCCAGATCTGCTTCTTCTTCAGTTCGCTGGCGGACGCGTTCAC
F29A	F29A-F	ACGGCCGAGGCGGCCGGTTCAAGGTG
	F29A-R	CACCTTGAACCCGGCCGCCTCGGCCGT
F29E	F29E-F	CTGACGGCCGAGGCGGAAGGGTTCAAGGTGAAC
	F29E-R	GTTCACCTTGAACCCCTCCGCCTCGGCCGTCAG

Table 4. Design of fascin mutants. All mutants were designed using the pEGFP-fascin WT DNA template.

Filename : pEGFP-fascin
Sequence Size : 6379

```

AgeI      610      620      630      640      650      660
ACCGGTGCGCCACCATGGTGAGCAAGGGCGAGGAGCTGTTACCCGGGGTGGTGCCCATCTG
      M V S K G E E L F T G V V P I L
      670      680      690      700      710      720
GTCGAGCTGGACGGCGACGTAACGGCCACAAGTTCAGCGTGTCCGGCGAGGGCGAGGGC
V E L D G D V N G H K F S V S G E G E G
      730      740      750      760      770      780
GATGCCACCTACGGCAAGCTGACCCTGAAGTTCATCTGCACCACCGGCAAGCTGCCCGTG
D A T Y G K L T L K F I C T T G K L P V
      790      800      810      820      830      840
CCCTGGCCCACCCTCGTGACCACCTGACCTACGGCGTGCAGTGTTCAGCCGCTACCCC
P W P T L V T T L T Y G V Q C F S R Y P
      850      860      870      880      890      900
GACCACATGAAGCAGCAGACTTCTTCAAGTCCGCCATGCCCGAAGGCTACGTCCAGGAG
D H M K Q H D F F K S A M P E G Y V Q E
      910      920      930      940      950      960
CGCACCATCTTCTTCAAGACGACGGCAACTACAAGACCCGCGCCGAGGTGAAGTTCGAG
R T I F F K D D G N Y K T R A E V K F E
      970      980      990      1000      1010      1020
GGCGACACCTGGTGAACCGCATCGAGCTGAAGGGCATCGACTTCAAGGAGGACGGCAAC
G D T L V N R I E L K G I D F K E D G N
      1030      1040      1050      1060      1070      1080
ATCCTGGGGCACAAGCTGGAGTACAAC TACAACAGCCACAACGTCTATATCATGGCCGAC
I L G H K L E Y N Y N S H N V Y I M A D
      1090      1100      1110      1120      1130      1140
AAGCAGAAGAACGGCATCAAGGTGAAC TCAAGATCCGCCACAACATCGAGGACGGCAGC
K Q K N G I K V N F K I R H N I E D G S
      1150      1160      1170      1180      1190      1200
GTGCAGCTCGCCGACCACTACCAGCAGAACACCCCATCGGCGACGGCCCCGTGCTGCTG
V Q L A D H Y Q Q N T P I G D G P V L L
      1210      1220      1230      1240      1250      1260
CCCGACAACCCTACCTGAGCACCAGTCCGCCCTGAGCAAAGACCCCAACGAGAAGCGC
P D N H Y L S T Q S A L S K D P N E K R
      1270      1280      1290      1300      1310      1320
GATCATATGGTCTCTGCTGGAGTTCGTGACCGCCGCCGGGATCACTCTCGGCATGGACGAG
D H M V L L E F V T A A G I T L G M D E
      BsrGI      BspEI/SmaI
      1350      1360      1370      1380
CTGTAGAGTCCGGGGGgccgcgagcggcctctcgtctactgccaccaccaccgccaac
L Y K S G G P R S G L S S T A T M T A N
      1390      1400      1410      1420      1430      1440
ggcacagccgagggcgtgagatccagttcggcctcatcaactgcccgaacaagtacctg
G T A E A V Q I Q F G L I N C G N K Y L
      1450      1460      1470      1480      1490      1500
acggccgagggcgttcgggttcaaggtgaacgcgtccgccagcagcctgaagaagaagcag
T A E A F G F K V N A S A S S L K K K Q
      1510      1520      1530      1540      1550      1560
atctggacgctggagcagccccctgacgagggcggcagcggcctgtgcctgcccagc
I W T L E Q P P D E A G S A A V C L R S
      1570      1580      1590      1600      1610      1620
cactggggcggctacctggcggcggacaaggacggcaacgtgacctgagcagcggaggtg
H L G R Y L A A D K D G N V T C E R E V
      1630      1640      1650      1660      1670      1680
ccccgtcccgactgcggtttcctcatcgtggcgcacgacgagcgtcgctggtcgctgag
P G P D C R F L I V A H D D G R W S L Q
      1690      1700      1710      1720      1730      1740
tccgagggcgcaccggcgtacttcggcggcaccgaggaccgctgtcctgcttcggcag
S E A H R R Y F G G T E D R L S C F A Q
      1750      1760      1770      1780      1790      1800
acgggtgtcccccgccgagaagtggagcgtgcacatcgccatgaccctcaggtcaacatc
T V S P A E K W S V H I A M H P Q V N I
      1810      1820      1830      1840      1850      1860
tacagcgtcaccgtaagcgtacgcgcacctgagcgcggcggccgagcagatcgcc
Y S V T R K R Y A H L S A R P A D E I A

```

EGFP

Start
Human
Fascin1

F29-A-E
TTC-GCC-GAA

S39-A-E
AGC-GCC-GAA

```

1870      1880      1890      1900      1910      1920
gtggaccgcgacgtgccctggggcgctcgactcgctcatcacctcgccttccaggaccag
V D R D V P W G V D S L I T L A F Q D Q
1930      1940      1950      1960      1970      1980
cgctacagcgtgcagaccgcccaccaccgcttctcgccacgacgggcccctggggcg
R Y S V Q T A D H R F L R H D G R L V A
1990      2000      2010      2020      2030      2040
cgccccgagccggccaactggctacacgctggagtccgctccggcaagggtggccttccgc
R P E P A T G Y T L E F R S G K V A F R
2050      2060      2070      2080      2090      2100
gactgcgaggccgcttacctggcgccgctcgggcccagcggcacgctcaaggcgggcaag
D C E G R Y L A P S G P S G T L K A G K
2110      2120      2130      2140      2150      2160
gccaccaaggtgggcaaggacgagctctttgctctggagcagagctgcgcccaggtcgtg
A T K V G K D E L F A L E Q S C A Q V V
2170      2180      2190      2200      2210      2220
ctgcagggcgcccaacgagaggaacgtgtccacgcgccagggtatggacctgtctgccaat
L Q A A N E R N V S T R Q G M D L S A N
2230      2240      2250      2260      2270      2280
caggacgaggagaccgaccaggagaccttccagctggagatcgaccgcgacacacaaaag
Q D E E T D Q E T F Q L E I D R D T K K
2290      2300      2310      2320      2330      2340
tgtgccttccgtaccacacgggcaagtactggacgctgacggccaccggggcggtgcag
C A F R T H T G K Y W T L T A T G G V Q
2350      2360      2370      2380      2390      2400
tccaccgcctccagcaagaatgccagctgctactttgacatcgagtggcgtgaccggcgc
S T A S S K N A S C Y F D I E W R D R R
2410      2420      2430      2440      2450      2460
atcacactgagggcgctccaatggcaagtttgtgacctccaagaagaatgggcagctggcc
I T L R A S N G K F V T S K K N G Q L A
2470      2480      2490      2500      2510      2520
gcctcggtaggacagcaggggactcagagctcttctcatgaagctcatcaaccgcccc
A S V E T A G D S E L F L M K L I N R P
2530      2540      2550      2560      2570      2580
atcatcgtgttccgcggggagcatggcttcatcggctgccgcaaggtcacgggcaccctg
I I V F R G E H G F I G C R K V T G T L
2590      2600      2610      2620      2630      2640
gacccaaccgctccagctatgacgtcttccagctggagttcaacgatggcgcctacaac
D A N R S S Y D V F Q L E F N D G A Y N
2650      2660      2670      2680      2690      2700
atcaaagactccacaggcaataactggacggtgggcagtgactccgtgggtcaccagcagc
I K D S T G K Y W T V G S D S V V T S S
2710      2720      2730      2740      2750      2760
ggcgacactcctgtggacttcttcttcgagttctgcgactataacaaggtggccatcaag
G D T P V D F F F E F C D Y N K V A I K
2770      2780      2790      2800      2810      2820
gtgggcccggcgtacctgaaggcgaccacgcaggcgtcctgaaggcctcggcggaaacc
V G G R Y L K G D H A G V L K A S A E T
2830      2840      2850      2860      2870      2880
Gtggacccgcctcgctctgggagtacaggccggcccgccttccccgcctgccca
V D P A S L W E Y *
2890      2900      2910      2920      2930      2940
catggcggctcctgccaacctcctgctaacccttctccgcccaggtgggctccagggc
2950      2960      2970      2980      2990      3000
gggaggcaagcccccttgcccttcaaactggaaccccagagaaaacggtgccccacct
3010      3020      3030      3040      3050      3060
gtgcgccctatggactccccactctcccctccgCCCGGGATCCACCGGATCTAGATAACT
SmaI BamHI

```

STOP
3'UTR

Figure 30. Sequence of human fascin1. cDNA and amino acid sequence. Position of mutations at F29 and S39 are shown in cyan and red, respectively. Sequence of EGFP precedes that of fascin.

Quantitative Immunoblotting

Cells were lysed in buffer containing 10mM Tris, [pH 7.5], 150mM NaCl, 1% Triton X-100, 10% glycerol, and protease inhibitor tablet (Roche). Lysate and purified fascin protein were loaded onto a SDS-PAGE (4-20% polyacrylamide) and immunoblotted with mouse monoclonal anti-fascin primary antibody (DAKO Cytomation) and secondary mouse antibody (Sigma) using standard protocols. The amount of fascin in cell lysates was evaluated by comparing the intensity of the bands of each sample (background subtracted) with the pure fascin standard by densitometry using NIH ImageJ software.

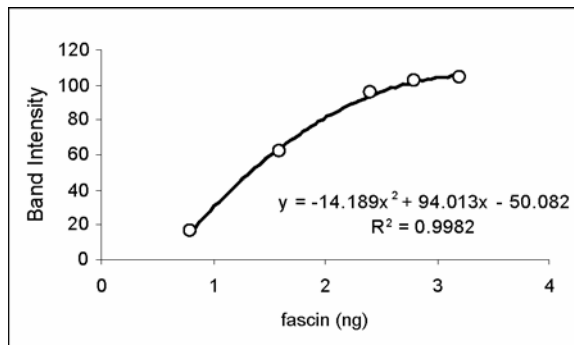


Figure 31. Protein standard curve.

Lysate fascin concentration was determined from protein standardization curve. Band intensities for fascin protein standards were measured and plotted versus amount of fascin loaded onto gel. A second order polynomial function was used to fit the data, with $x = \text{fascin (ng)}$ and $y = \text{band intensity}$. To calculate amount of protein in lysate, lysate band intensities (y -axis) were located on plot and matched with corresponding fascin concentration (x -axis), or determined from curve fitting equation. This plot corresponds to standard curve for western blot in figure 18.

Immunofluorescent staining of fixed cells

Immunostaining was performed after cell extraction for 3 to 10 min in 1% Triton X-100 in PEM buffer (100 mM Pipes, pH 6.9, 1 mM MgCl₂, and 1 mM EGTA), containing 4% polyethylene glycol, mol wt 40,000 (SERVA), and 2 μ M phalloidin (Sigma-Aldrich), followed by fixation with 0.2% glutaraldehyde and quenching with NaBH₄. For phalloidin staining, 0.033 μ M Texas Red phalloidin (Molecular Probes, Inc.) was added to the extraction solution instead of unlabeled phalloidin. GFP-fascin expressing cells were stained with Texas Red phalloidin after fixation of unextracted cells, followed by permeabilization with 1% Triton X-100 in PBS.

Microscopy

Epi-fluorescent microscopy

Light microscopy was performed using an Eclipse TE2000 microscope (Nikon) equipped with a Plan 100x 1.3 NA objective (Nikon) and a back-illuminated cooled CCD camera (CH250, Roper Scientific). MetaMorph Imaging software (Universal Imaging Corp) was used for image acquisition and analysis. For live cell imaging, cells were kept in a CO₂-independent culture medium (L-15, Gibco) at 37 °C.

FRAP and FLIP

FRAP and FLIP experiments were performed on a Zeiss LSM 510 Meta confocal microscope with a 100x/1.3 N.A. planapochromat oil objective. TMR-actin was excited with the 543nm line of a HeNe laser (1mW) while GFP- and Alexa488-tagged proteins were excited with the 488nm line of an argon laser (25mW). We photobleached fluorescence using a rectangular region of 1 μ m² area for 0.7-1.7 seconds using 100% laser power for photobleaching and recorded images at attenuated laser settings.

FRAP data was analyzed as follows: the average intensity in the bleached zone was measured over the time course of the experiment. Prior to quantifying the fluorescence recovery, the measurements

were corrected for photobleaching during image acquisition by a bleaching correction factor. This factor was determined by curve-fitting the fluorescence decay of a filopodium located far from the site of bleaching during a FRAP experiment (non-bleached bundle in the *in vitro* experiments) with a single exponential function, $\exp(-k_{decay}t)$, to extract a decay constant, k_{decay} . We then multiplied the intensity in the bleached zone by the correction factor, $\exp(-k_{decay}t)$, for each time point, t , in the experiment to obtain a normalized recovery profile. We curve fit the *in vivo* FRAP profile with a double exponential function, $I(t) = I_f - 0.75 * \exp(-k_{fast}t) - 0.25 * \exp(-k_{slow}t)$, and single exponential function, $I(t) = I_f + (I_o - I_f)\exp(-k_{fast}t)$, for the *in vitro* experiment since fluorescence recovered rapidly to pre-bleach values, where I_f is the intensity of the bleached zone at the final time of the experiment relative to the pre-bleach state, I_o is the intensity immediately post bleach relative to the pre-bleach state, k_{fast} is the constant reflecting the recovery to quasi-steady state when fascin cross-links have redistributed evenly within the filopodium, and k_{slow} is the constant reflecting the recovery to pre-bleach intensity. The half time for dissociation was calculated as $t_{1/2} = \ln 2/k_{fast}$, with average values along with their 95% confidence interval reported.

FLIP data was analyzed by measuring the loss in fluorescence near the filopodial tip. The intensity loss was multiplied by a photobleaching correction factor, which was determined in the same manner as above. Once normalized, the decay in fluorescence was fit with a single exponential function, $I(t) = I_o \exp(-k_{off}t)$, where I_o is the initial intensity relative to the pre-bleach state and k_{off} is the dissociation rate constant.

Chapter 7: References

- Adams, J. C. (1997). Characterization of cell-matrix adhesion requirements for the formation of fascin microspikes. *Mol. Biol. Cell.* 8, 2345-2363.
- Adams, J.C., J.D. Clelland, G.D. Collett, F. Matsumura, S. Yamashiro, and L. Zhang. (1999). Cell-matrix adhesions differentially regulate fascin phosphorylation. *Mol. Biol. Cell.* 10, 4177-4190.
- Adams, J.C. and M.A. Schwartz. (2000). Stimulation of fascin spikes by thrombospondin-1 is mediated by the GTPases Rac and Cdc42. *J. Cell Biol.* 150, 807-822.
- Adams, J.C. (2002). Regulation of protrusive and contractile cell-matrix contacts. *J. Cell Sci.* 115, 257-265.
- Adams, J.C. (2004). Roles of fascin in cell adhesion and motility. *Curr. Opin. Cell Biol.* 16, 590-596.
- Albrecht-Buehler, G. (1976). Filopodia of spreading 3T3 cells. Do they have a substrate-exploring function? *J Cell Biol.* 69, 275-286.
- Anilkumar, N., M. Parsons, R. Monk, T. Ng, and J.C. Adams. (2003). Interaction of fascin and protein kinase C α : a novel intersection in cell adhesion and motility. *EMBO J.* 22, 5390-5402.
- Aratyn, Y., T.E. Schaus, E.W. Taylor, and G.G. Borisy. (2007). Intrinsic dynamic behavior of fascin in filopodia. *Mol. Biol. Cell.* 18, 3092-.
- Bamburg, J.R. (1999). Proteins of the ADF/cofilin family: essential regulators of actin dynamics. *Annu. Rev. Cell Dev. Biol.* 15, 185-230.
- Bartles, J.R. (2000). Parallel actin bundles and their multiple actin-bundling proteins. *Curr. Opin. Cell Biol.* 12, 72-78.
- Belyantseva, I.A., Boger, E.T. and T.B. Friedman. (2003). Myosin XVa localizes to the tips of inner ear sensory cell stereocilia and is essential for staircase formation of the hair bundle. *Proc. Natl Acad. Sci. USA*, 100, 13958–13963.
- Bentley, D. and A. Toroian-Raymond (1986). Disoriented pathfinding by pioneer neuron growth cones deprived of filopodia by cytochalasin treatment. *Nature* 323, 712-715.
- Berg, J.S., and R.E. Cheney. (2002). Myosin-X is an unconventional myosin that undergoes intrafilopodial motility. *Nat. Cell Biol.* 4, 246-250.
- Brieher, W.M., M. Coughlin, and T.J. Mitchison. (2004). Fascin-mediated propulsion of *Listeria monocytogenes* independent of frequent nucleation by the Arp2/3 complex. *J Cell Biol.* 165, 233-242.
- Bryan, J., and R.E. Kane. (1978). Separation and interaction of the major components of sea urchin actin gel. *J Mol Biol.* 125, 207-224.
- Bryan, J., R. Edwards, P. Matsudaira, J. Otto, and J. Wulfkuhle. (1993) Fascin, an echinoid actin-bundling protein, is a homolog of the *Drosophila* singed gene product. *Proc Natl Acad Sci USA* 90, 9115-9119.
- Carey, J., Ed. (2002). Brain Facts: A primer on the brain and nervous system. Washington, DC, The Society for Neuroscience.

- Carrier, M.F. and D. Pantaloni. (1997). Control of actin dynamics in cell motility. *J. Mol. Biol.* 269, 45-67.
- Cant, K. and L. Cooley. (1996) Single amino acid mutations in *Drosophila* fascin disrupt actin bundling function *in vivo*. *Genetics*. 143, 249-258.
- Cohan, C. S., Welnhof, E. A., Zhao, L., Matsumura, F., and S. Yamashiro. (2001). Role of the actin bundling protein fascin in growth cone morphogenesis: localization in filopodia and lamellipodia. *Cell Motil. Cytoskeleton* 48, 109-120.
- DesMarais, V., I. Ichetovkin, J. Condeelis, and S.E. Hitchcock-DeGregori. (2002). Spatial regulation of actin dynamics: a tropomyosin-free, actin-rich compartment at the leading edge. *J. Cell Sci.* 115, 4649-4660.
- Edwards, R. A., H. Herrera-Sosa, J. Otto, and J. Bryan. (1995). Cloning and expression of a murine fascin homolog from mouse brain. *J. Biol. Chem.* 270, 10764-10770.
- Fath, K.R., S.D. Obenauf, and D.R. Burgess. (1990). Cytoskeletal proteins and mRNA accumulation during brush border formation in adult chicken enterocytes. *Development*. 106, 407-419.
- Fedorov, A.A., E.V. Fedorov, S. Ono, F. Matsumura, and S.C. Almo. (1999) Crystal structure of human fascin, an actin-crosslinking protein. *RCSB Protein Data Bank*, 1DFC.
- McClay D.R. (1999) The role of thin filopodia in motility and morphogenesis. *Exp. Cell Res.* 253, 296-301.
- Davenport, R.W., P. Dou, V. Rehder, and S.B. Kater. (1993). A sensory role for neuronal growth cone filopodia. *Nature*. 361, 721-724.
- Dent, E.W. and F.B. Gertler. (2003). Cytoskeletal dynamics and transport in growth cone motility and axon guidance. *Neuron*. 40, 209-227.
- Goldberg D.J., and D.W. Burmeister. (1986). Stages in axon formation: Observations of growth of *Aplysia* axons in culture using video-enhanced contrast-differential interference contrast microscopy. *J Cell Biol.* 103, 1921-1931.
- Goncharuk, V.N., J.S. Ross, and J.A. Carlson. (2002). Actin-binding protein fascin expression in skin neoplasia. *J. Cutan. Pathol.* 29, 430-438.
- Govind. S., R. Kozma, C. Monfries, L. Lim, and S. Ahmed. (2001). Cdc42Hs facilitates cytoskeletal reorganization and neurite outgrowth by localizing the 58-kD insulin receptor substrate to filamentous actin. *J. Cell Biol.* 152, 579-594.
- Grothey A., R. Hashizume, A.A. Sahin, and P.D. McCrea. (2000). Fascin, an actin-bundling protein associated with cell motility, is upregulated in hormone receptor negative breast cancer. *Br. J. Cancer*. 83, 870-873.
- Gundersen, R.W. and J.N. Barrett. (1980). Characterization of the turning response of dorsal root neurites toward nerve growth factor. *J. Cell Biol.* 87, 546-554.
- Gupta, G.P. and J. Massague. (2005). Cancer metastasis: Building a framework. *Cell*. 127, 679-695.
- Harris E.S., F. Li, and H.N. Higgs. (2004). The mouse formin, FRL α , slows actin filament barbed end elongation, competes with capping protein, accelerates polymerization from monomers, and severs filaments. *J. Biol. Chem.* 279, 20076-20087.

- Harrison, W.L., M.E. Schneider, and B. Kachar. (2005) When size matters: the dynamic regulation of stereocilia lengths. *Curr. Opin. Cell Biol.* 17, 55-61.
- Hashimoto, Y., M. Skacel, J.C. Adams. (2005). Roles of fascin in human carcinoma motility and signaling: Prospects for a novel biomarker? *IJBCB* 37, 1787-1804.
- Hashimoto, Y., M. Skacel, I.C. Lavery, A.L. Mukherjee, G. Casey, and J.C. Adams. (2006). Prognostic significance of fascin expression in advanced colorectal cancer: an immunohistochemical study of colorectal adenomas and adenocarcinomas. *BMC Cancer.* 6, 241-252.
- Heidemann, S.R., P. Lamoureux, R.E. Buxbaum. (1990). Growth cone behavior and production of traction force. *J. Cell Biol.* 111, 1949-1957.
- Honda, M., K. Takiguchi, S. Ishikawa, and H. Hotani. (1999). Morphogenesis of liposomes encapsulating actin depends on the type of actin cross-linking. *J. Mol. Biol.* 287, 293-300.
- Hu W., P.D. McCrea, M. Deavers, J.J. Kavanagh, A.P. Kudelka, and C.F. Verschraegen. (2000). Increased expression of fascin, motility associated protein, in cell cultures derived from ovarian cancer and in borderline and carcinomatous ovarian tumors. *Clin. Exp. Metastasis.* 18, 83-88.
- Isambert H., P. Venier, A.C. Maggs, A. Fattoum, R. Kassab, D. Pantaloni, and M.F. Carlier. (1995). Flexibility of actin filaments derived from thermal fluctuations. Effect of bound nucleotide, phalloidin, and muscle regulatory proteins. *J. Biol. Chem.* 270, 11437-44.
- Ishikawa, R., S. Yamashiro, K. Kohama, and F. Matsumura. (1998). Regulation of actin binding and actin bundling activities of fascin by caldesmon coupled with tropomyosin. *J. Biol. Chem.* 273, 26991-26997.
- Ishikawa, R., T. Sakamoto, T. Ando, S. Higashi-Fujima, and K. Kohama. (2003). Polarized actin bundles formed by human fascin-1; their sliding and disassembly on myosin II and myosin V *in vitro*. *J. Neurochem.* 87, 676-685.
- Jamora, C. and E. Fuchs. (2002). Intercellular adhesion, signaling and the cytoskeleton. *Nat. Cell Biol.* 4, 101-108.
- Janmey, P.A., U. Euteneuer, P. Traub, and M. Schliwa. (1991). Viscoelastic properties of vimentin compared with other filamentous biopolymer networks. *J Cell Biol.* 113, 155-160.
- Jawhari, A.U., A. Buda, M. Jenkins, K. Shehzad, C. Sarraf, M. Noda, M.J.G. Farthing, M. Pignatelli, and J.C. Adams. (2003). Fascin, an actin-bundling protein, modulates colonic epithelial cell invasiveness and differentiation *in vitro*. *Am. J. Path.* 162, 69-80.
- Kabukcuoglu, S., S.S. Ozalp, U. Oner, M.F. Acikalin, O.T. Yalcin, and E. Colak. (2005) Fascin, an actin-bundling protein expression in cervical neoplasms. *Eur J. Gynecol. Oncol.* 26, 636-641.
- Koleske, A.J. (2003). Do Filopodia Enable the Growth Cone to Find Its Way? *Science stke.* 2003(183), pe20.
- Kovar D.R., J.R. Kuhn, A.L. Tichy, and T.D. Pollard. (2003). The fission yeast cytokinesis formin Cdc12p is a barbed end actin filament capping protein gated by profilin. *J. Cell Biol.* 161, 875-887.
- Kovar D.R. and T.D. Pollard. (2004) Progressing actin: Formin as a processive elongation machine. *Nat. Cell Biol.* 6, 1158-1159.

- Kranewitter, W.J., C. Danninger, and M. Gimona. (2001). GEF at work: Vav in protruding filopodia. *Cell Motil Cytoskeleton*. 49, 154-160.
- Kureishy, N., V. Sapountzi, S. Prag, N. Anilkumar, and J.C. Adams. (2002). Fascins, and their role in cell structure and function. *Bioessays*. 24, 350-361.
- Lanier, L.M., M.A. Gates, W. Witke, A.S. Menzies, A.M. Wehman, J.D. Macklis, D. Kwiatkowski, P. Soriano, and F.B. Gertler. (1999). Mena is required for neurulation and commissure formation. *Neuron*. 22, 313-325.
- Letourneau, P.C. (1996). The cytoskeleton in nerve growth cone motility and axonal pathfinding. *Perspect Dev Neurosci*. 4, 111-123.
- Lewis, A.K., and P.C. Bridgman. (1992). Nerve growth cone lamellipodia contain two populations of actin filaments that differ in organization and polarity. *J Cell Biol*. 119, 1219-1243.
- Mallavarapu, A., and T. Mitchison. (1999). Regulated actin cytoskeleton assembly at filopodium tips controls their extension and retraction. *J Cell Biol*. 146, 1097-1106.
- Martin-Blanco, E. and E. Fuchs. (2001) Epithelial morphogenesis: Filopodia at work. *Curr. Biol*. 11, R28-R31.
- Matus, A (2000). Actin-based plasticity in dendritic spines. *Science* 290, 754-758.
- McClay, D.R. (1999). The role of thin filopodia in motility and morphogenesis. *Exp. Cell Res*. 253, 296-301.
- Meyer, R.K. and U. Aebi. (1990). Bundling of actin filaments by alpha-actinin depends on its molecular length. *J. Cell. Biol*. 110, 2013-2024.
- Medeiros, N.A., D.T. Burnette, and P. Forscher. (2006). Myosin II functions in actin-bundle turnover in neuronal growth cones. *Nature* 8, 215-226.
- Mitchison, T. and M. Kirschner. (1988). Cytoskeletal dynamics and nerve growth. *Neuron*. 1, 761-722.
- Mitchison, T. and L.P. Cramer. (1996). Actin-based cell motility and cell locomotion. *Cell* 84, 371-379.
- Mullins, R.D., J.A. Heuser, and T.D. Pollard (1998). The interaction of Arp2/3 complex with actin: nucleation, high affinity pointed end capping, and formation of branched networks of filaments. *Proc. Natl. Acad. Sci. USA*. 95, 6181-6186.
- Mogilner, A., and B. Rubinstein. (2005). The physics of filopodial protrusion. *Biophys J*. 89, 782-795.
- Nakagawa, H., A.G. Terasaki, H. Suzuki, K. Ohashi, and S. Miyamoto. (2006). Short-term retention of actin filament binding proteins on lamellipodial actin bundles. *Febbs Letters*. 580, 3223-3228.
- Neuhaus J.M., M. Wanger, T. Keiser, and A. Wegner. (1983). Treadmilling of actin. *J Muscle Res Cell Motil*. 4, 507-527.
- Ono, S., Y. Yamakita S. Yamashiro P.T. Matsudaira J.R., Gnarra T. Obinata, and F. Matsumura. (1997). Identification of an actin binding region and a protein kinase C phosphorylation site on human fascin. *J Biol Chem*. 272, 2527-2533.
- Otto, J.J., R.E. Kane, J. Bryan. (1979) Formation of filopodia in coelomocytes: localization of fascin, a 58,000 dalton actin cross-linking protein. *Cell*. 17, 285-293.

- Pantaloni, D., C. Le Clairche, and M.F. Carrier. (2001). Mechanism of actin-based motility. *Science* 292, 1502-1506.
- Parker, K.P., A.L. Brocke, C. Brangwynne, R.J. Mannix, N. Wang, E. Ostuni, N.A. Geisse, J.C. Adams, G.M. Whitesides, D.E. Ingber. (2002). Directional control of lamelliipodia extension by constraining cell shape and orientating cell tractional forces. *FASEB J.* 16, 1195-1204.
- Pellegrin, S. and H. Mellor. (2005). The Rho family GTPase Rif induces filopodia through mDia2. *Curr. Biol.* 15, 129-133.
- Pelosi, G., F. Pasini, F. Fraggetta, U. Pastorino, A. Iannucci, P. Maissoneuve, G. Arrigoni, G. De Manzoni, E. Bresola, and G. Viale. (2003a). Independent value of fascin immunoreactivity for predicting lymph node metastases in typical and atypical pulmonary carcinoids. *Lung Cancer.* 42, 203-13.
- Pelosi, G., U. Pastorino, F. Pasini, P. Maissoneuve, F. Fraggetta, A. Iannucci, A. Sonzogni, G. De Manzoni, A. Terzi, E. Durante, E. Bresola, F. Pezzella, and G. Viale. (2003b). Independent prognostic value of fascin immunoreactivity in stage I nonsmall cell lung cancer. *Br. J. Cancer.* 88, 537-547.
- Peng, J., B.J. Wallar, A. Flanders, P.J. Swiatek, and A.S. Alberts. (2003). Disruption of the Diaphanous-related formin Drf1 gene encoding mDia1 reveals a role for Drf3 as an effector for Cdc42. *Curr. Biol.* 13, 534-545.
- Ponting, C.P. and R.B. Russell. (2000) Identification of distant homologues of fibroblast growth factors suggests a common ancestor for all beta-trefoil proteins. *J. Mol. Biol.* 302, 1041-1047.
- Pollard, T.D. (1986). Rate constants for the reactions of ATP- and ADP-actin with the ends of actin filaments. *J. Cell Biol.* 103, 2747-2754.
- Pollard, T.D. and G.G. Borisy. (2003). Cellular motility driven by assembly and disassembly of actin filaments. *Cell* 112, 453-465.
- Pollard T.D., L. Satterwhite, L. Cisek, J. Corden, M. Sato, and P. Maupin. (1990). Actin and myosin biochemistry in relation to cytokinesis. *Ann NY Acad Sci.* 582, 120-130.
- Pellegrin S. and H. Mellor. (2005). The Rho family GTPase Rif induces filopodia through mDia2. *Curr. Biol.* 15, 129-133.
- Pruyne D., M. Evangelista, C. Yang, E. Bi, S. Zigmond, A. Bretsher, and C. Boone. (2002). Role of formins in actin assembly: Nucleation and barbed end association. *Science* 297, 612-615.
- Rock, R. S., M. Rief, A.D. Mehta, and J.A. Spudich. (2000). In vitro assays of processive myosin motors. *Methods* 22, 373-81.
- Rzadzinska, A., M. Schneider, K. Noben-Trauth, J.R. Bartles, and B. Kachar. (2005) Balanced levels of espin are critical for stereociliary growth and length maintenance. *Cell Mot. Cyt.* 62, 157-165.
- Rzadzinska, A., M.E. Schneider, C. Davies, G.P. Riordan, and B. Kachar. (2004). An actin molecular treadmill and myosins maintain stereocilia functional architecture and self-renewal. *J. Cell Biol.* 164, 887-897.
- Sagot I., S.K. Klee, and D. Pellman. (2002). Yeast formins regulate cell polarity by controlling the assembly of actin cables. *Nat. Cell Biol.* 4, E29-30.

- Sala, C. (2002). Molecular regulation of dendritic spine shape and function. *Neurosignals*. 11, 213-223.
- Sanchez, A.A., P.A. Newmark, S.M. Robb, and R. Juste. (2002). The *Schmidtea mediterranea* database as a molecular resource for studying platyhelminthes, stem cells and regeneration. *Development*. 129, 5659-5665.
- Sato M., W.H. Schwarz, and T.D. Pollard. (1987). Dependence of the mechanical properties of actin/ α -actinin gels on deformation rate. *Nature*. 325, 828-830.
- Schaus, T.E., E.W. Taylor, and G.G. Borisy. (2007). Self-organization of actin filament orientation in the dendritic nucleation array treadmilling model. *PNAS* 104, 7086-7091.
- Schirenbeck A., T. Bretshneider, R. Arasada, M. Schleicher, and J. Faix. (2005) The Diaphanous-related formin dDia2 is required for the formation and maintenance of filopodia. *Nat. Cell Biol.* 2, 619-625.
- Sheetz M.P., D.B. Wayne, and A.L. Pearlman. (1992). Extension of filopodia by motor-dependent actin assembly. *Cell Motility and the Cytoskeleton*. 22, 160-169.
- Shonukan, O., I. Bagayogo, P. McCrea, M. Chao, and B. Hempstead. (2003). Neurotrophin-induced melanoma cell migration is mediated through the actin-bundling protein fascin. *Oncogene*. 22, 3616-3623.
- Smith, C.L. (1994). Cytoskeletal movements and substrate interactions during initiation of neurite outgrowth by sympathetic neuron *in vitro*. *J. Neurosci*. 22, 8071-8083.
- Sprague B.L., R. L. Pego, D.A. Stavreva, and J.G. McNally. (2004). Analysis of binding reactions by fluorescence recovery after photobleaching. *Biophys. J.* 86, 3473-3495.
- Spudich J. and S. Watt. (1971). The regulation of rabbit skeletal muscle contraction. *J Biol Chem*. 246, 4866-4871.
- Steketee M.K., K. Balazovich, and K.W. Tosney. (2001). Filopodial initiation and a novel filament-organizing center, the focal ring. *Mol. Biol. Cell*. 12, 2378-2395.
- Stokes, D.L., and D.J. DeRosier. (1991). Growth conditions control the size and order of actin bundles *in vitro*. *Biophys. J.* 59, 456-465.
- Stradal, T., K.D. Courtney, K. Rottner, P. Hahne, J.V. Small, and A.M. Pendergaast. (2001). The Abl interactor proteins localize to sites of actin polymerization at the tips of lamellipodia and filopodia. *Curr. Biol*. 11, 891-895.
- Suter, D.M. and P. Forscher. (2000). Substrate-cytoskeletal coupling as a mechanism for the regulation of growth cone motility and guidance. *J. Neurobiol.* 44, 97-113.
- Suter, D.M., L.D. Errante, V. Belotserkovsky, P. Forscher. (1998). The Ig superfamily cell adhesion molecule, apCAM, mediates growth cone steering by substrate cytoskeletal coupling. *J. Cell Biol.* 141, 227-240.
- Svitkina, T.M., and G.G. Borisy. (1999). Arp2/3 complex and actin depolymerization factor/cofilin in dendritic organization and treadmilling of actin filament array in lamellipodia. *J. Cell Biol.* 145, 1009-1026.

- Svitkina, T.M., E.A. Bulanova, O.Y. Chaga, D.M. Vignjevic, S. Kojima, J.M. Vasiliev, and G.G. Borisy. (2003). Mechanism of filopodia initiation by reorganization of a dendritic network. *J Cell Biol.* 160, 409-421.
- Swaminathan, R., C.P. Hoang, and A.S. Verkman. (1997). Photobleaching recovery and anisotropy decay of green fluorescent protein GFP-S65T in solution and cells: cytoplasmic viscosity probed by green fluorescent protein translational and rotational diffusion. *Biophys. J.* 72, 1900-1907.
- Tilney, L.G., E.M. Bonder, and D.J. DeRosier. (1981). Actin filaments elongate from their membrane-associated ends. *J. Cell Biol.* 90, 485-494.
- Tilney, L.G., P.S. Connelly, L. Ruggiero, K.A. Vranich, and G.M. Guild. (2003). Actin filament turnover regulated by cross-linking accounts for the size, shape, location, and number of actin bundles in *Drosophila* bristles. *Mol. Biol. Cell.* 14, 3953-3966.
- Tilney, L.G., P.S. Connelly, K.A. Vranich, M.K. Shaw, and G.M. Guild. (2000). Regulation of actin filament cross-linking and bundle shape in *Drosophila* bristles. *J. Cell Biol.* 14, 87-100.
- Tilney, L.G., M.S. Tilney, and G.M. Guild. (1992). Actin filaments, stereocilia, and hair cells of bird cochlea: how cells count and measure. *Annu. Rev. Cell Biol.* 8, 257-274.
- Tilney, L.G. and D.J. DeRosier. (1986). Actin filaments, stereocilia, and hair cells of the bird cochlea IV. How the actin filaments become organized in developing stereocilia and in the cuticular plat. *Dev. Biol.* 116, 119-129.
- Tilney, L.G. and D.J. DeRosier. (2000) F-actin bundles are derivatives of microvilli: what does this tell us about how bundles might form? *J. Cell Biol.* 148, 1-6.
- Tilney, L.G. and D.J. DeRosier. (2005). How to make a curved *Drosophila* bristle using straight actin bundles. *PNAS.* 102, 18785-18792.
- Tokuo, H. and M. Ikebe. (2004). Myosin X transports Mena/VASP to the tip of filopodia. *Biochem. Biophys. Res. Commun.* 319, 214-220.
- Tseng, Y., E. Federov, J.M. McCaffery, S.C. Almo, and D. Wirtz. (2001). Micromechanics and ultrastructure of actin filament networks crosslinked by human fascin: a comparison with alpha-actinin. *J. Mol. Biol.* 310, 351-366.
- Tseng, Y. B.W. Schafer, S.C. Almo, and D. Wirtz. (2002). Functional synergy of actin filament cross-linking proteins. *J. Biol. Chem.* 277, 25609-25616.
- Vasioukhin, V. and E. Fuchs. (2001) Actin dynamics and cell-cell adhesion in epithelia. *Curr. Opin. Cell Biol.* 13, 76-84.
- Vignjevic, D, S.I. Kojima, Y. Aratyn, O. Danciu, and G. Borisy. (2006). Role of fascin in filopodial protrusion. *J Cell Biol.* 174, 863-875.
- Vignjevic, D. M. Schoumacher, N. Gavert, K. Janssen, G. Jih, M. Lae, D. Louvard, A. Ben-Ze'ev, and S. Robine. (2007). Fascin, a novel target of β -catenin-TCF signaling, is expressed at the invasive front of human colon cancer. *Cancer Res.* 67, 6844-6853.
- Vignjevic, D., D. Yarar, M.D. Welch, J. Peloquin, T. Svitkina, and G.G. Borisy. (2003). Formation of filopodia-like bundles in vitro from a dendritic network. *J Cell Biol.* 160, 951-962.

- Wang, A., H. Liu, and Y. Zhang. (2007). Increased expression of fascin associated with malignant transformation of sinonasal inverted papilloma. *Chinese Med. J.* 120, 375-379.
- Wolenski, J.S. (1995). Regulation of calmodulin-binding myosins. *Trends Cell Biol.* 5, 310-316.
- Wong W. T. and R. O. L. Wong (2001). Changing specificity of neurotransmitter and regulation of rapid dendritic remodeling during synaptogenesis. *Nature* 4, 351-352.
- Wood W., A. Jacinto, R. Grose, S. Woolner, J. Gale, C. Wilson, and P. Martin. (2002). Wound healing recapitulates morphogenesis in *Drosophila* embryos. *Nat. Cell Biol.* 4, 907-912.
- Wu, J.Q. and T.D. Pollard. (2005). Counting cytokinesis proteins globally and locally in fission yeast. *Science.* 310, 310-314.
- Xu J., Y. Tseng, and D. Wirtz. (2000). Strain hardening of actin filament networks; regulation by the dynamic cross-linking protein α -actinin. *J Biol Chem.* 275(46), 35886-35892.
- Xu J., D. Wirtz, and T.D. Pollard. (1998). Dynamic cross-linking by α -actinin determines properties of actin filament networks. *J Biol Chem.* 273(16), 9570-9576.
- Yamagishi, A. M. Masuda, T. Ohki, H. Onishi, and N. Mochizuki. (2004). A novel actin bundling/filopodium-forming domain conserved in insulin receptor tyrosine kinase substrate p53 and missing in metastasis protein. *J. Biol. Chem.* 279, 14929-14936.
- Yamakita Y., S. Ono, F. Matsumura, and S. Yamashiro. (1996). Phosphorylation of human fascin inhibits its actin binding and bundling activities. *J Biol Chem.* 271, 12632-12638.
- Yamashiro-Matsumura S and Matsumura F. (1985) Purification and characterization of an F-actin-bundling 55-kilodalton protein from HeLa cells. *J Biol Chem* 260: 5087-5097.
- Yoder B.J., E. Tso, M. Skacel, J. Pettay, S. Tarr, T. Budd, R.R. Tubbs, J.C. Adams, and D.G. Hicks. (2005). The expression of fascin, an actin-bundling motility protein, correlates with hormone receptor-negative breast cancer and a more aggressive clinical course. *Clin. Cancer Res.* 11, 186-192.
- Yonemura, S., M. Hirao, D. Yoshinori, N. Takahashi, T. Kondo, S. Tsukita, and S. Tsukita. (1998). Ezrin/radixin/moesin (ERM) proteins bind to a positively charged amino acid cluster in the justa-membrane cytoplasmic domain of CD44, CD43, and ICAM-2. *J. Cell Biol.* 140, 885-895.
- Yuste, R. and T. Bonhoeffer. (2004). Genesis of dendritic spines: insights from ultrastructural and imaging studies. *Nature Reviews Neuroscience* 5, 24-34.
- Zhai Y. and G.G. Borisy. (1994). Quantitative determination of the proportion of microtubule polymer present during the mitosis-interphase transition. *J Cell Sci.* 107, 881-890.
- Zheng, J.Q., J.J. Wan, and M.M. Poo. (1996). Essential role of filopodia in chemotropic turning of nerve growth cone induced by a glutamate gradient. *J. Neurosci.* 16, 1140-1149.
- Zhou, F. Q. and C. S. Cohan (2001). Growth cone collapse through coincident loss of actin bundles and leading edge actin without actin depolymerization. *J. Cell Biol.* 153, 1071-1084.
- Zigmond S.H., M. Evangelista, C. Boone, C. Yang, A.C. Dar, F. Sicheri, J. Forkey, and M. Pring. (2003). Formin leaky cap allows elongation in the presence of tight capping proteins. *Curr. Biol.* 13, 1820-1823.

Zigmond S.H. (2004). Fomin-induced nucleation of actin filaments. *Curr. Opin. In Cell Biol.* 16, 99-105.

YVONNE S. ARATYN

University of Chicago
 Institute of Biophysical Dynamics
 Gordon Center for Integrated Science, E223
 929 E. 57th St.
 Chicago, IL 60637
 Phone: (773) 817-1313
 Email: yaratyn@gmail.com

CURRENT POSITION:

Postdoctoral Fellow, Institute for Biophysical Dynamics, University of Chicago *October 2007*

EDUCATION:

Doctor of Philosophy, Cell and Molecular Biology

Northwestern University Medical School, Chicago, Illinois

August 2007

Thesis advisor: *Gary Borisy*

- PhD Thesis: Fascin Dynamics in Filopodia
- Designed and expressed mutants of fascin to characterize regulatory features of actin cross-linking in filopodia.
- Used Confocal Scanning Microscopy to perform *in vivo* and *in vitro* fluorescence recovery after photobleaching (FRAP) and fluorescence loss in photobleaching (FLIP) experiments on fluorescently-tagged fascin and actin proteins
- Designed a combinatorial approach to calculating local concentration of protein in filopodia using fluorescence microscopy and quantitative immunoblotting

Master of Science, Mechanical Engineering

Northwestern University, Evanston, Illinois

August 2003

Thesis advisor: *Seth Lichter*

- M.S. Thesis: Modeling Structure and Function relationships for β -lactamase
- Developed a computational model to characterize the structure and function of β -lactamase
- Expressed, purified, and performed kinetic and thermodynamic assays on mutants of AmpC β -lactamase

Bachelor of Science, Engineering Mechanics

University of Illinois at Urbana-Champaign

May 2000

- Courses emphasizing applied mathematics and fluid dynamics
- Engineering Senior Design Project: designed environmentally safe cellular phone housing for Motorola

WORK EXPERIENCE:**Research Intern****Phase Transformation of Semiconductors***University of Illinois at Urbana-Champaign**May 1999 – August 2000**Materials Science Department**University of Illinois at Chicago**Mechanical Engineering Department*

- Conducted Raman spectroscopy on silicon
- Conducted temperature dependency tests on properties of semiconductors using a Nikon High Temperature Microhardness Tester

Research Assistant**MBE growth and characterization of semiconductors***University of Illinois at Chicago**May 1997 – August 1998**Physics Department*

- Preparation of silicon wafers for Molecular Beam Epitaxy (MBE)
- Assisted with materials research on MBE growth of cadmium telluride grown on silicon (CdTe/Si) for infrared detector applications

PUBLICATIONS:

- Vignjevic D., Kojima S., **Aratyn Y.**, Danciu O., Svitkina T., and G. Borisy. "Role of Fascin in Filopodia Protrusion." (2006) *Journal of Cell Biology*, 174:863-875.
- **Aratyn Y.**, Schaus, T., Taylor, E., and G. Borisy. "Intrinsic Dynamic Behavior of Fascin in Filopodia." (2007) *Molecular Biology of the Cell*, 18,3928-3940.

DISTINCTIONS:

Northwestern University, Cancer Center

July 2006

Katten Munchin Rosenman Travel Award

Northwestern University Graduate School Travel Award

August 2006

NIH National Research Service Award (Rank top 7.5%)

April 2006-April 2008

NSF Integrative Graduate Education and

June 2001 – September 2003

Research Training (IGERT) Fellow

Northwestern University Scholar

June 2001

Walter P. Murphy Fellow

September 2000 – June 2001

Licensed Engineer-in-Training, State of Illinois

October 2000

Dean's list, University of Illinois College of Engineering

Three Semesters

Honorable Mention for Material Research Society's (MRS)

1999

Undergraduate Materials Research Initiative (UMRI)

Proposal title: Raman Analysis of Silicon and Germanium after High-Temperature Hardness Tests